P U R D U E U N I V E R S I T Y
Lafayette, Indiana

School of Mechanical Engineering

HEAT TRANSFER LABORATORY

Annual Report No. 1
NAS 8-20222

IMPROVED FLUID DYNAMICS SIMILARITY ANALYSIS AND VERIFICATION

June 29, 1965 - June 28, 1966

to

NATIONAL AERONAUTICS AND SPACE ADMINISTRATION
George C. Marshall Space Flight Center
Applied Mechanical Research Branch
Propulsion Division
Propulsion and Vehicle Engineering Laboratory
Huntsville, Alabama

IMPROVED FLUID DYNAMICS SIMILARITY, ANALYSIS AND VERIFICATION

First Annual Report

Period Covered: June 29, 1965 - June 28, 1966

Submitted by

School of Mechanical Engineering
Purdue University
Lafayette, Indiana

Principal Investigators:

E. R. F. Winter and R. J. Schoenhals

to

NATIONAL AERONAUTICS AND SPACE ADMINISTRATION
George C. Marshall Space Flight Center
Applied Mechanical Research Branch
Propulsion Division
Propulsion and Vehicle Engineering Laboratory
Huntsville, Alabama

Contracting Officer's Representative: Hugh M. Campbell

Contract Number: NAS 8-20222
Control Number: DCN 1-5-52-01195-01 (1F) & S1 (1F)

Authors: Roger Griebe
W. J. Leech
Terry Libby
M. A. Ramayya
R. J. Schoenhals
E. R. F. Winter
A. Wong

August 25, 1966

ABSTRACT

This report describes research accomplished from June 29, 1965 to June 28, 1966 under Contract No. NAS 8-20222, Improved Fluid Dynamics Similarity, Analysis and Verification. Results are presented for three major areas of study:

1. Single phase flow during discharge of liquids
2. Two phase flow in the absence of heat transfer
3. Fluid flow and energy transport in a confined liquid subjected to heat transfer

Similarity parameters obtained by means of dimensional analysis are given. Analytical results, incorporating the various physical effects of importance, are presented graphically in terms of the similarity parameters obtained. Experimental data are also presented graphically in order to verify the similarity parameters, to indicate the operating ranges for which these parameters are important, and to evaluate the accuracy of the analytical results.

TABLE OF CONTENTS

LIST OF SYMBOLS

a	Cross sectional area of discharge pipe
a	Width of the heated container
A	Cross-sectional area of discharge tank
A, As,	Cross-sectional area of the heated container
b	Length of the heated container
B	$\frac{C_D \sqrt{g/2}}{\beta}$
c	Specific heat of fluid at T_w
C	Contraction coefficient
C_D	Discharge coefficient
C_D	Dimensionless drag coefficient
C_f	Skin friction coefficient
c_p	Specific heat of liquid
C_v	Velocity coefficient
d	Discharge tube diameter
D	Container diameter
f	Darcy-Wesbach friction factor
F	Froude number
g	Gravitational accelleration
Gr	Grashof number
$\bar{h}$	Film heat transfer coefficient
h	Initial fluid height
h_d	height difference between points 1 and 2

h_e	Entrance head loss
h_f	Frictional head loss
h_f	Specific enthalpy of liquid
h_{fg}	Latent specific heat of vaporization
h_i	Total head loss
H	Initial height of liquid in the discharge tank
H	Total head
H	Height of heated container
H_{sv}	Total suction head above vapor pressure
k	Thermal conductivity of the heated container walk
K	$\frac{3}{4}$ nRT
K	Entrance loss coefficient
L	Discharge tube length
$\dot{m}$	Mass flow rate
m_f	Mass of liquid
m_g	Mass of vapor generated
n	Number of moles
n	Number of data points
P	Heated perimeter
P	Pressure
ΔP	Pressure drop
P_g	Partial pressure of gas
P_ℓ	Local liquid pressure
P_n	Absolute pressure at point n, n = 0, 1, 2, -----
Pr	Prandtl Number
P_v	Vapor pressure

q	Heat transfer
Q	Sum of the squares of the deviation
r	Radius
R	Universal gas constant
Re	Reynolds number
S	$(h + \Delta P/\rho g)^{1/2}$
S	Wetted area of a ship
t	Time
T	Temperature
T_{bi}	Initial temperature of the bulk fluid
T_w	Temperature of the heated walls
v_f	Specific volume of liquid
v_g	Specific volume of vapor
v_o	Velocity at reference o
$\bar{v}_f$	Total Volume of liquid
$\bar{v}_g$	Total volume of vapor
w	Drag on a ship
y	Liquid surface height
$\hat{y}_i$	Value of y at time t_i given by equation (D4)
y_i	Experimental value of y at time t_i
z_o	Liquid heat

α	Thermal diffusivity, $\frac{k}{\rho c}$
α	Surface tension of liquid
β	$\sqrt{\left(\frac{a}{A}\right)^2 - 1}$ geometric parameter
β	ξ_c/ξ relative vapor ratio
β	Coefficient of thermal expansion
Δ	Stratification thickness
ε_i	Deviation of i^{th} data point
θ	Dimensionless time, $\frac{\alpha t}{aH}$
μ	Absolute viscosity
ν	Kinematic viscosity
ξ	Head loss coefficient with cavitation
ξ_c	Head loss coefficient with cavitation
π_n	π - factors (n = 1, 2 -----)
ρ	Density
σ	Cavitation number
σ_d	Desinent cavitation number
σ_H	Thoma's similarity number
σ_i	Incipient cavitation number
τ	Frictional force
ψ	Fineness coefficient

LIST OF FIGURES

INTRODUCTION

Full scale testing of large liquid propellant and oxidizer supply systems can be time consuming, expensive, and in some cases inconvenient. For these reasons it is frequently appropriate that scaled down laboratory models be considered. It might be desirable, for example, to ascertain the performance of a large system in advance of its construction in order to evaluate the soundness of a particular design or to provide concrete evidence of the need for engineering changes if laboratory tests on a model should indicate weaknesses in a tentative design. Where a large scale system has alreay been built, the ability to predict overall performance is not as important. However, in this situation certain unexpected features of operational behavior in the large system may become evident. If they do, then further study may be required to establish confidence in the existing system or to determine the necessary changes which will eliminate any of these features which are found to be undesirable. In cases such as this it may be more convenient, realistic, and economical to simulate the actual system with a laboratory apparatus of smaller size. There are some occasions when only a portion of a system requires intensive study, and a scaled down laboratory model of an individual system component may allow

large numbers of experimental measurements to be obtained rapidly and easily.

In order to exactly duplicate the behavior of a large system with a corresponding laboratory model, it is required that complete similarity be achieved. This can sometimes be accomplished if fairly simple processes are involved. However, the task of attaining complete similarity becomes increasingly difficult when a number of physical phenomena all occur simultaneously and interact with each other within a single system. In the less complex situations it is important that the simulation be made essentially exact in order to maximize the usefulness of the laboratory data. For the more complex cases, where exact simulation may not be attainable, it is important to ascertain the limitations of the laboratory simulation and to formulate a laboratory program which minimizes these limitations as much as possible.

It is clear that the procedures outlined above can be carried out effectively only if the similarity parameters have been obtained and if the relationships between them have been roughly established, perhaps by means of approximate analytical techniques or from previously obtained experimental measurements. The second point is very important if exact similarity cannot be achieved. In this situation similarity should be maintained with respect to those parameters which are dominant, and should be sacrificed only with respect to those parameters which are known to have a minor effect within the range of operation considered. The

present investigation was undertaken in order to provide:

1. A better understanding of the similarity relationships associated with some of the fluid dynamics phenomena occuring in propellant and oxidizer supply systems.
2. A basis for obtaining a given amount of needed information from a minimum of similarity experiments conducted with scaled laboratory models.
3. A basis for obtaining maximum information from a given number of similarity experiments conducted with scaled laboratory models.
4. A basis for suggesting improved techniques that may facilitate future similarity investigations whose goals are related to any of the three items above.

Three major areas were selected for individual study in the present investigation, and the results are reported herein. These areas are briefly described as:

1. Single phase flow during discharge of liquids.
2. Two phase flow in the absence of heat transfer.
3. Fluid flow and energy transport in a confined liquid subjected to heat transfer.

In each of these areas similarity parameters were obtained by means of dimensional analysis. Analytical results, based on approximate physical models, were derived and the solutions were expressed in terms of the similarity parameters obtained. Finally, experimental measurements were made in order to verify the significance and importance of the similarity parameters obtained, and to establish the validity and limitations associated with the approximate analytical solutions.

SIMILARITY STUDIES OF GRAVITY AND PRESSURE DRIVEN LIQUID DISCHARGE

In this section a study of gravity and pressure driven discharge of liquids is described. A typical situation of interest is illustrated in FIG. 1. Attention is directed toward the mass flow rate of the discharging liquid ($\dot{m}$) and its dependence on time, on the geometry and size of the system, the liquid properties, pressure drop, and gravitational field strength. The liquid is considered to be initially at rest before the discharge process is started.

The study was divided into three separate phases. The first phase involved application of dimensional analysis for the purpose of determining the pertinent dimensionless parameters describing systems of the type shown in FIG. 1. In the second phase, analytical results based on various physical models were obtained. The simplest of these models yielded concise expressions which were readily evaluated numerically, but accuracy was sacrificed since not all of the physical effects were properly accounted for. The more complex physical models were more accurate, but they also involved more lengthy analyses. For these cases, digital computer calculations were carried out in order to obtain numerical results. In the third phase of the study, experimental measurements were made in order to verify the

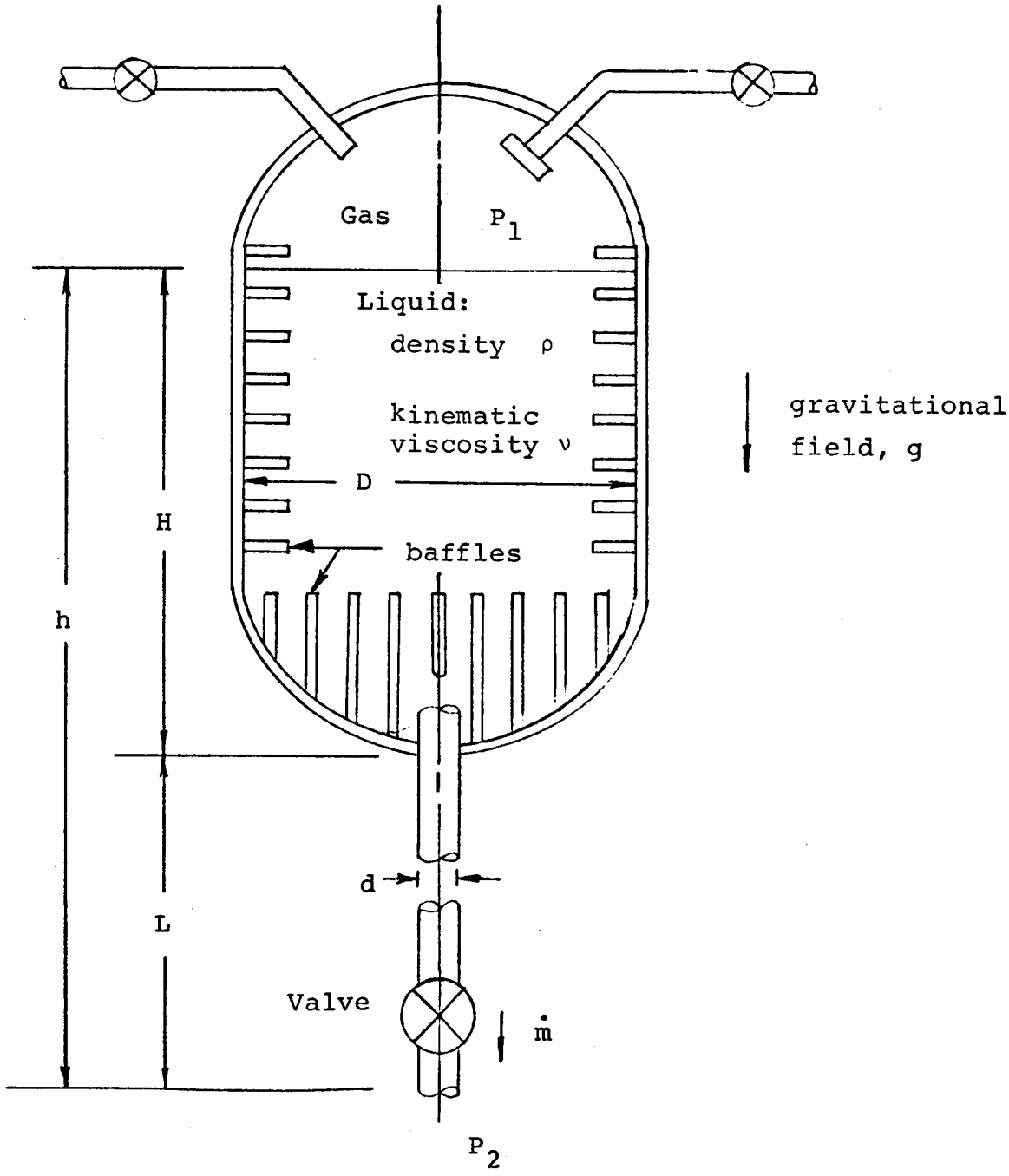

FIG. 1 ILLUSTRATION OF A LIQUID DISCHARGE SYSTEM

significance and importance of the dimensionless parameters obtained in the first phase, and to establish the validity and limitations associated with the analytical results obtained in the second phase. To facilitate the analytical and experimental portions of this study, a more simplified geometry (FIG. 2) was used.

In the discussion which follows a survey of related research is summarized first, and then a description of the important physical effects associated with the discharge process is given. This is followed by the details of the three study phases described above and appropriate comparisons of the results obtained.

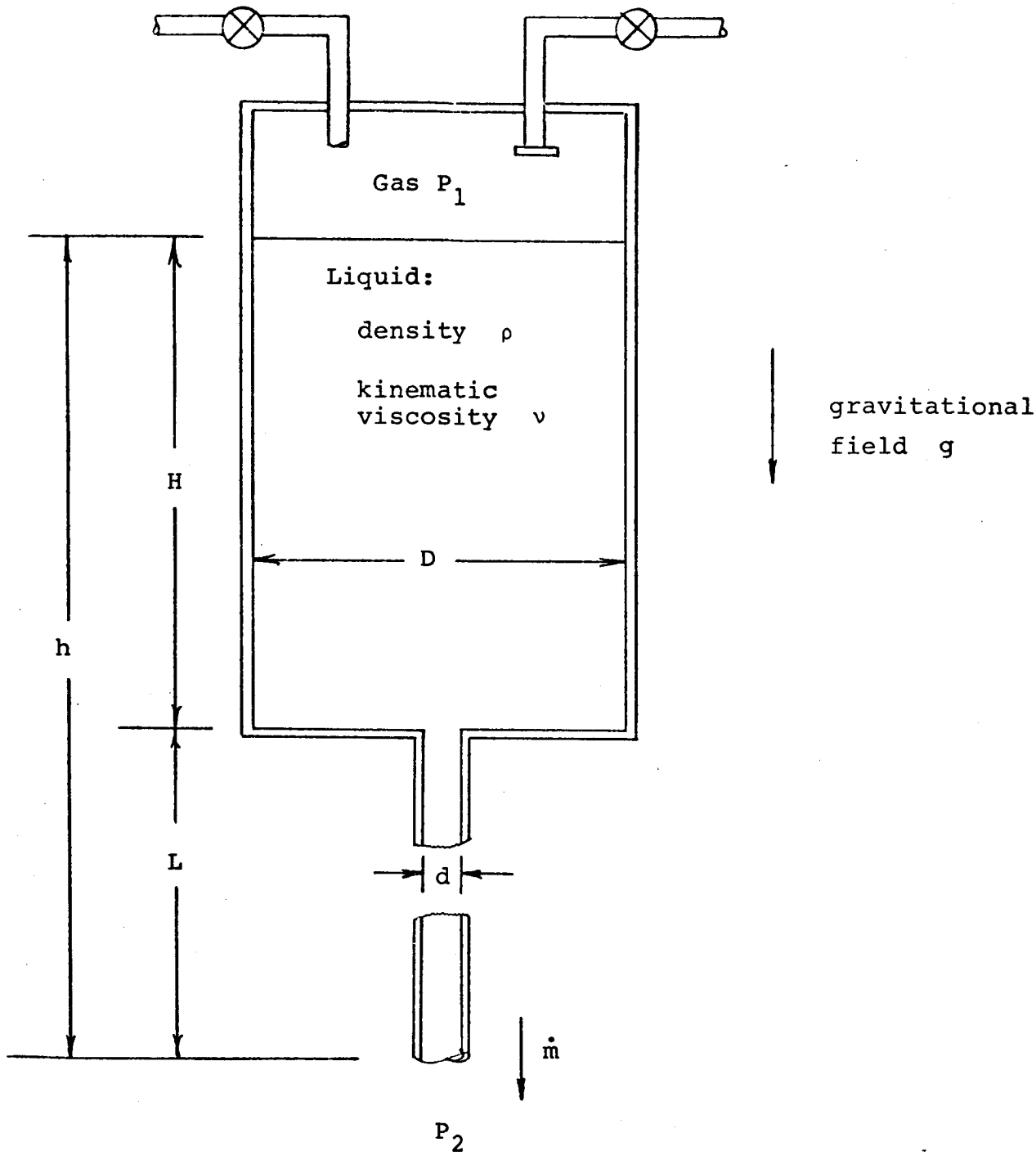

FIG. 2 SIMPLIFIED GEOMETRY USED FOR ANALYTICAL AND EXPERIMENTAL STUDIES

SURVEY OF LITERATURE

As mentioned earlier, one aim of the present research is to investigate the possibility of predicting propellant discharge rates for prototype rockets from tests on scaled down models. The performance of a liquid fuel rocket depends, among other things, on the rate of supply of fuel and oxygen to the rocket engine. Scaling of rocket engines has been discussed by Penner (Ref. 1), who indicated that scaling of chemical reactors with complete similarity is not possible. For the liquid fuel rocket engines, scaling with loss of geometric and dynamic similarity were considered. For small scale units, Penner's analysis suggests a reasonable approach to the interpretation of experimental data. It was concluded that once the relationship between the various parameters has been established from a large number of experiments, rational scaling to larger units should be possible. The present investigation is mainly limited to a consideration of the supply rates of fuel or oxidizer to the engine.

The discharge of containers through ofifices and pipes has been studied for many years by hydraulic engineers (Ref. 2, 3), whose main aim was the design of water supply tanks. Pure gravity discharge is encountered in such designs and Bernoulli's Equation (Ref. 4), with emperical corrections

for the viscous and geometric effects (Ref. 5), yields reasonably accurate results for the times and rates of discharge. So, many of the modeling techniques developed by hydraulic engineers (Ref. 6), were concerned with river dams, spillways, open channel flows, etc, and little attention has been paid to the problem of modeling rapid discharge of containers.

One of the most powerful methods for dealing with such problems is Dimensional Analysis. This technique yields the similarity parameters involved, through an application of Buckingham's π - Theorem (Ref. 7), in that it groups the pertinent variables into appropriate dimensionless parameters. Though dimensional analysis gives the dimensionless parameters involved, it does not give the form of dependence among these parameters. Neither can it predict which of the parameters are significant and which of them can be neglected. Sometimes it may appear that conflicting requirements must be satisfied for scaling, from which it may be prematurely concluded that no scaling is possible at all. For example, in the case of ship motion it turns out (Ref. 8) that for geometrically similar hull shapes, the dimensionless drag coefficient is giver by

$$C_D = \frac{W}{\rho S V^2} = f(\psi, F, Re).$$

where ψ = Fineness coefficient

F = Froude Number for the flow = $\frac{V^2}{gL}$

Re = Reynolds Number = $\frac{\rho VL}{\mu}$

This relation implies that if ψ, F, R are the same for two geometrically similar shapes, C_D must be the same. If the same fluid is used, to keep $F = \frac{V^2}{gL}$ constant, the velocity must decrease with decrease in model size, whereas to keep $R = \frac{\rho VL}{\mu}$ the same, V must increase with decreasing model size. However, the practical possibility of scaling tests for ship hulls stems from the fact that the drag can be separated into two parts, one depending on the Reynolds Number and the other on the fineness coefficient and the Froude Number. Hence, dimensional analysis must be supplemented by experiment, experience, and mathematical analysis wherever possible.

There is another problem. Sometimes it is very difficult to match one of the non-dimensional parameters. A case in point is the Reynolds Number in the wind tunnel testings of aircraft models (Ref. 9, 10). In such instances, the models are tested at a Reynolds Number which is different from the full scale one, and the results are extrapolated using some known behaviour. Flanigan and Putnam (Ref. 11) discuss the principles of similitude in fluid flow and classify modeling programs into four general catagories as

(a) diagnostic;

(b) predictive;

(c) developmental

(d) basic.

As was suggested in their paper, the application of modeling to practical problems usually involves more than one category. The problem of scaling and testing of distorted models for valid scale model work was discussed by Ezra (Ref. 12). Various methods for distinguishing the independent and dependent similarity parameters and finding the relationships between them were suggested there Methods for scale model work, even when one or more independent parameters cannot be scaled and when there is no knowledge of mathematical relationships between the independent and dependent variables, were given by Ezra. In short the problem treated in this report involves a twofold attempt to:

(i) match the relevant non-dimensional parameters for scaled down and full scale rocket propellant containers so that the non-dimensional mass flow coefficient remains the same, and

(ii) predict its variation with each of the other parameters.

The problem at hand is that of modeling the discharge of a cryogenic fluid. In the most general terms, two phase

flow of a stratified fluid, with cavitation and heat transfer, through multiple outlets from a single tank is to be considered. In addition, the effect of varying gravitational field is to be considered, though this may be hard to simulate. The processes involved are very complicated, with numerous effects to be taken into account. For instance, Roudebush and Mandell (Ref. 13) consider pressurization of a liquid hydrogen tank during outflow. It can be easily seen from the assumptions, the final equation obtained and the parametric analysis carried out in that paper, how complicated an apparently simple problem of pressurizing a container becomes when dealing with cryogenic fluids. The dimensional analysis for this problem, carried out by Nein and Thompson (Ref. 14) indicates that the dimensionless pressurant mass is dependent on at least 9 π - factors. Clark (Ref. 15) has reviewed the literature regarding the various problems (pressurization, stratification, and interfacial phenomena) involved with large rocket propellant tank systems. Fischer (Ref. 16) presented the conditions for similarity for two phase flows with simultaneous heat transfer. He concludes that for two two-phase flows to be similar not only the characteristic Reynolds, Euler and Froude numbers for the individual phases must be the same in the two flows, but also the density and the dynamic viscosity ratios for the two phases in both flows must be the same.

In summary, it can be said that although there have been numerous investigations with regard to individual phenomena, further attention is needed with respect to the modeling of rapid discharge of a cryogenic fluid from a container. This is the aim of the present investigation.

PHYSICAL EFFECTS

FIGURES 1 and 2 illustrate systems studied in this research. Forces act on the fluid to produce fluid acceleration during the discharge process. The various kinds of forces, and the corresponding two types of fluid acceleration that result from the action of these forces, are indicated below.

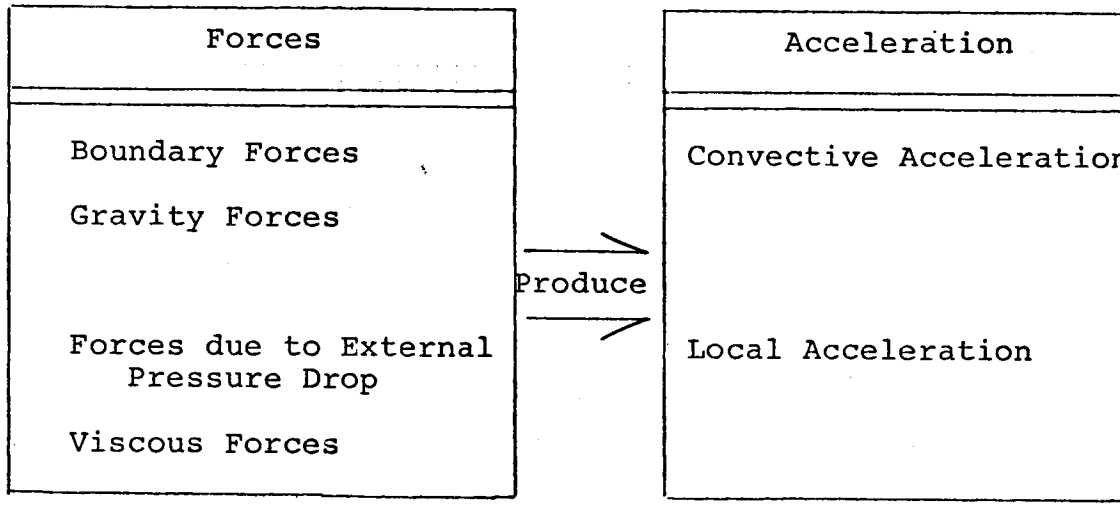

The boundary forces (forces perpendicular to the walls) are sufficient to prevent the fluid from moving normal to the boundaries, the structure being considered rigid. Downward gravity and the external pressure drop (from the top to the bottom of the fluid column) contribute to downward acceleration of the fluid column, while viscous forces impede this acceleration. Convective acceleration is associated with

the change in velocity of a fluid particle as it travels from a region of one velocity into a region having a different velocity. Thus, convective acceleration can be produced even if the flow is steady. Local acceleration of the fluid is associated with the time varying, or transient, condition of the flow. This acceleration, at any point in the system, is equal to the time rate of change of velocity at that point. The two acceleration contributions, when added together at any particular point in the system, give the actual acceleration of the fluid particle passing through that point at a particular instant of time. In each of the analyses which follow, the physical effects accounted for are indicated, and errors produced by omitting certain physical effects are evaluated.

In general, the pressure drop across the system, $(P_1 - P_2)$, may possibly vary with time. The effective gravitational field, g, may also vary in accordance with changes in vehicle thrust. If local pressures are low enough cavitation may occur. Surface tension effects may conceivably be important if the system dimensions are small enough. Also, in practical applications the valve setting may vary with time. This, however, amounts to a time varying change in the system geometry and is beyond the scope of this report. In order to keep the discussion brief, ΔP and g are taken as constants. Additionally, surface tension, phenomena associated with cavitation, and variable valve settings are omitted.

DIMENSIONAL ANALYSIS

In this section dimensional analysis results are given along with discussion to illustrate how these results are related to the physical effects discussed in the previous section. The systems illustrated in FIGS. 1 and 2 are considered. For all geometrically similar systems only one length is needed in order to specify all other length dimensions for a particular enclosing container. For example, D/d and L/d are fixed constants for geometrically similar containers, and h/D is also a constant for any class of similarly shaped containers having similar liquid geometries at the start of the process. Thus, for all systems having a prescribed initial geometry, for both the container and the liquid, it is only necessary to specify one length parameter in order to fix the size of the system and all of its dimensions. For this situation, the mass discharge rate (FIG. 1 or FIG. 2) is related to the fluid properties, the system dimensions, the effective gravitational field, and the time elapsed from initiation of discharge. Thus,

$$\dot{m} = f(\rho, g, \Delta P, \nu, h, t). \qquad (1)$$

The variables are listed below, along with their dimensions in terms of mass (M), length (L), and time (T).

Symbol	Parameter	Dimensions
$\dot{m}$	mass flow rate	MT^{-1}
ρ	density	ML^{-3}
g	gravitational field	LT^{-2}
ΔP	pressure drop	$ML^{-1}T^{-2}$
ν	kinematic viscosity	$L^{2}T^{-1}$
h	initial fluid height	L
t	time	T

Use of Buckingham's theorem and the repeated variable technique (see Appendix A) results in the following dimensionless parameters.

$\frac{\dot{m}}{\rho\left(\frac{\pi d^2}{4}\right)\sqrt{2gh}}$, dimensionless mass flow rate

$\frac{t}{\sqrt{2h/g}}$, dimensionless time

$\frac{\Delta P/\rho g}{h}$, ratio of pressure head to initial hydrostatic head

$\frac{d\sqrt{2gh}}{\nu}$, a characteristic Reynolds number

Since the discharge diameter d has a fixed value relative to h for all geometrically similar systems, h has been arbitrarily replaced by d in those instances where its use produces greater physical insight, but this does not represent an increase in the number of parameters beyond those given in equation (1). Along the same lines, numerical values have also been inserted for the purpose of attaching more direct physical meanings to some of the quantities contained in the dimensionless parameters given above. $(\pi d^2/4)$ is the discharge area, $\sqrt{2gh}$ is the velocity attained by an object initially at rest which falls freely through a distance h under the influence of gravitational field g, and $\sqrt{2h/g}$ is the time of free fall. The resulting relation among the dimensionless quantities is written as

$$\frac{\dot{m}}{\rho\left(\frac{\pi d^2}{4}\right)\sqrt{2gh}} = F\left[\frac{t}{\sqrt{2h/g}}, \frac{\Delta P/\rho g}{h}, \frac{d\sqrt{2gh}}{\nu}\right] \qquad (2a)$$

Consideration of systems of the type indicated in FIG. 2 having different geometries (as specified by various values of d, D, and L for a given value of h) gives three additional length ratios. Equation (2a) is correspondingly modified to account for these geometrical changes and is rewritten as

$$\frac{\dot{m}}{\rho\left(\frac{\pi d^2}{4}\right)\sqrt{2gh}} = F\left[\frac{t}{\sqrt{2h/g}}, \frac{\Delta P/\rho g}{h}, \frac{d\sqrt{2gh}}{\nu}, \frac{h}{d}, \frac{D}{d}, \frac{L}{d}\right] \qquad (2b)$$

A procedure for obtaining this more complete result is given in Appendix A. Equation (2a) represents the results for a class of systems all characterized by similar geometry as specified by a fixed set of values for h/d, D/d, and L/d.

In the experimental portion of the investigation it was found that the height of the liquid surface could be measured more conveniently than the mass flow rate. It is therefore appropriate to consider the dimensionless ratios associated with the time variation of the liquid surface height, y. Application of the dimensional analysis procedure indicated above gives

$$\frac{y}{h} = G\left[\frac{t}{\sqrt{2h/g}}, \frac{\Delta P/\rho g}{h}, \frac{d\sqrt{2gh}}{\nu}\right] \tag{3a}$$

and

$$\frac{y}{h} = G\left[\frac{t}{2h/g}, \frac{\Delta P/\rho g}{h}, \frac{d\sqrt{2gh}}{\nu}, \frac{h}{d}, \frac{D}{d}, \frac{L}{d}\right] \tag{3b}$$

as alternate expressions for equations (2a) and (2b) respectively.

ANALYSIS

In this section various analyses are carried out which vary in complexity, in the geometry associated with the system being studied, and in the physical effects which are accounted for. The liquid is considered to be incompressible for all of the cases studied. For each situation the simplest possible analysis is carried out first, and the additional complexities are subsequently added so that the relative magnitude of each physical effect can be illustrated for various operating ranges.

Liquid Discharge Through an Opening

Consider the system shown in Fig. 3 which represents a special case of that shown in Fig. 2, that is, the case of $L/d = 0$. For the initial study of this system the pressure drop, $(P_1 - P_2)$, is omitted, while viscous and local acceleration effects are neglected. The physical effects accounted for are indicated below.

Forces		Fluid Acceleration	
[X]	Boundary Forces	[ ]	Local Acceleration
[X]	Gravity Forces		
[ ]	Forces due to External Pressure Drop	[X]	Convective Acceleration
[ ]	Viscous Forces		

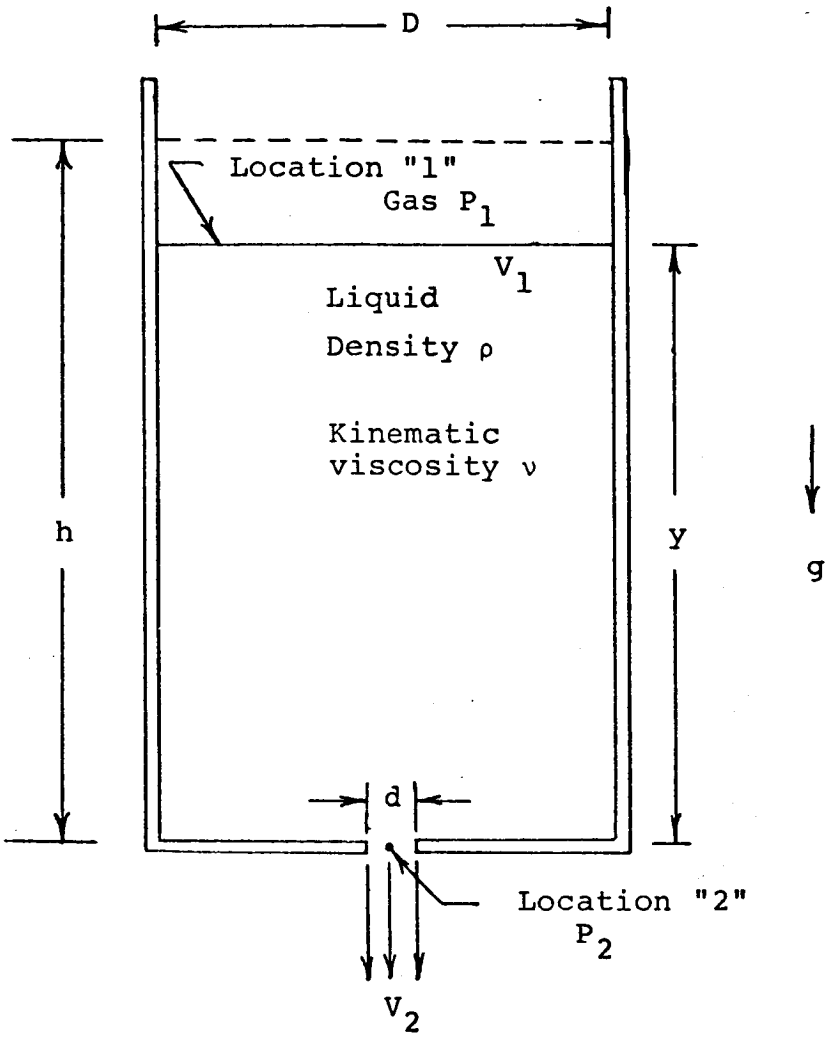

FIG. 3 GEOMETRY AND COORDINATE SYSTEM FOR ANALYSIS OF LIQUID DISCHARGE THROUGH AN OPENING.

The analysis associated with the above conditions is based on quasi - steady flow (since local acceleration is neglected) in the absence of viscous effects for zero pressure drop.

It is assumed that the velocity of the fluid is constant over any cross-section. Also, the surface of the fluid is assumed to be horizontal at all times. The discharge mass flow rate $\dot{m}$ is given by $\rho a V_2$, and continuity requires that

$$\rho A V_1 = \rho a V_2 \tag{4}$$

where V_1 and V_2 are the fluid velocities at locations 1 and 2 respectively. For the conditions indicated in the table above, Bernoulli's equation applies. Thus,

$$P_1 + \rho\, g\, y + \frac{1}{2}\rho\, V_1^2 = P_2 + \frac{1}{2}\rho\, V_2^2 \tag{5}$$

For the coordinate system shown, $V_1 = -\frac{dy}{dt}$ and $V_2 = -\frac{A}{a}\frac{dy}{dt}$. Since $P_1 = P_2$, equation (5) becomes

$$\rho\, g\, y + \frac{1}{2}\rho\left(-\frac{dy}{dt}\right)^2 = \frac{1}{2}\rho\left(-\frac{A}{a}\frac{dy}{dt}\right)^2 \tag{6}$$

Solving for dy/dt gives

$$\frac{dy}{dt} = -\frac{1}{\beta}\sqrt{2\, g\, y} \tag{7}$$

where $\beta^2 = \left[\left(\frac{A}{a}\right)^2 - 1\right]$, a parameter depending only on the geometry of the system. Note that the negative sign appears because y decreases as t increases. Integration of equation (7) yields

$$\int_0^t dt = -\frac{\beta}{\sqrt{2\,g}} \int_h^y \frac{dy}{\sqrt{y}} \,. \tag{8}$$

Finally,

$$t = \beta\left[\sqrt{\frac{2\,h}{g}} - \sqrt{\frac{2\,y}{g}}\right] \tag{9}$$

which relates the instantaneous height of liquid to time after initiation of discharge. Equation (9) can be re-written as

$$\frac{y}{h} = 1 - \left(\frac{1}{\beta}\right)\left(\frac{t}{\sqrt{2h/g}}\right) \tag{10}$$

which shows that the instantaneous height is related to time parabolically. Also, this result implies that the total discharge time is $\left(\beta\sqrt{\frac{2h}{g}}\right)$. These results are represented graphically in FIG. 4. Notice that equation (10) contains the two dimensionless parameters predicted by equation (3a), y/h and $\frac{t}{\sqrt{2h/g}}$. The two remaining parameters in equation (3a) do not appear in equation (10) since effects of pressure drop and liquid viscosity have not been considered in the present analysis.

The instantaneous rate of discharge is $\rho A \left(-\frac{dy}{dt}\right)$ where $\frac{dy}{dt}$ is given by equation (7). Thus,

$$\dot{m} = \frac{\rho\, A}{\beta}\ \sqrt{2\,g\,y} \tag{11}$$

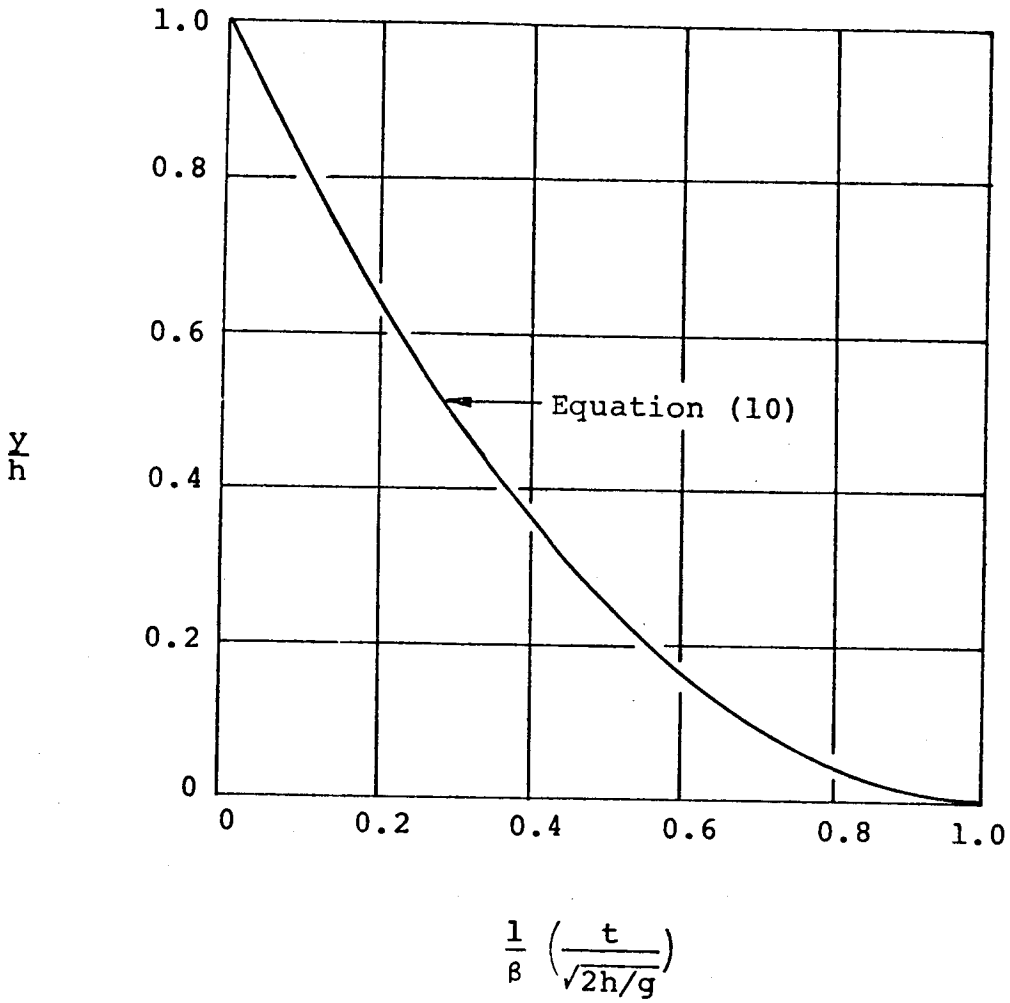

FIG. 4 VARIATION OF LIQUID HEIGHT WITH TIME FROM ANALYSIS BASED ON QUASI-STEADY FLOW IN THE ABSENCE OF VISCOUS EFFECTS FOR ZERO PRESSURE DROP

But from equation (9),

$$\sqrt{2gy} = \sqrt{2gh} - \frac{gt}{\beta} \tag{12}$$

Therefore, equation (11) becomes

$$\dot{m} = \frac{\rho A}{\beta}\left[\sqrt{2gh} - \frac{gt}{\beta}\right]. \tag{13}$$

Rearrangement of this equation provides the result in dimensionless form, which is

$$\sqrt{1 - \left(\frac{a}{A}\right)^2}\left[\frac{\dot{m}}{\rho\left(\frac{\pi d^2}{4}\right)\sqrt{2gh}}\right] = 1 - \frac{1}{\beta}\left(\frac{t}{\sqrt{2h/g}}\right). \tag{14}$$

For systems having fixed geometry, $\sqrt{1 - (a/A)^2}$ and β both have constant values so that $\left[\frac{\dot{m}}{\rho\left(\frac{\pi d^2}{4}\right)\sqrt{2gh}}\right]$ is purely a function of $\left[\frac{t}{\sqrt{2h/g}}\right]$ according to equation (14). This is in agreement with the dimensional analysis result given in equation (2a). Equation (14) does not contain $\frac{\Delta P/\rho g}{h}$ and $\frac{d\sqrt{2gh}}{\nu}$ because the preceding analysis was carried out only for the case in which $\Delta P = 0$, while viscous effects were omitted.

A plot of equation (14) is given in FIG. 5 which shows that the predicted discharge rate decreases linearly with time. This decrease with time is associated with the drop-off in the hydrostatic head y, (which corresponds to the gravitational driving potential) as liquid is removed from the container.

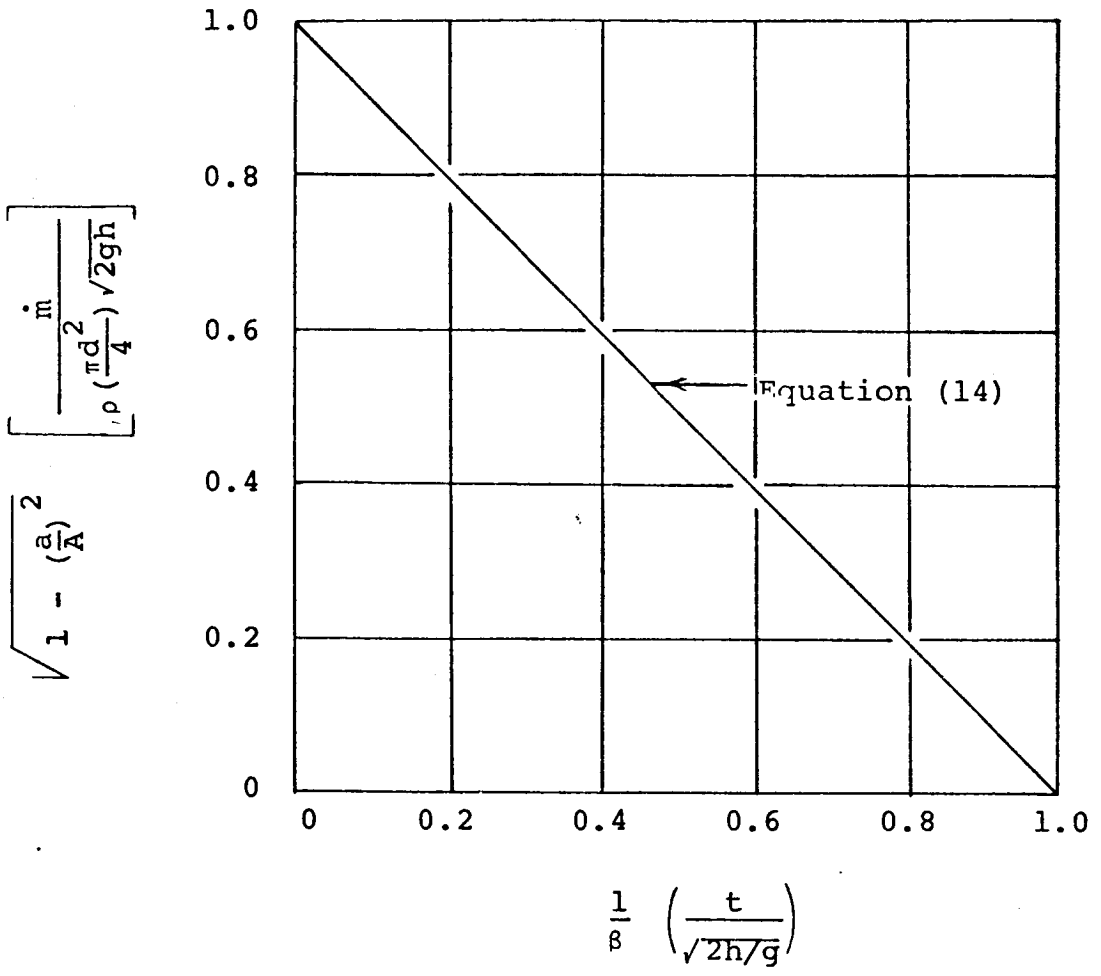

FIG. 5 VARIATION OF MASS FLOW RATE WITH TIME FROM ANALYSIS BASED ON QUASI-STEADY FLOW IN THE ABSENCE OF VISCOUS EFFECTS FOR ZERO PRESSURE DROP

A simplification of equation (14) is possible when $a/A \ll 1$. For this situation $\beta = \sqrt{(A/a)^2 - 1} \approx \frac{A}{a}$, and equation (14) reduces to

$$\frac{\dot{m}}{\rho\left(\frac{\pi d^2}{4}\right)\sqrt{2gh}} \approx 1 - \left(\frac{a}{A}\right)\left(\frac{t}{\sqrt{2h/g}}\right). \qquad (15)$$

The process studied and described in this report involves the behavior of a liquid, initially at rest, when it is discharged from a container. This implies that the initial flow rate (at t = 0) must be zero. Although the actual flow rate may in reality rise very rapidly with itme, the inertia of the fluid prevents acceleration to the maximum flow rate in zero time (as indicated in FIG. 5). On this basis the model analyzed in this section is physically unacceptable, at least for small values of time. During this initial time period local acceleration effects, not considered in the above analysis, are appreciable when the fluid accelerates from rest. An analysis which considers these aspects is given in Appendix B. The physical effects accounted for are indicated below.

Forces		Fluid Acceleration	
[X]	Boundary Forces	[X]	Local Acceleration
[X]	Gravity Forces		
[ ]	Forces due to External Pressure Drop	[X]	Convective Acceleration
[ ]	Viscous Forces		

The above description includes the inertia of the fluid as associated with the time varying, or transient, condition of the flow. The corresponding analysis (Appendix B) is based on transient flow in the absence of viscous effects for zero pressure drop. The results are shown in FIG. 6 and 7. The fluid is at rest initially, and all of the curves exhibit a zero discharge velocity and mass flow rate at $t = 0$. For small discharge openings ($a << A$ and $\beta >> 1$) the flow accelerates rapidly, with respect to the total discharge time, and the system behavior, after the initial brief period of acceleration, closely approximates that predicted previously (FIG. 4 and 5). For larger discharge openings the flow is considerably retarded over relatively longer times due to the inertia of the fluid during its initial period of acceleration. However, the predicted total discharge times are, for all practical purposes, fairly independent of β except in the range where β decreases to values smaller than 2. Even though the fluid inertia retards the flow initially for these situations, it also has the effect of maintaining the flow rate at higher values during the deceleration period so that the overall discharge time is almost unaffected.

FIGURES 6 and 7 can be used to ascertain the range of usefulness of the results given in FIG. 4 and 5, which do not account for local acceleration effects. For many typical situations (where $\beta >> 1$) predictions based on the quasi-steady

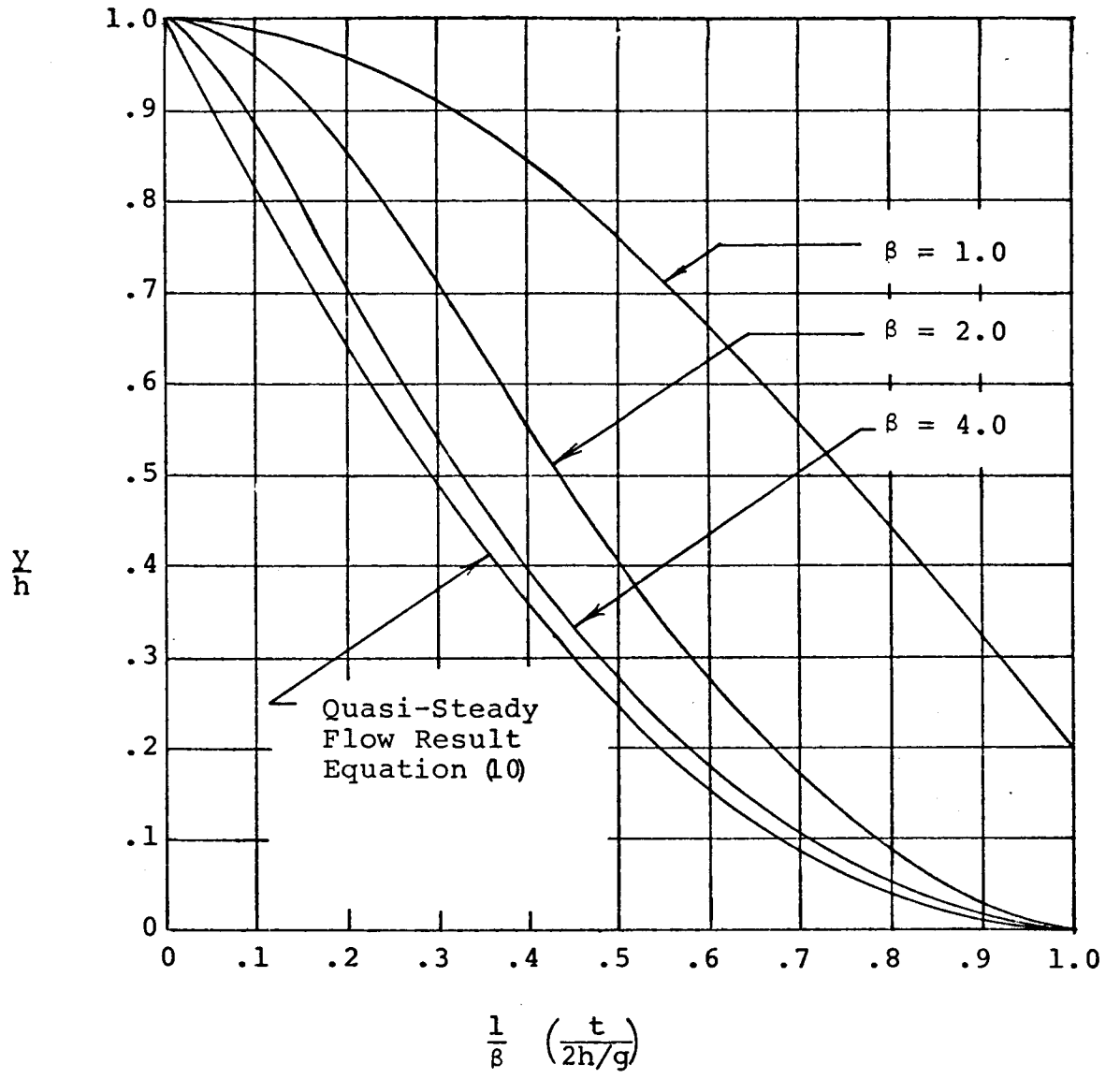

FIG. 6 VARIATION OF LIQUID HEIGHT WITH TIME FROM ANALYSIS BASED ON TRANSIENT FLOW IN THE ABSENCE OF VISCOUS EFFECTS FOR ZERO PRESSURE DROP

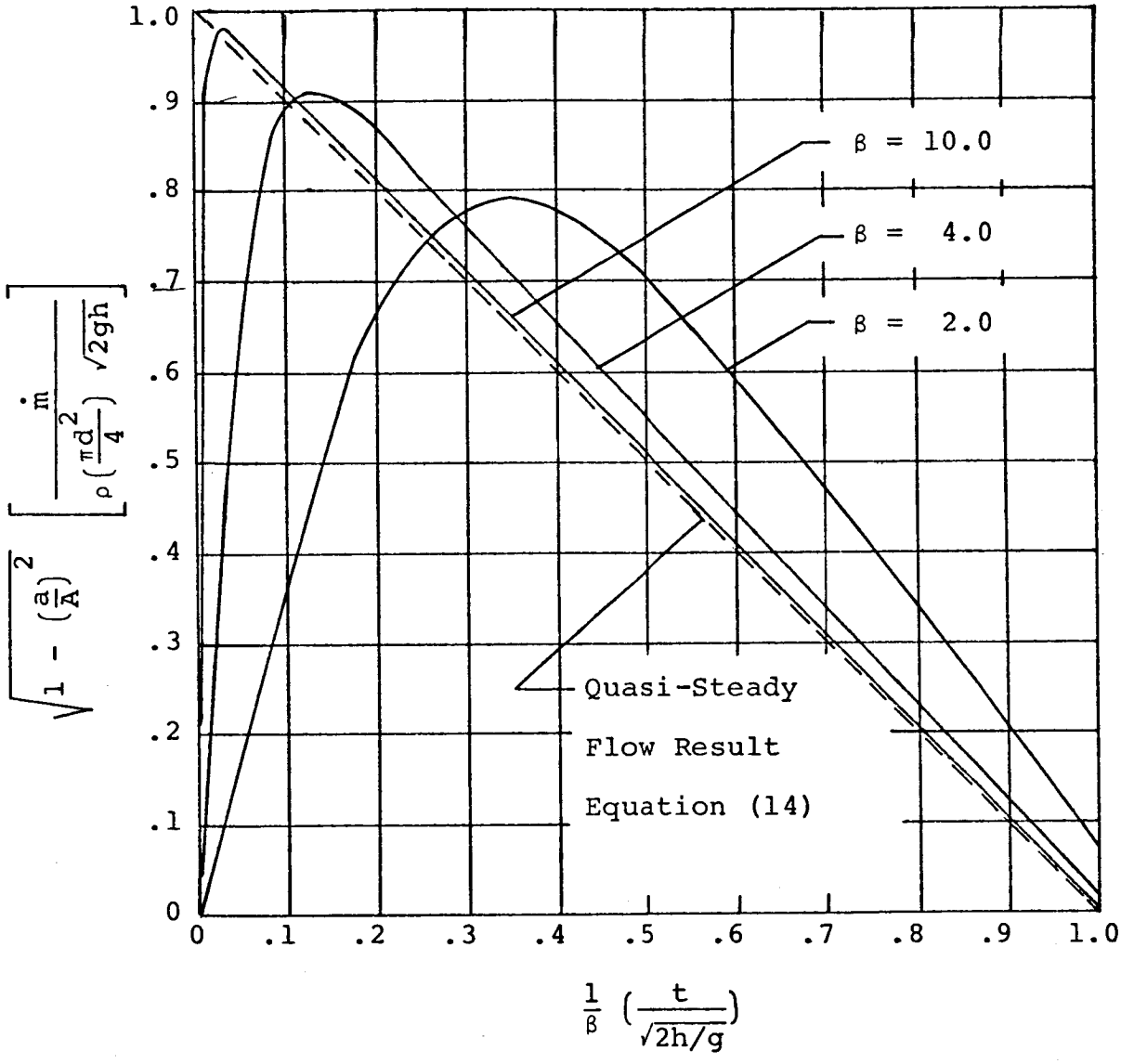

FIG. 7 VARIATION OF MASS FLOW RATE WITH TIME FROM ANALYSIS BASED ON TRANSIENT FLOW IN THE ABSENCE OF VISCOUS EFFECTS FOR ZERO PRESSURE DROP

flow model (FIG. 4 and 5) are quite adequate for engineering purposes. FIGURES 6 and 7 show that although the inertia effect tends to retard the discharge initially, there is very little overall effect on the height versus time curve or the total discharge time unless β is small, that is, unless the discharge area, a, is of the same order of magnitude as the container area A.

Now that the effect of fluid local acceleration has been evaluated for $\Delta P = 0$, it is appropriate to study the discharge process under the influence of a pressure difference, ΔP, which is not zero. In order to isolate the qualitative effect of such a pressure difference, and to keep the analysis simple, both viscous and local acceleration effects are ignored. The latter implies that the results will not be accurate for very small time values and also that β must be somewhat larger than one for the results to be valid physically over most of the transient period (see FIG. 6 and 7). The effects which are considered are summarized below.

Forces		Fluid Acceleration	
[X]	Boundary Forces	[ ]	Local Acceleration
[X]	Gravity Forces		
[X]	Forces due to External Pressure Drop	[X]	Convective Acceleration
[ ]	Viscous Forces		

For the conditions indicated above equations (4) and (5) apply, but in this case P_1 and P_2 are not equal. Therefore, equation (6) is corrected to include ΔP, and the procedure indicated in equations (7) through (14), modified to include the ΔP term, yields

$$\frac{y}{h} = 1 - 2\sqrt{1 + \frac{\Delta P/\rho g}{h}} \cdot \left(\frac{1}{\beta} \cdot \frac{t}{\sqrt{2h/g}}\right) + \left(\frac{1}{\beta} \cdot \frac{t}{\sqrt{2h/g}}\right)^2 \qquad (15)$$

$$\sqrt{1 - (a/A)^2}\left[\frac{\dot{m}}{\rho\left(\frac{\pi d^2}{4}\right)\sqrt{2gh}}\right] = \sqrt{1 + \frac{\Delta P/\rho g}{h}} - \left(\frac{1}{\beta}\frac{t}{\sqrt{2h/g}}\right) \qquad (16)$$

Notice that equations (15) and (16) are in agreement with the dimensional analysis results given in equations (2a) and (3a) respectively, with three of the four dimensionless groups appearing explicitly in each of the analytical expressions above. Equations (15) and (16) do not contain $\frac{d\sqrt{2gh}}{\nu}$ because the preceding analysis does not account for viscous effects. The two quantities, $\sqrt{1 - (a/A)^2}$ and β, which appear have fixed numerical values for any particular geometry.

The results given by equations (15) and (16) are illustrated in FIG. 8 and 9 along with those given previously in FIG. 4 and 5 for the case of $\frac{\Delta P/\rho g}{h} = 0$. The predicted liquid height still decreases parabolically with time, but at a faster rate than that which occurs in the absence of a pressure drop. The total discharge time is correspondingly

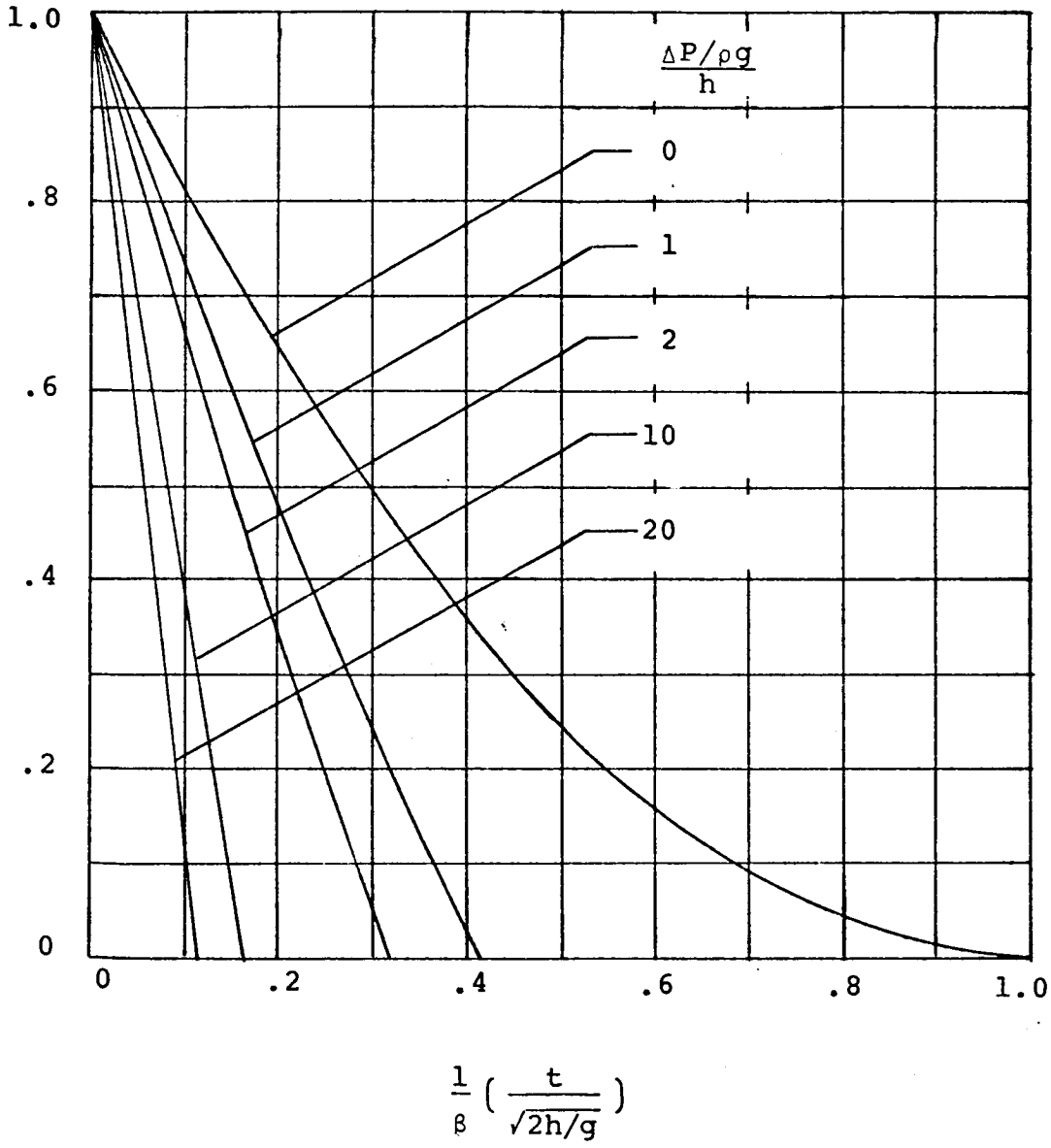

FIG. 8 VARIATION OF LIQUID HEIGHT WITH TIME FROM ANALYSIS BASED ON QUASI-STEADY FLOW IN THE ABSENCE OF VISCOUS EFFECTS FOR NON-ZERO PRESSURE DROP

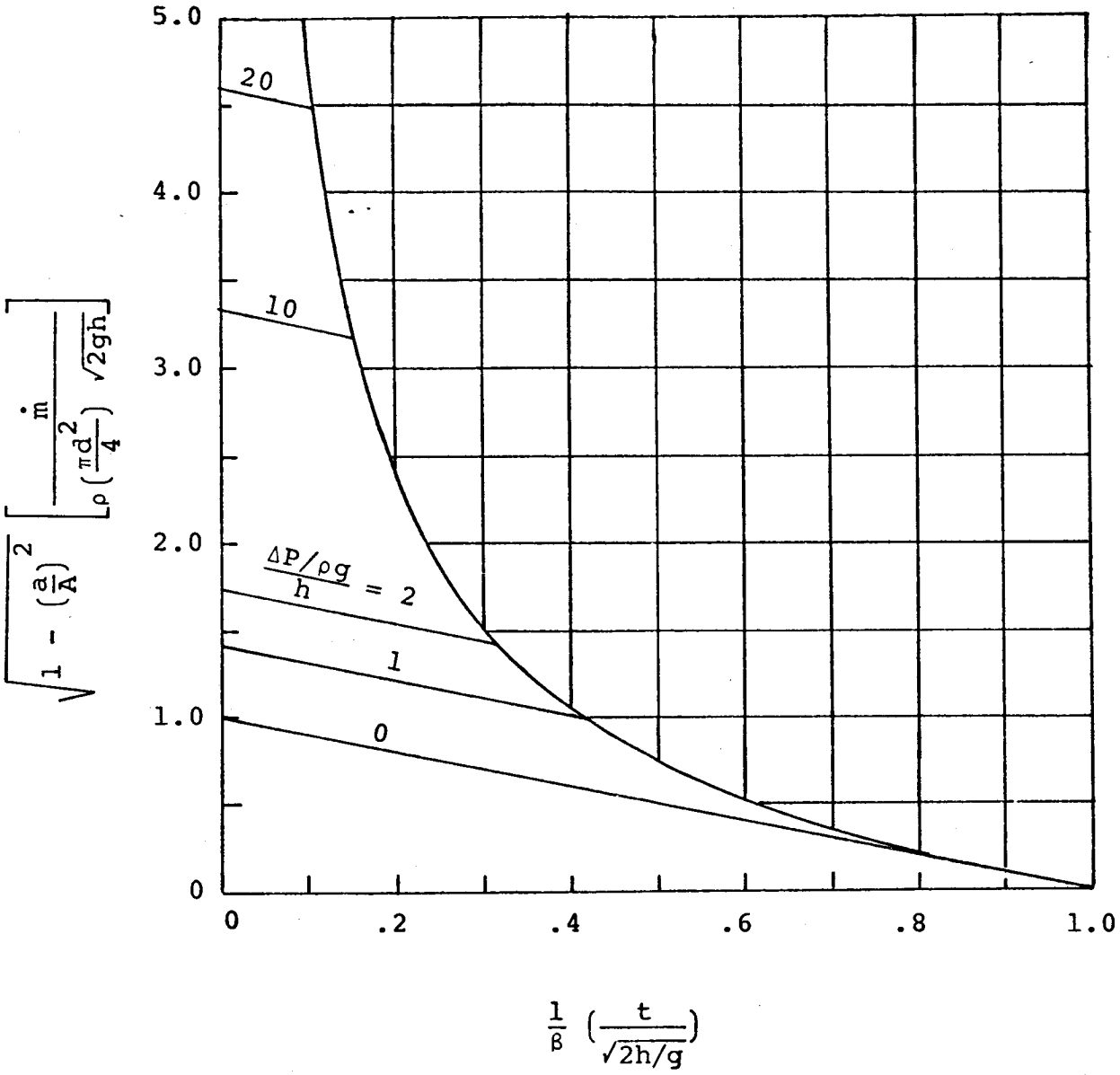

FIG. 9 VARIATION OF MASS FLOW RATE WITH TIME FROM ANALYSIS BASED ON QUASI-STEADY FLOW IN THE ABSENCE OF VISCOUS EFFECTS FOR NON-ZERO PRESSURE DROP

reduced. The flow rate still decreases linearly with time due to the dropoff in the hydrostatic head y (gravitational driving potential) as liquid is removed from the container.

In each of the analyses considered thus far viscous effects have been neglected. Also, it has been assumed that the streamlines are all perpendicular to the cross-sectional area at the location of the opening (FIG. 10). Under certain conditions, which depend, in general, on geometry and on a Reynolds number associated with the flow, the discharge stream may contract to a smaller diameter as shown in FIG. 11. For this situation the streamlines at the discharge opening are not all perpendicular to the cross-sectional area of the opening. At the location where the streamlines do become perpendicular to the cross section, the area of the stream is somewhat reduced. Both viscous effects (FIG. 10 and 11) and the contraction effects (FIG. 11) tend to retard the flow. They can be accounted for in a conventional manner (Ref. 4) and are now superimposed upon the treatment yielding the results summarized in the previous paragraph. The corresponding physical model is based on the description below.

Forces		Fluid Acceleration	
[X]	Boundary Forces	[ ]	Local Acceleration
[X]	Gravity Forces		
[X]	Forces due to External Pressure Drop	[X]	Convective Acceleration
[X]	Viscous Forces		

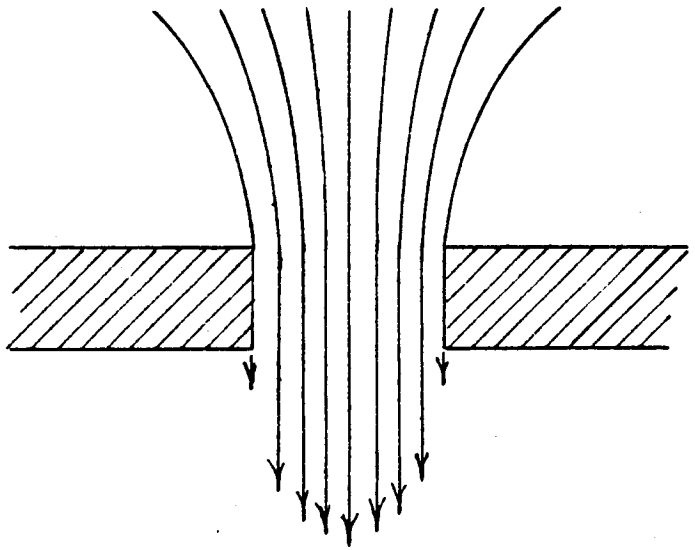

$C_v = 0.82$

$C_c = 1.00$

$C_D = 0.82$

FIG. 10 DISCHARGE WITH VISCOUS EFFECTS WITHOUT CONTRACTION (Ref. 5)

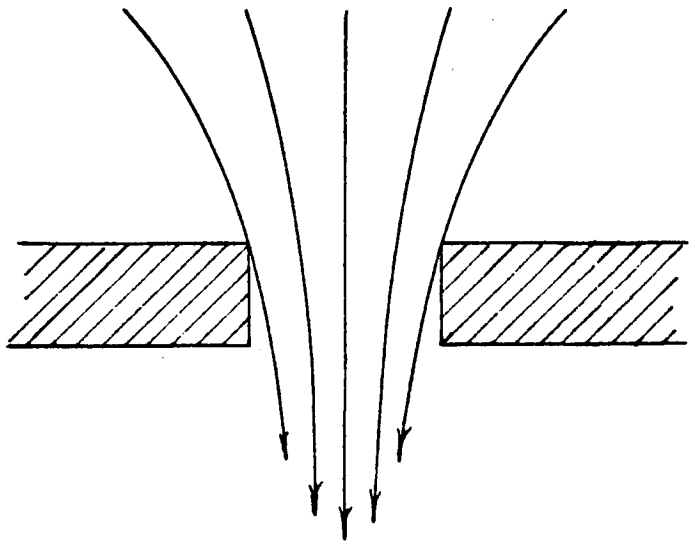

$C_v = 0.98$

$C_c = 0.61$

$C_D = 0.60$

FIG. 11 DISCHARGE WITH VISCOUS EFFECTS WITH CONTRACTION (Ref. 5)

In the analysis which follows fluid local acceleration effects are omitted for the sake of simplicity. The remaining physical effects considered in this report are all accounted for, at least approximately. The viscous retardation of the flow is specified by means of a velocity coefficient, C_v, and a contraction coefficient, C_c (see Ref. 4). The reduction in flow rate due to both effects is specified in terms of a discharge coefficient, C_D, which is the product of C_v and C_c. Typical values of these coefficients (obtained from Ref. 5) are indicated in FIG. 10 and 11.

The discharge coefficient is the ratio of the actual discharge rate to the idealized rate predicted for the same situation, but with viscous and contraction effects omitted. Thus equation (11), which gives the idealized rate for a given liquid height y when $\Delta P = 0$, is altered to

$$\dot{m} = C_D \cdot \left[\frac{\rho A}{\beta} \sqrt{2g(y + \Delta P/\rho g)} \right] . \qquad (17)$$

The effect of a non-zero pressure drop has also been included in the idealized rate expression (in brackets) as was done in the previous analysis. The procedure indicated by equations (7) through (14), when carried out with the discharge coefficient included, yields results identical to those given by equations (15) and (16) except that $1/\beta$ is replaced by C_D/β. These results are

$$\frac{y}{h} = 1 - 2 \sqrt{1 + \frac{\Delta P/\rho g}{h}} \left(\frac{C_D}{\beta} \cdot \frac{t}{\sqrt{2h/g}}\right) + \left(\frac{C_D}{\beta} \frac{t}{\sqrt{2h/g}}\right)^2 \qquad (18)$$

$$\sqrt{1-\left(\frac{a}{A}\right)^2}\left[\frac{\dot{m}}{\rho\left(\frac{\pi d^2}{4}\right)\sqrt{2gh}}\right]=C_D\sqrt{1+\frac{\Delta P/\rho g}{h}}-\left(\frac{C_D}{\beta}\ \frac{t}{\sqrt{2h/g}}\right) \qquad (19)$$

FIGURE 12 shows the variation of C_D with Reynolds number (based on total head), as given by Vennard (Ref.18), which is applicable to quasi-steady flow conditions when $y/d > 5$ and for $\frac{D}{d} >> 1$. When $y/d \approx 1$ or smaller, the lowering of the liquid surface into the vicinity of the outlet obviously causes considerable variation in the fluid streamline pattern at the exit. Thus, for small values of y/d some deviation from the C_D curve of FIG. 12 can be expected. Since $\left(\frac{y}{d}\right) = \left(\frac{h}{d}\right)\left(\frac{y}{h}\right)$, this implies that even when $\frac{d\sqrt{2gh}}{\nu}$, $\frac{y}{h}$, and $\frac{\Delta P/\rho g}{h}$ are held constant, various values of C_D can be obtained by varying $\frac{h}{d}$ in the operating range where $\left(\frac{h}{d}\right)\cdot\left(\frac{y}{h}\right)$ is small. Also, the curve of FIG. 12 applies only if $\frac{D}{d} >> 1$. When d is large, approaching the value of D, the cylindrical container wall affects the streamline pattern in the vicinity of the outlet, so that C_D varies with $\frac{D}{d}$ in general. This can be expected on the basis of C_D values obtained for flow through an orifice in a tube full of liquid (FIG. 13), a situation which is not quite the same as the case discussed here, but is somewhat similar.

On the basis of the discussion above, it is clear that C_D is somewhat dependent on h/d and D/d in addition to the dimensionless ratios appearing in the abscissa of FIG. 12.

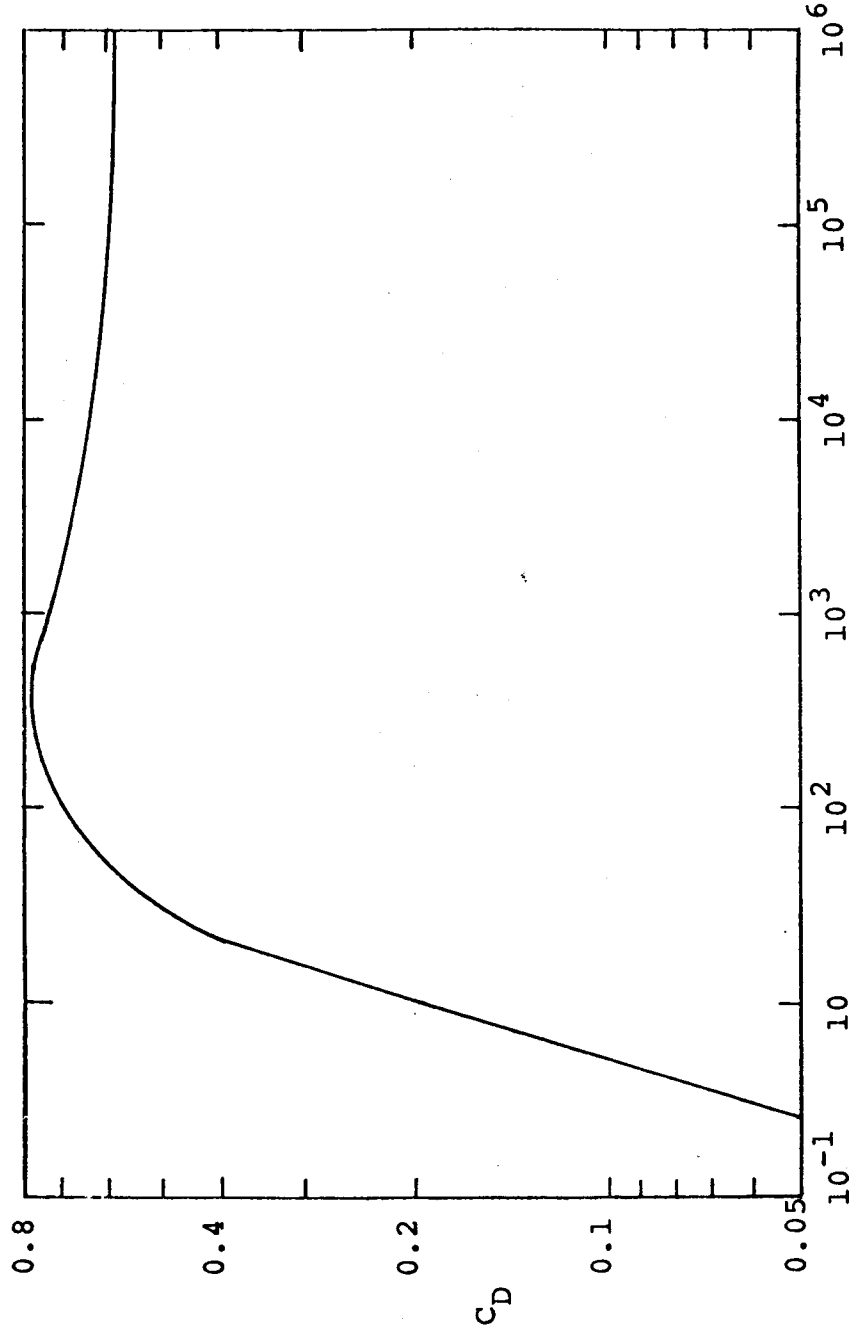

FIG. 12 VARIATION OF DISCHARGE COEFFICIENT FOR $y/d >$ AND $D/d >> 1$ FROM REF. 18

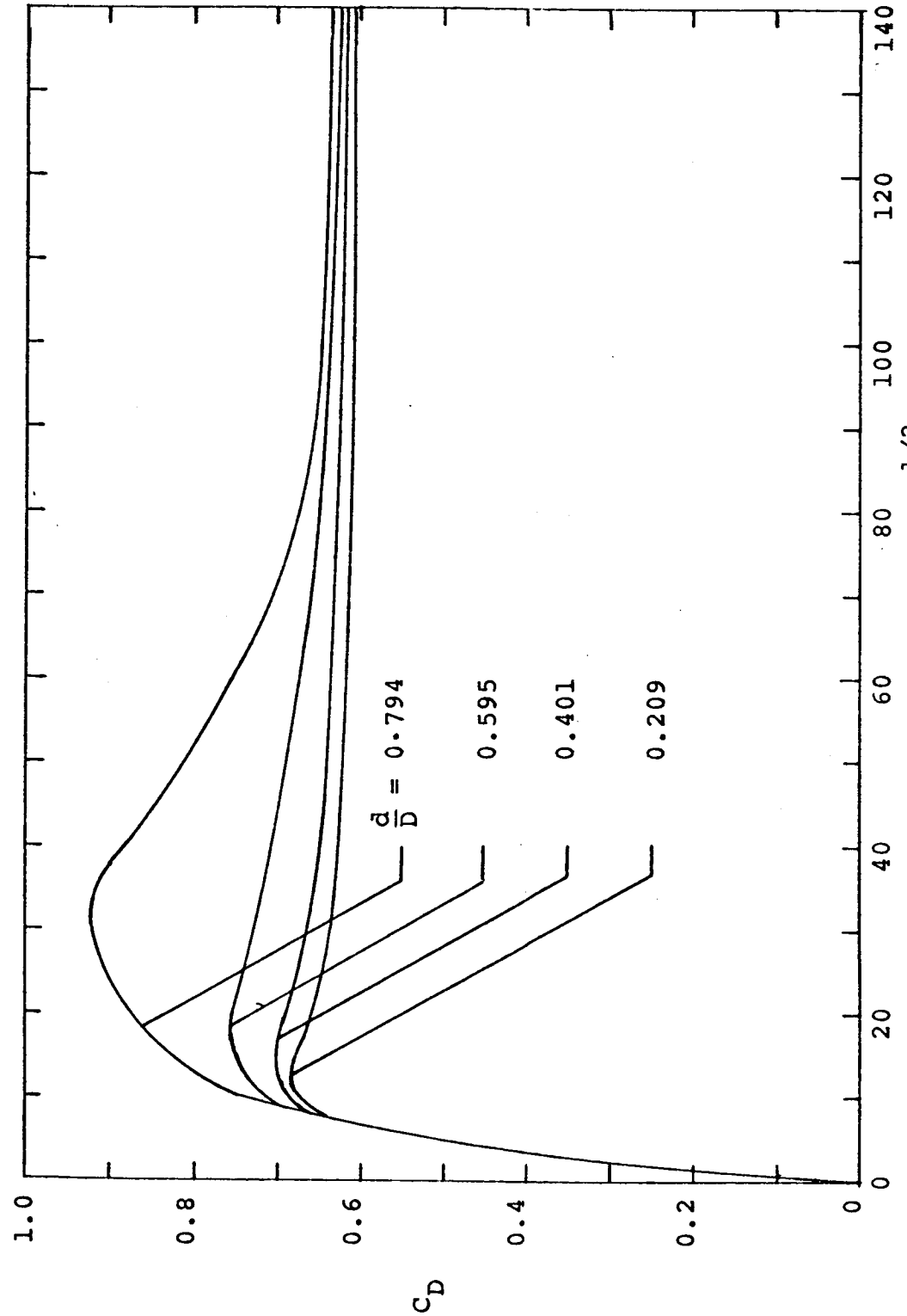

FIG. 13 VARIATIONS OF DISCHARGE COEFFICIENT FOR FLOW THROUGH AN ORIFICE IN A TUBE (REF. 17)

Therefore, all of the dimensionless parameters given initially in equations (2b) and (3b) are appropriately included in the results given by equations (18) and (19)[1]. However, the results given by equations (18) and (19) are not exact in general since C_D was assumed constant throughout the discharge period in their derivation. In reality C_D may be expected to vary somewhat with time as y decreases (FIG. 12). Despite this fact, use of a constant C_D value for an entire transient run can be expected to produce reasonably accurate results in many typical situations where $\frac{d\sqrt{2gh}}{\nu}\sqrt{\frac{y}{h}+\frac{\Delta P/\rho g}{h}}$ remains somewhat above 10^4 throughout most of the discharge period (FIG. 12). In this case C_D is very close to 0.6 during the entire process (provided that $h/d >> 1$), except for possible changes in C_D occurring at the very end of the process ($y/d \approx 1$, or smaller) brought about by an alteration of the flow pattern as the liquid surface is lowered into the region of the exit.

On the other hand, for transient runs involving modified Reynolds numbers (abscissa of FIG. 12) which drop from 10^4 or above down to about 100, increases in C_D during the discharge occur, from 0.6 to about 0.8. Furthermore, C_D can drop from about 0.7 to zero if the Reynolds number range is at the lower end, say between 100 and zero (FIG. 12).

---

[1] Note that $L/d = 0$ in this treatment, while $a/A = (d/D)^2$ and $\beta = \sqrt{\left(\frac{D}{d}\right)^4 - 1}$ in equations (18) and (19).

In this situation viscous effects become highly dominant, and the strong variation of C_D would cause equations (18) and (19) to be inaccurate. Thus, a word of caution is in order with respect to the ability of equations (18) and (19) to predict the actual discharge behavior for some operating ranges. Even in the more severe cases, however, these equations can yield fairly good approximate results provided that a good estimate is made of an appropriate C_D value to be used with these equations. This may be difficult to do for situations where the actual C_D value varies drastically over the discharge period, so that considerable experience and sound judgement may be required to produce successful predictions for these conditions.

For modified Reynolds numbers above 30 (abscissa of FIG. 12), C_D can be expected to lie between 0.5 and 1.0. FIGURES 14 and 15 contain plots of equations (18) and (19) which illustrate the retardation effect produced by C_D values corresponding to the lower Reynolds numbers (FIG. 12). For a situation involving a variable C_D during a discharge process, an average C_D value can be estimated (FIG. 12) in order to obtain the approximate time variations of the liquid surface height and mass flow rate (FIG. 14 and 15). The corresponding actual curves would fall in the vicinity of the idealized curves, plotted in the manner indicated in FIG. 14 and 15, but would deviate somewhat in shape.

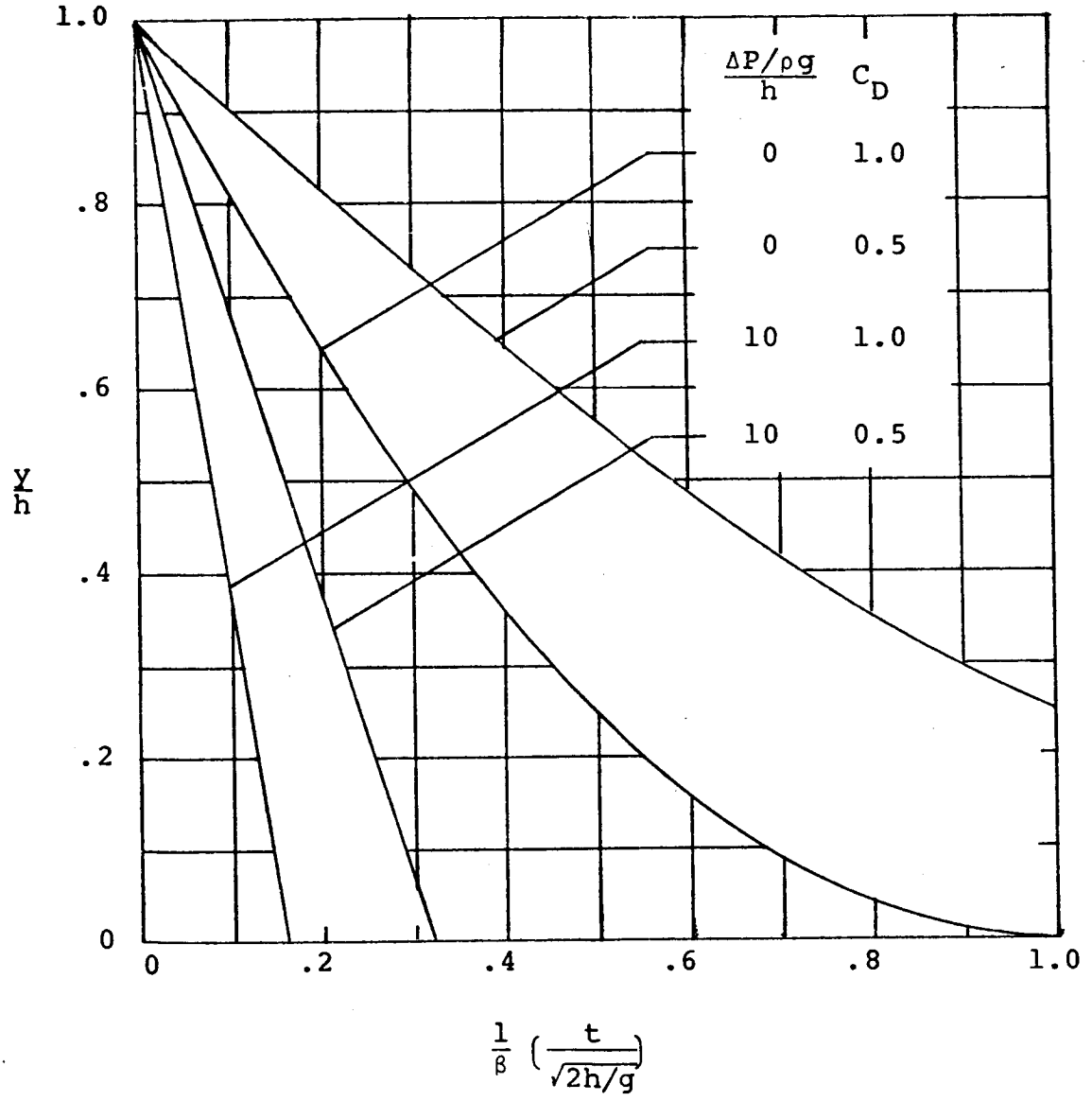

FIG. 14 VARIATION OF LIQUID HEIGHT WITH TIME FROM ANALYSIS BASED ON QUASI-STEADY FLOW IN THE PRESENCE OF VISCOUS EFFECTS FOR NON-ZERO PRESSURE DROP EQUATION (18)

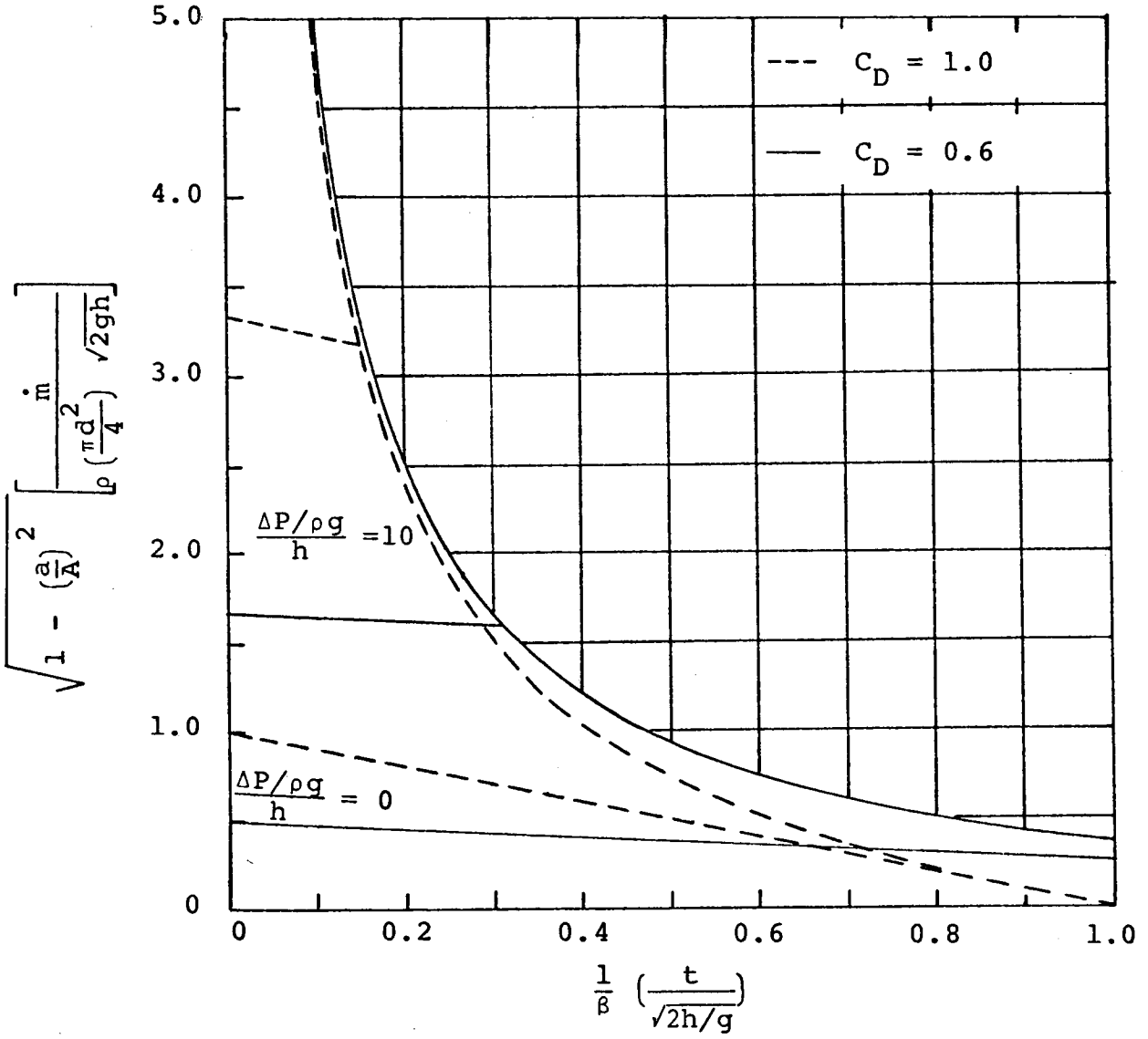

FIG. 15 VARIATION OF MASS FLOW RATE WITH TIME FROM ANALYSIS BASED ON QUASI-STEADY FLOW INCLUDING VISCOUS EFFECTS FOR NON-ZERO PRESSURE DROP, EQUATION (19)

Liquid Discharge Through a Tube

The previously presented analytical results apply to liquid discharge through an opening (FIG. 3) and correspond to the special case of $L/d = 0$. These results can also be applied, when combined with certain additional procedures, to discharge through a tube (FIG. 2) with $L/d > 0$. Equations (18) and (19) give the results, based on quasi-steady flow, which account for all of the physical effects except those due to local acceleration. Recall that these effects were found to be important only if the size of the discharge opening approaches the cross-sectional area of the container (β approaching an order of magnitude of unity). If local acceleration is not important, then equations (18) and (19) can be used for prediction purposes provided that C_D can be determined with reasonable accuracy. Before directing attention toward the determination of C_D, it is appropriate that the physical effects associated with the procedure outlined above be indicated. These are summarized below.

Forces	Fluid Acceleration
[X] Boundary Forces	[ ] Local Acceleration
[X] Gravity Forces	
[X] Forces due to External Pressure Drop	[X] Convective Acceleration
[X] Viscous Forces	

Application of Bernoulli's equation to the system shown in FIG. 2 gives a modified form of equation (5) which accounts for viscous effects by means of a head loss, h_L. This relation is

$$P_1 + \rho g y + \frac{1}{2}\rho V_1^2 = P_2 + \frac{1}{2}\rho V_2^2 + h_L \qquad (20)$$

where the liquid surface height, y, is measured from the exit location. Equation (6) is correspondingly modified to account for ΔP and h_L, and equation (11) becomes

$$\dot{m} = \frac{\rho A}{\beta} \sqrt{2g(y + \Delta P/\rho g - h_L)} \; . \qquad (21)$$

If the discharge stream should be contracted at the exit, this relation is further altered to

$$\dot{m} = C_c \frac{\rho A}{\beta} \sqrt{2g(y + \Delta P/\rho g - h_L)} \; . \qquad (22)$$

The definition of C_D, given previously by equation (17), is

$$\dot{m} = C_D \frac{\rho A}{\beta} \sqrt{2g(y + \Delta P/\rho g)} \; . \qquad (23)$$

Combining equations (22) and (23) gives

$$(y + \Delta P/\rho g) = \frac{h_L}{1 - C_D^2/C_c^2} \; . \qquad (24)$$

Now the total head loss is composed of the entrance head loss, h_e, due to the reduction in cross-sectional area at the inlet of the tube, and the frictional head loss, h_f, due to

viscous effects within the discharge tube. Thus,

$$h_L = h_e + h_f \quad . \tag{25}$$

These two head loss components are given by

$$h_e = K \frac{V_2^2}{2g} \tag{26}$$

and

$$h_f = f \frac{L}{d} \frac{V_2^2}{2g} \quad . \tag{27}$$

K is the entrance loss coefficient (Ref. 4) and f is the Darcy-Weisbach friction factor for flow in a tube (Ref. 4). The total head loss is

$$h_L = (K + f \frac{L}{d}) \frac{V_2^2}{2g} \quad . \tag{28}$$

Since $\dot{m} = \rho a V_2$, equations (23), (24), and (28) can be combined to give

$$C_D = \frac{C_c}{\sqrt{1 + \left[\frac{K + f \frac{L}{d}}{1 - (a/A)^2}\right] C_c^2}} \quad . \tag{29}$$

Over most operating ranges encountered, K is about 0.5 (Ref. 4). The friction factor, f, is dependent upon the Reynolds number of the flow in the tube and can be obtained (Ref. 4) from the Moody Chart (FIG. 16). This information for K and f applies only if the liquid fills the tube, in which case $C_c = 1$. For very short tubes, $f \frac{L}{d}$ is negligible

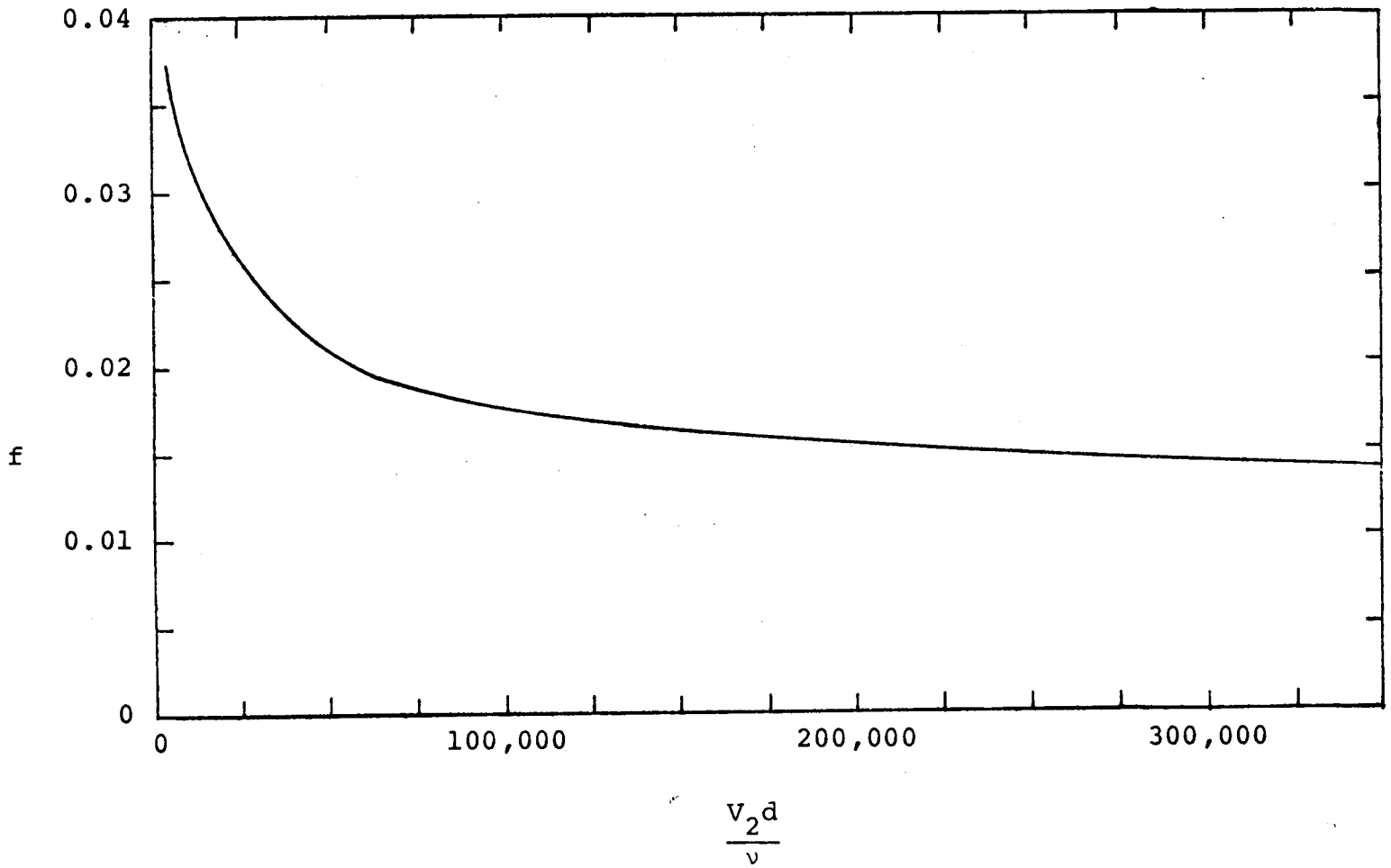

FIG. 16 MOODY CHART (REF. 4) GIVING DEPENDENCE OF THE SMOOTH TUBE FRICTION FACTOR ON THE TUBE REYNOLDS NUMBER

compared to K and equation (29) gives $C_D = 0.82$ for $C_c = 1$, $K = 0.5$ and $\left(\frac{a}{A}\right)^2 << 1$. This value of C_D is in good agreement with the nominal value of 0.8 given for short tubes by Vennard (Ref. 18) and agrees exactly with the nominal value for discharge through an opening in the absence of contraction given in Ref. 5. The latter situation occurs in some instances when the thickness to diameter ratio of the opening is not negligible, so that the opening really corresponds to the case of a short tube (FIG. 10). If contraction occurs so that the liquid does not fill the tube crossection at the exit, then $C_c < 1$ (see FIG. 11) and $f\frac{L}{d}$ should be eliminated from the generalized relation for C_D given by equation (29). For this case C_c is a little larger than 0.6 for most typical situations, and K is normally only slightly greater than zero (see FIG. 11).

FIGURE 17 shows curves for C_D, plotted according to equation (29), for $C_c = 1$ and $a/A << 1$. In generating these curves K was taken to be 0.5 and f was obtained from FIG. 16. Notice that the resulting C_D values are strongly dependent on L/d, but they do not vary appreciably over a large range of the Reynolds number. This implies that C_D is relatively constant even if $\dot{m}$ varies during a transient discharge process provided that the Reynolds number remains in this range. Strictly speaking, C_D can be shown to depend upon D/d and y/d as well as the Reynolds number and L/d. This can be expected on the basis that K depends somewhat on D/d and on y/d, if y/d is small, in addition to varying with

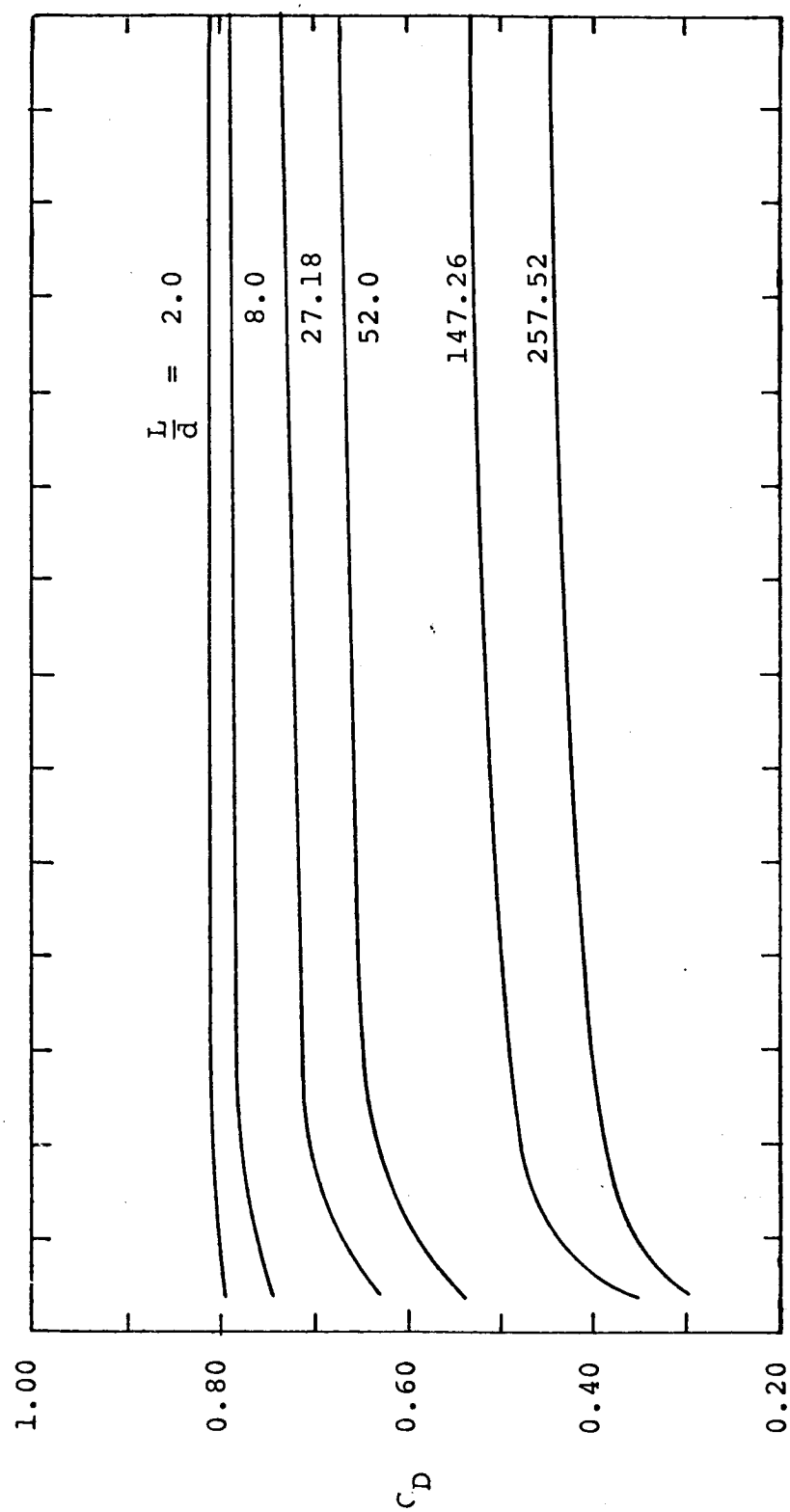

FIG. 17 PREDICTION OF DISCHARGE COEFFICIENT BASED ON C_c = 1.0, K = 0.5 AND f FROM MOODY CHART (FIG. 16) FOR a/A << 1

the Reynolds number (recall discussion of C_D for flow through an opening contained in the previous section).

In order to obtain approximate analytical results equations (18) and (19) are used (recall that C_D is assumed constant over the discharge period). FIGURES 18 and 19 show typical results which correspond to L/h = 0.5, plotted for C_D equal to 0.35 and 1.0 and for two values of $\frac{\Delta P/\rho g}{h}$. According to FIG. 17 the C_D range covered by these plots corresponds to values of L/d up to about 250.

An analysis which accounts for the additional effect of local acceleration is presented in Appendix C. The physical effects accounted for are summarized in the following table (see diagram in FIG. 20).

Forces	Fluid Acceleration
[X] Boundary Forces	[X] Local Acceleration
[X] Gravity Forces	
[X] Forces due to External Pressure Drop	[X] Convective Acceleration
[X] Viscous Forces	

The results of the analysis, under the assumptions mentioned in Appendix C, are presented in FIG. 21 through 30. From equation (C4) and FIG. 21 through 30, it can be seen that the dimensionless liquid height, or analogously the dimensionless mass flow rate, is a function of the

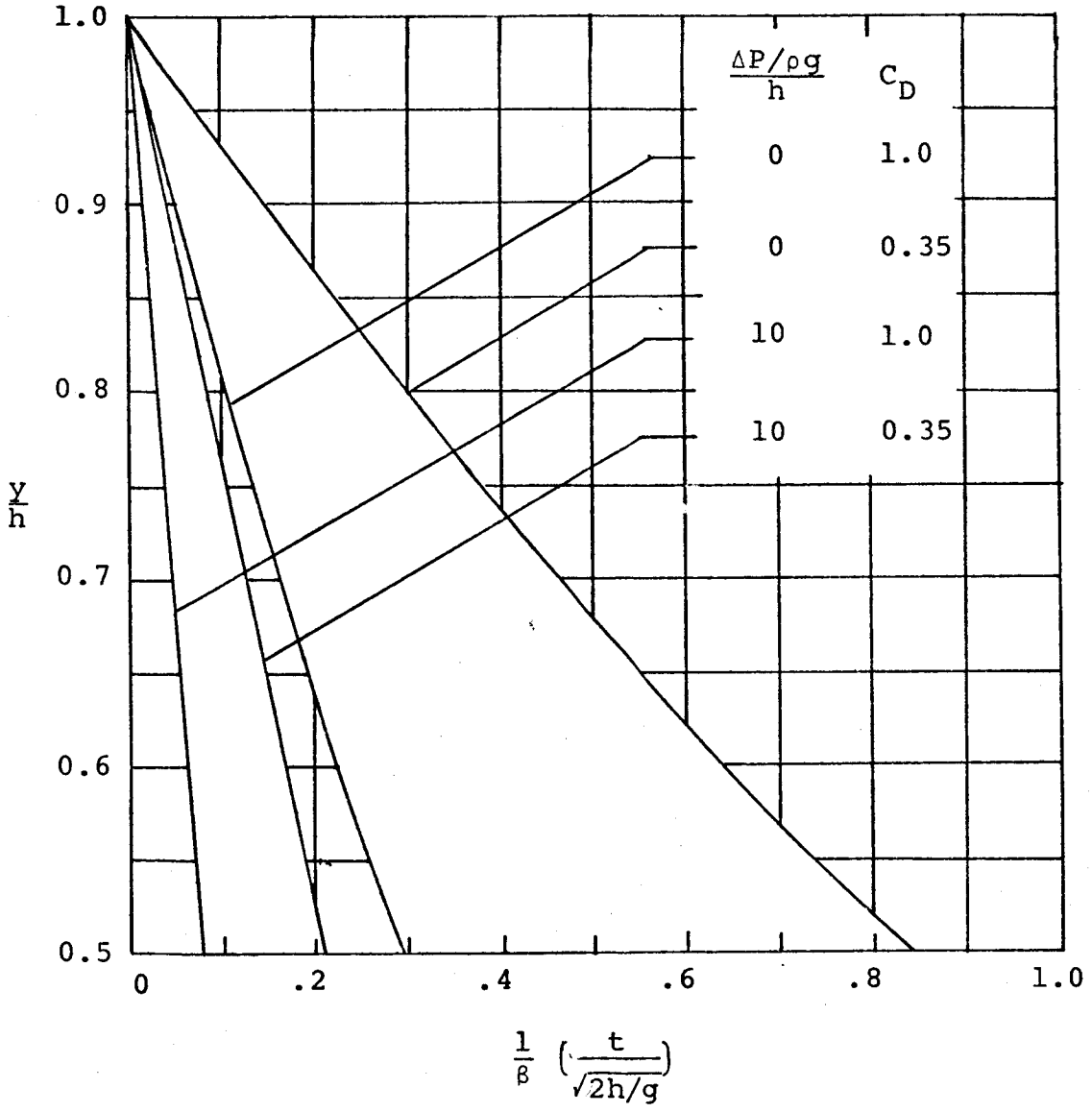

FIG. 18 VARIATION OF LIQUID HEIGHT WITH TIME FROM ANALYSIS BASED ON QUASI-STEADY FLOW IN THE PRESENCE OF VISCOUS EFFECTS FOR NON-ZERO PRESSURE DROP, EQUATION (18), FOR $\frac{L}{h} = 0.5$

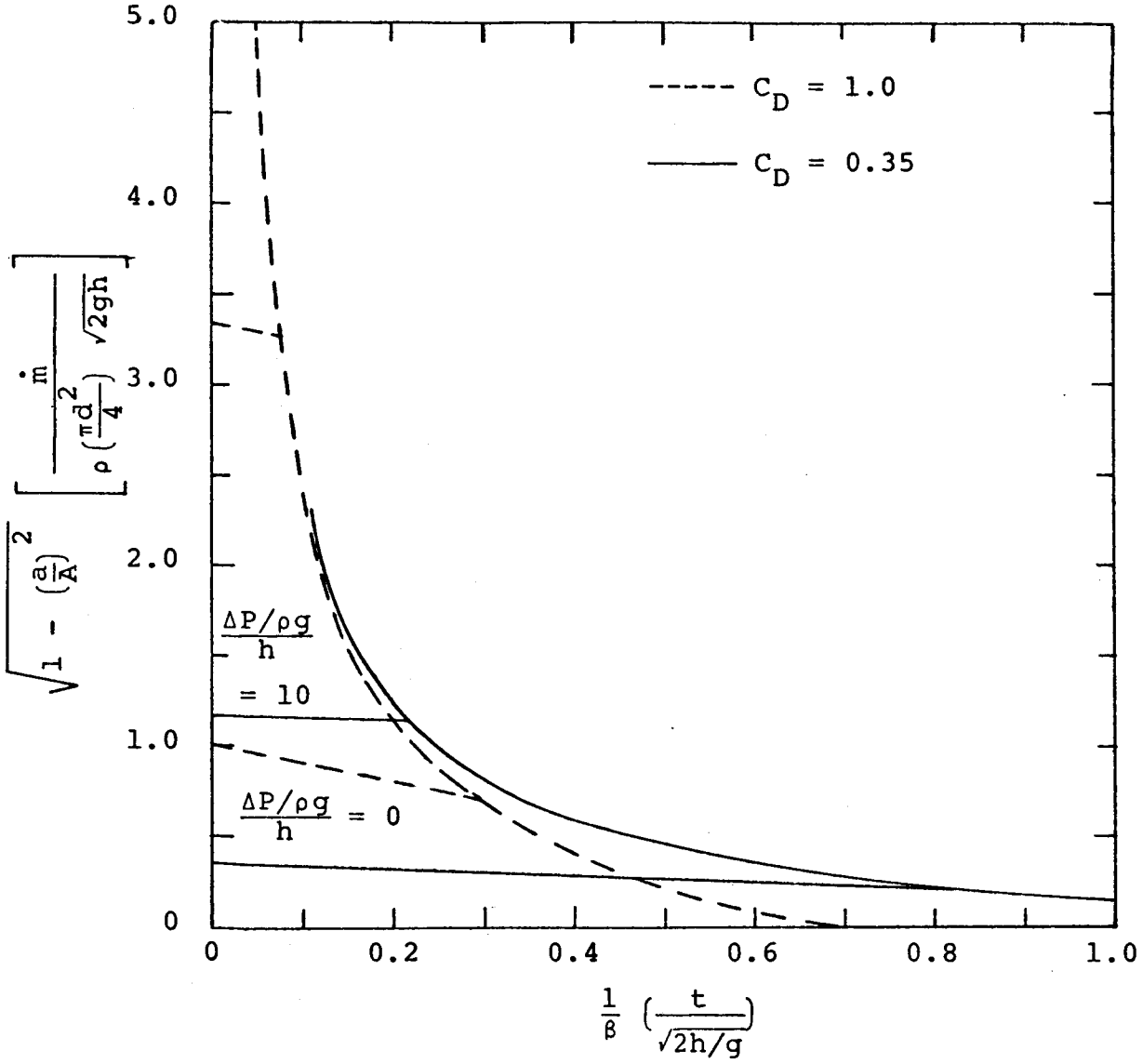

FIG. 19 VARIATION OF MASS FLOW RATE WITH TIME FROM ANALYSIS BASED ON QUASI-STEADY FLOW INCLUDING VISCOUS EFFECTS AND NON-ZERO PRESSURE DROP, EQUATION (19) FOR L/h = 0.5

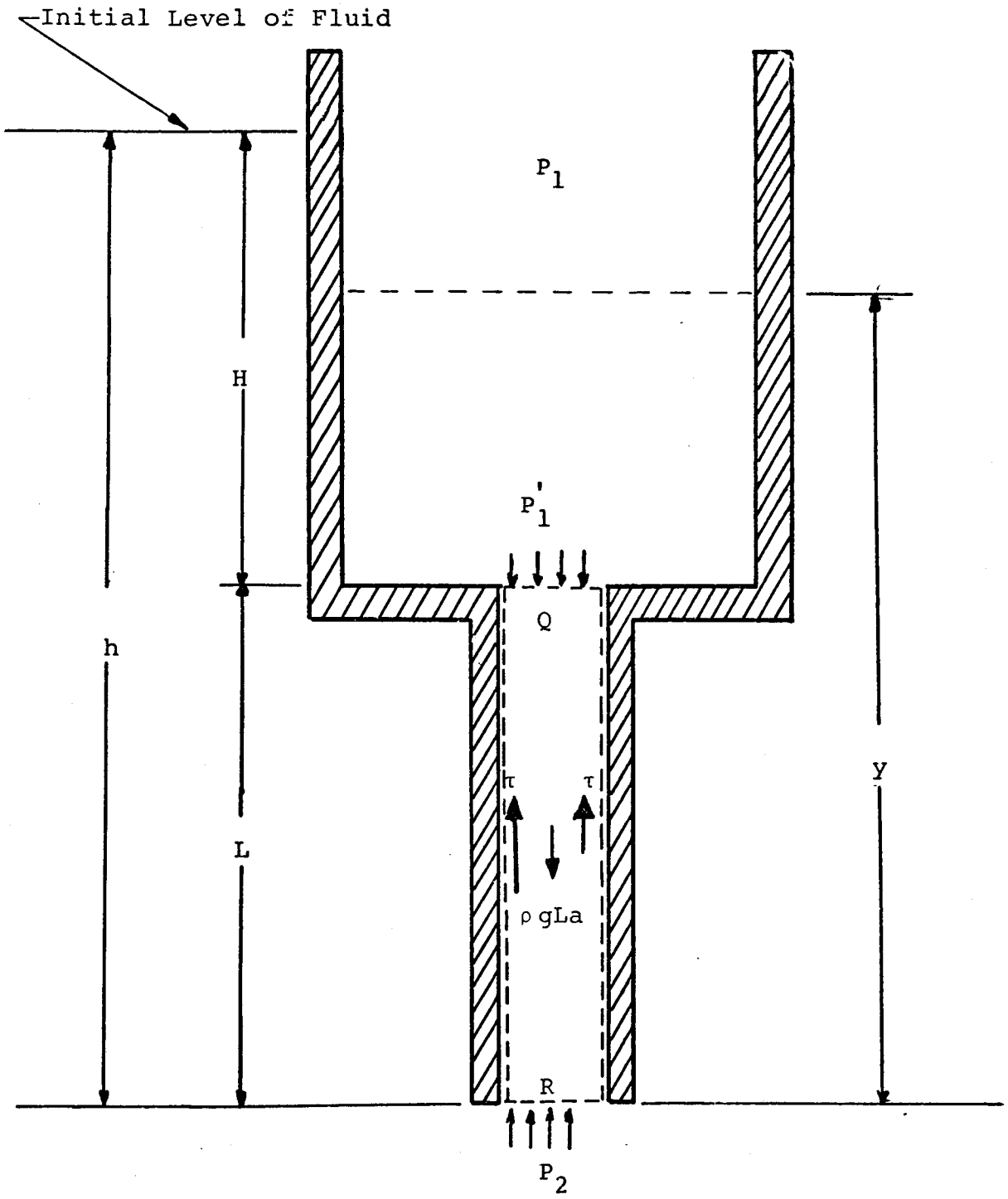

FIG. 20 SYSTEM CONFIGURATION AT ANY INSTANT OF TIME

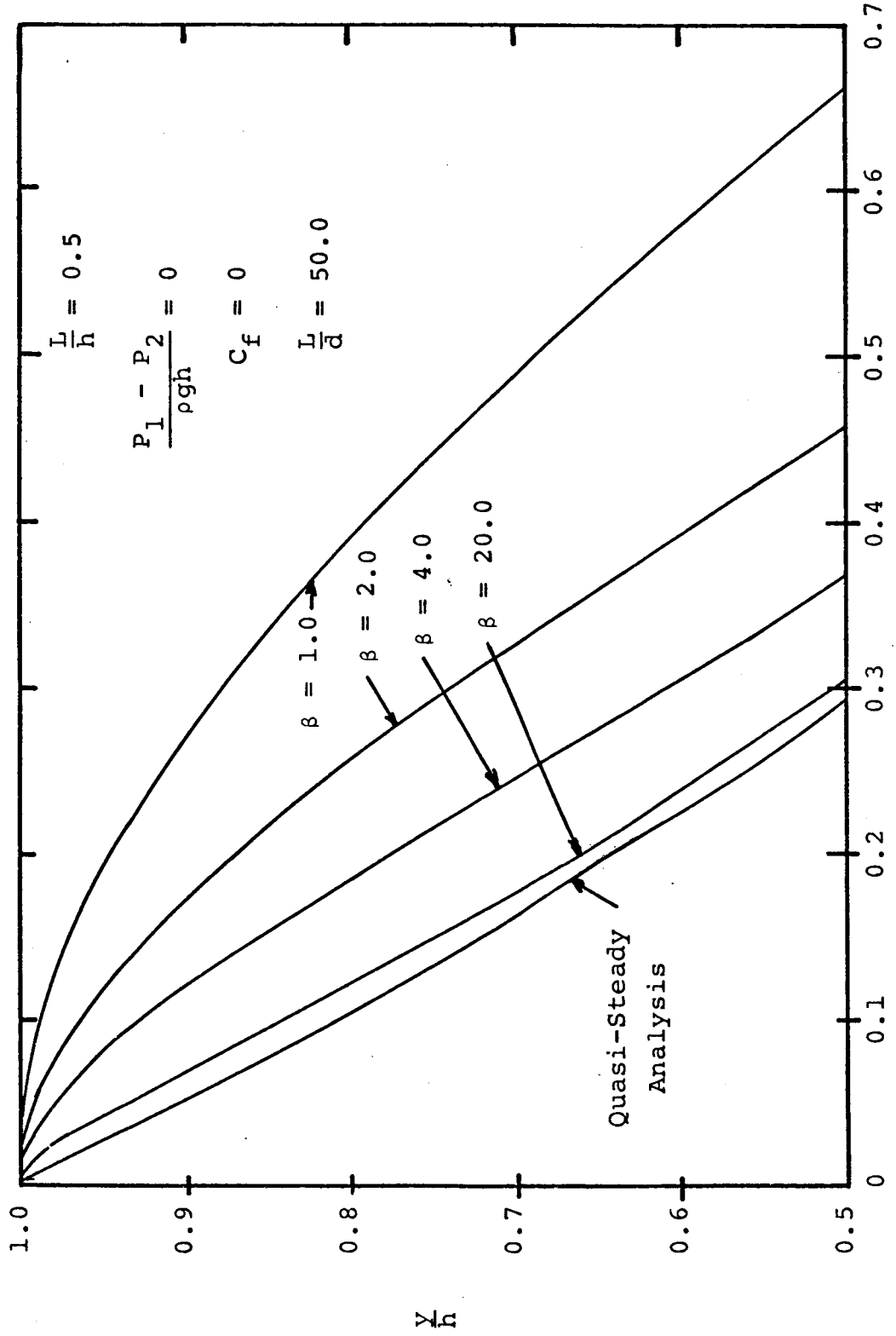

FIG. 21 VARIATION OF DIMENSIONLESS LIQUID HEIGHT WITH DIMENSIONLESS TIME FOR VARIOUS VALUES OF THE PARAMETER β

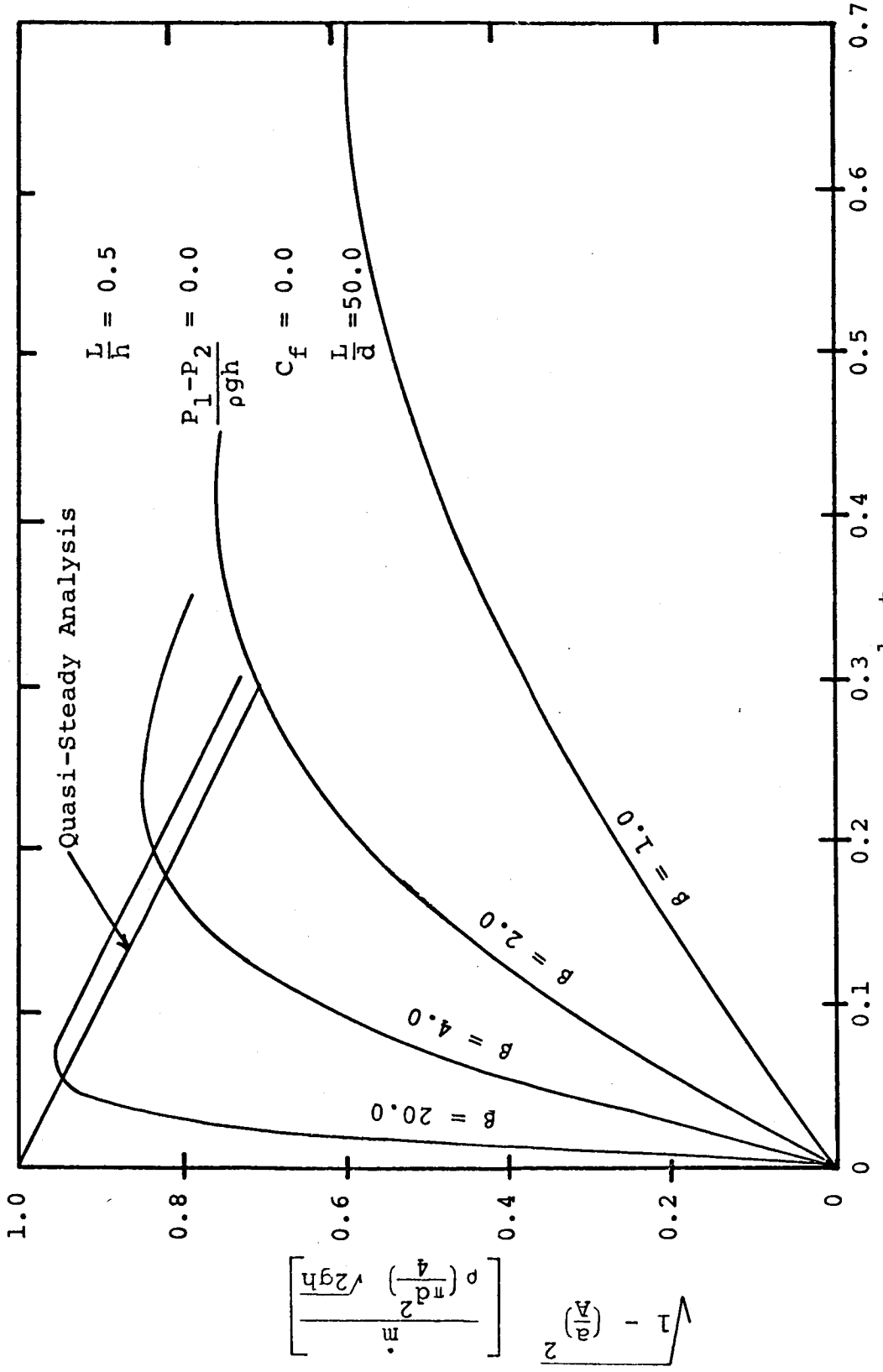

FIG. 22 VARIATION OF DIMENSIONLESS MASS FLOW RATE WITH DIMENSIONLESS TIME FOR VARIOUS VALUES OF THE PARAMETER β

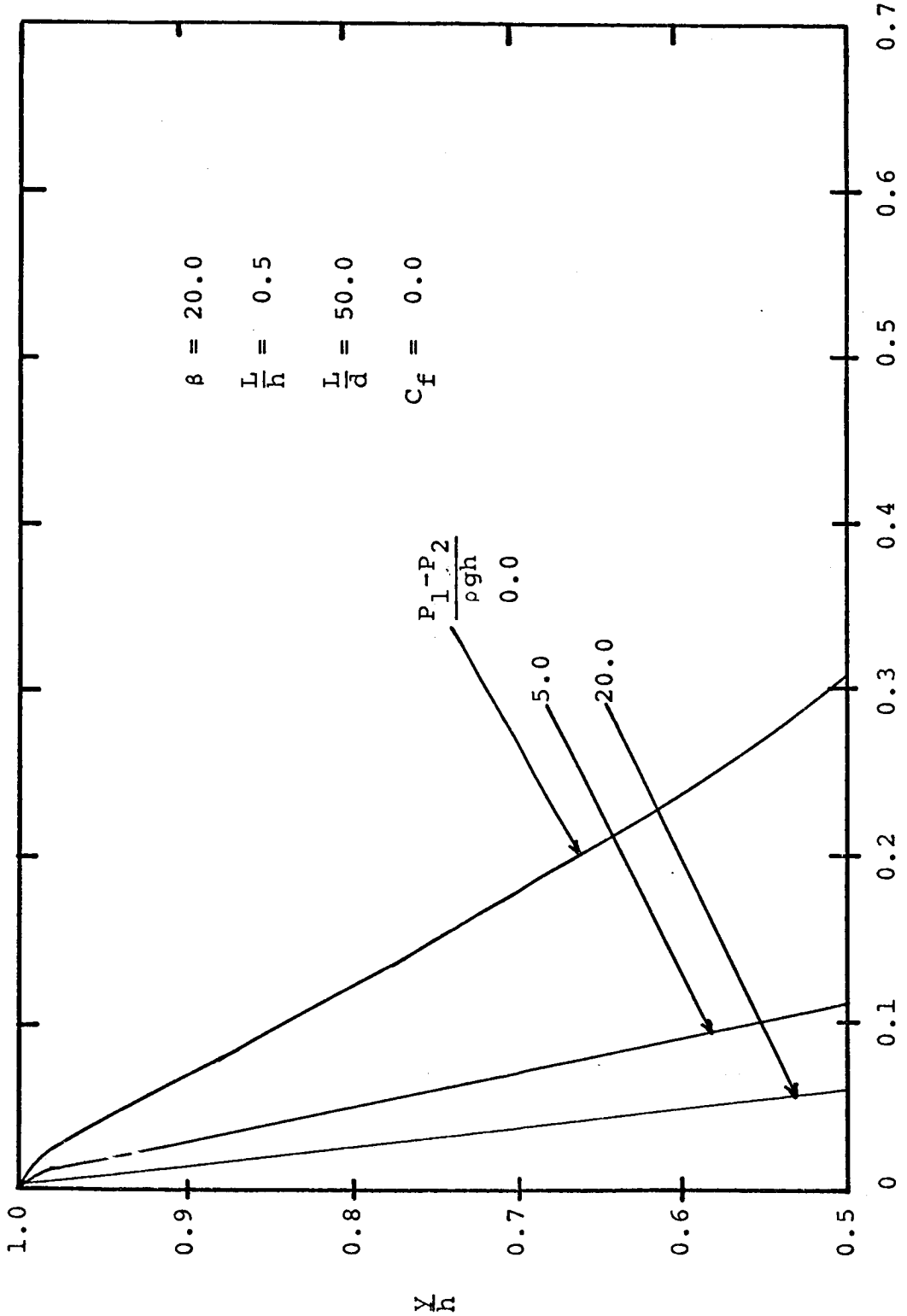

FIG. 23 VARIATION OF DIMENSIONLESS LIQUID HEIGHT WITH DIMENSIONLESS TIME FOR VARIOUS VALUES OF THE PARAMETER $\left(\frac{P_1-P_2}{\rho gh}\right)$

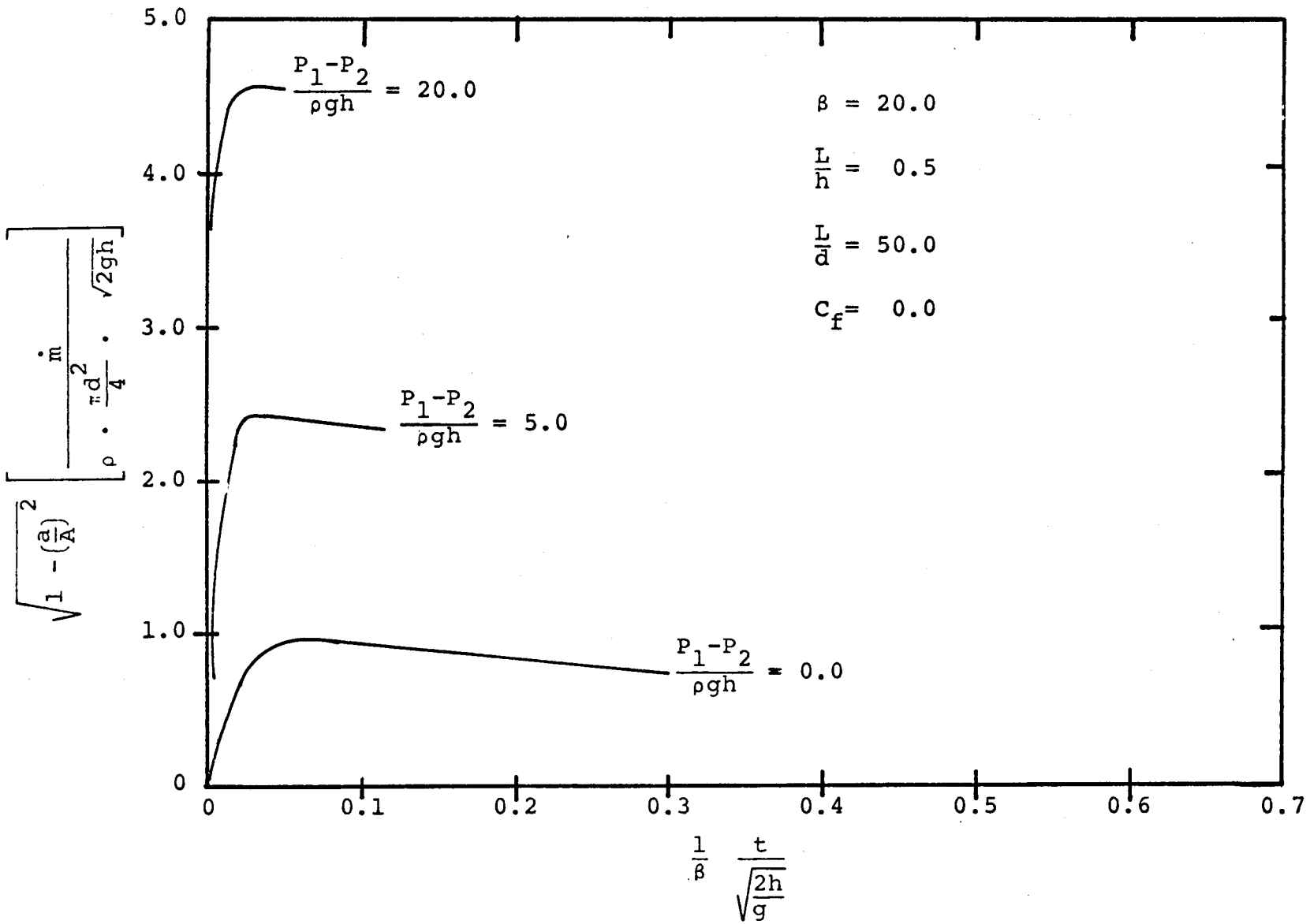

FIG. 24 VARIATION OF DIMENSIONLESS MASS FLOW RATE WITH DIMENSIONLESS TIME FOR VARIOUS VALUES OF THE PARAMETER $\left(\frac{P_1-P_2}{\rho gh}\right)$

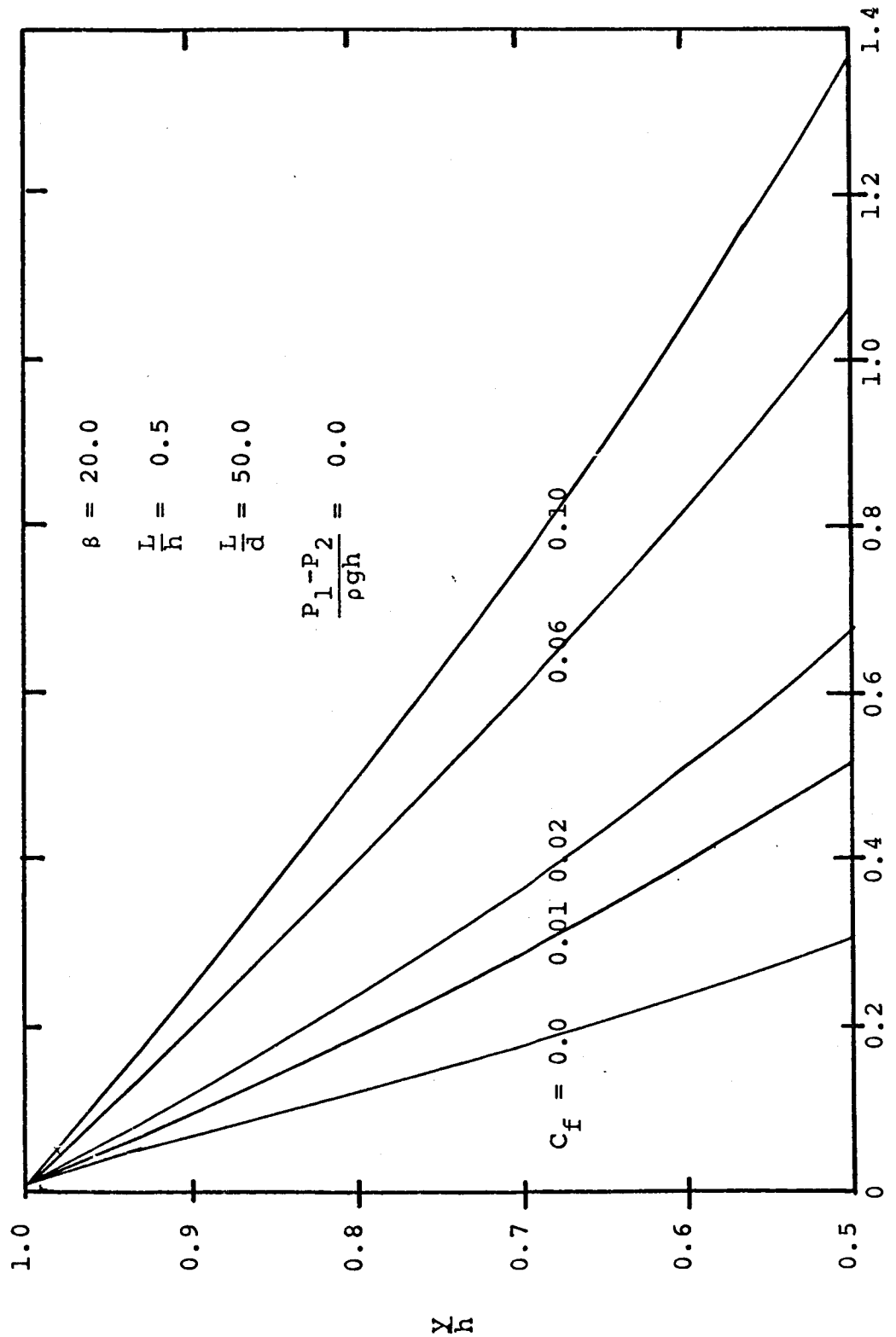

FIG. 25 VARIATION OF DIMENSIONLESS LIQUID WEIGHT WITH DIMENSIONLESS TIME FOR VARIOUS VALUES OF THE SKIN FRICTION COEFFICIENT, C_f (i.e., THE PARAMETER $\frac{d\sqrt{2gh}}{\nu}$)

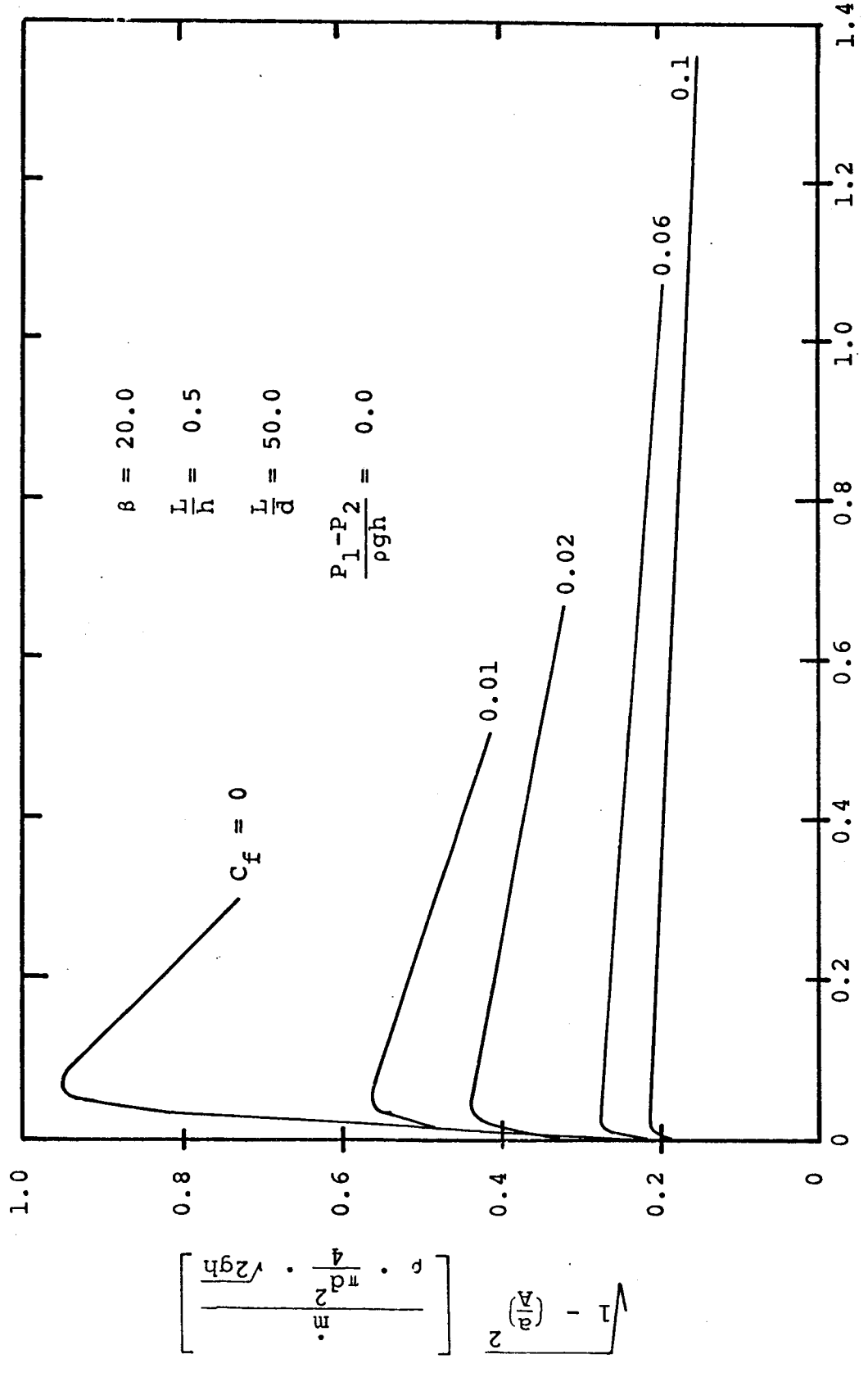

FIG. 26 VARIATION DIMENSIONLESS MASS FLOW RATE WITH DIMENSIONLESS TIME FOR VARIOUS VALUES OF THE SKIN FRICTION COEFFICIENT C_f

(i.e., THE PARAMETER $\frac{d\sqrt{2gh}}{\nu}$)

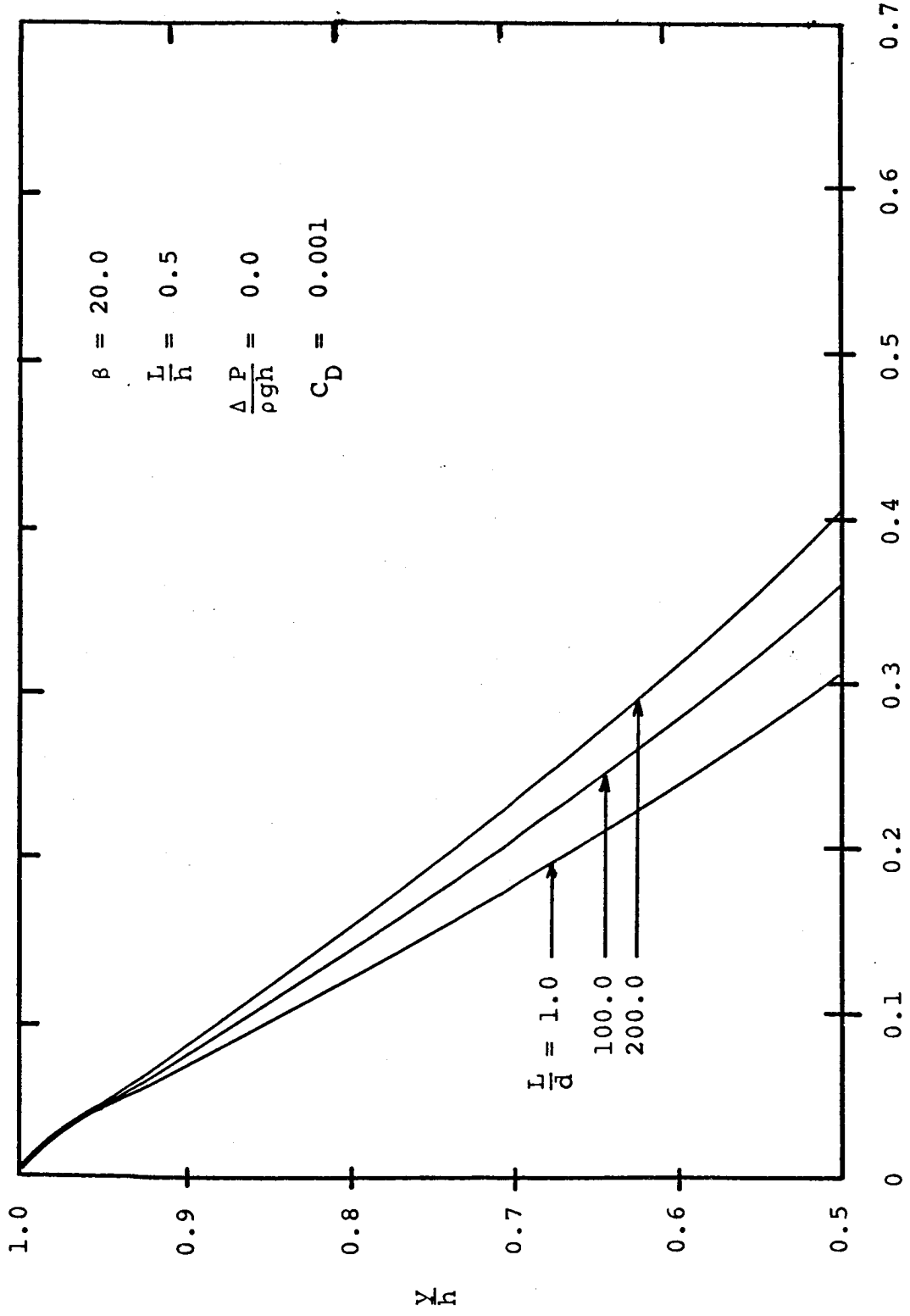

FIG. 27 VARIATION OF DIMENSIONLESS LIQUID HEIGHT WITH DIMENSIONLESS TIME FOR VARIOUS VALUES OF THE PARAMETER $\frac{L}{d}$

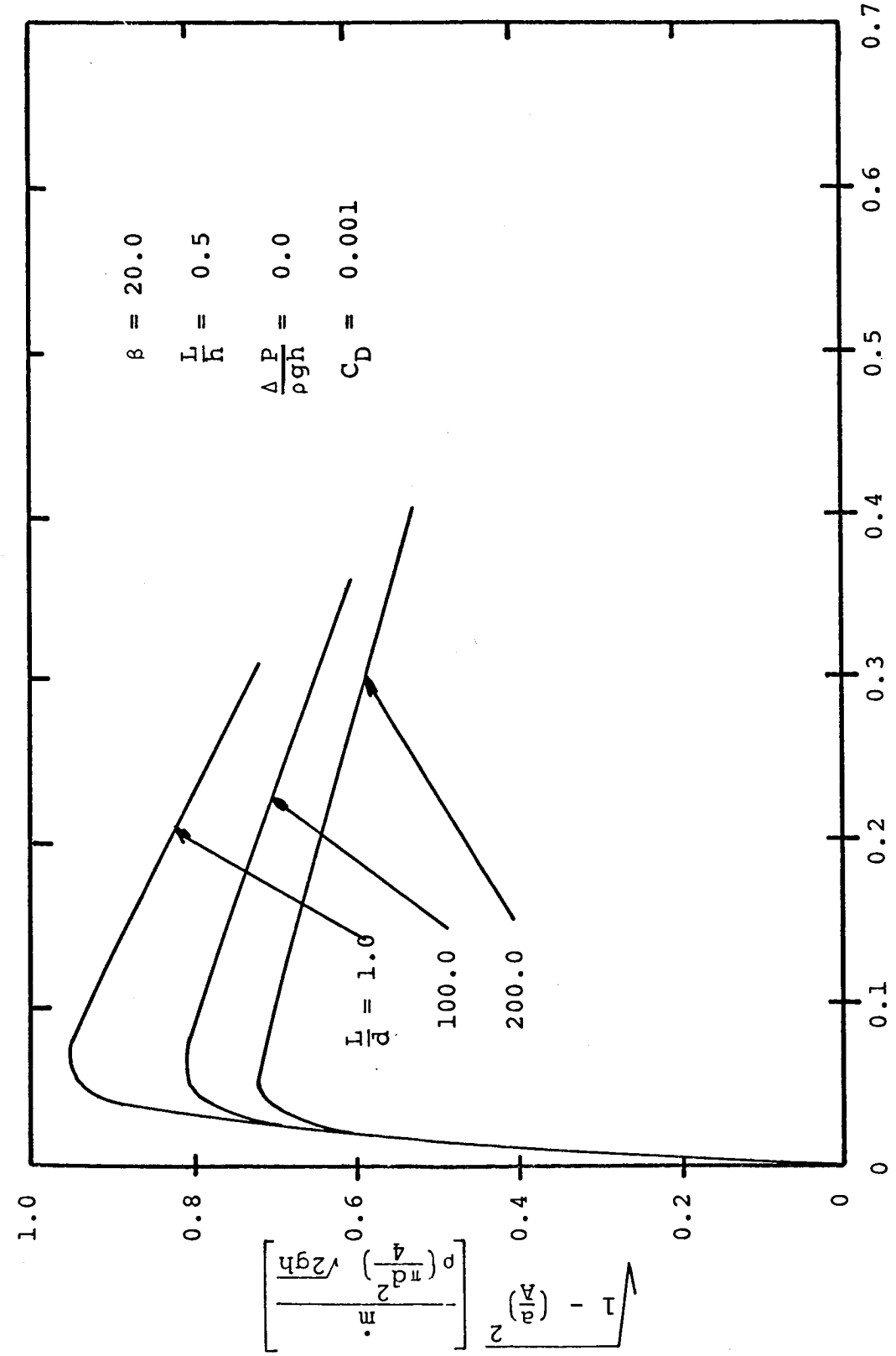

FIG. 28 VARIATION OF DIMENSIONLESS MASS FLOW RATE WITH DIMENSIONLESS TIME FOR VARIOUS VALUES OF THE PARAMETER $\frac{L}{d}$

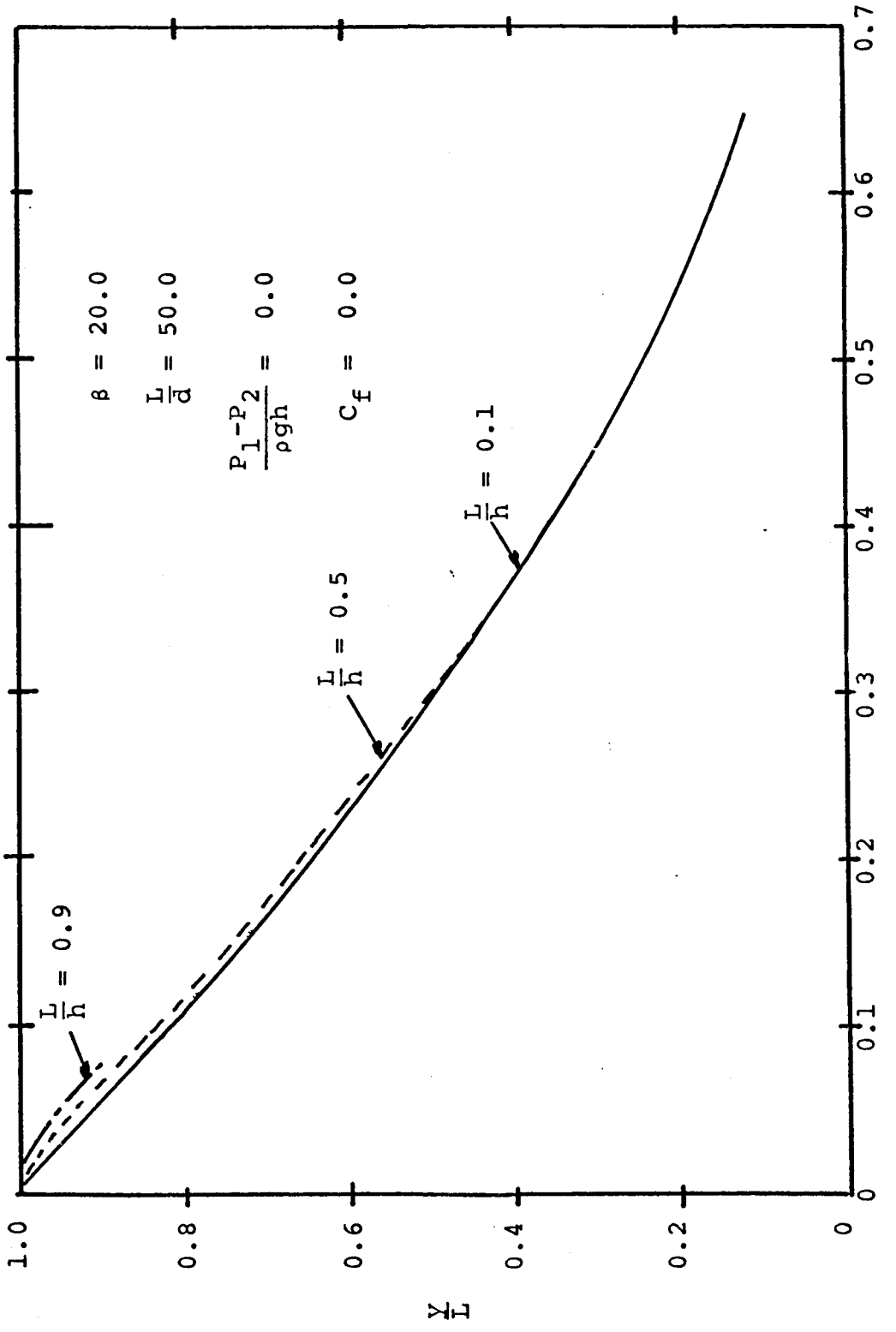

FIG. 29 VARIATION OF DIMENSIONLESS LIQUID HEIGHT WITH DIMENSIONAL TIME FOR VARIOUS VALUES OF THE PARAMETER $\frac{L}{h}$

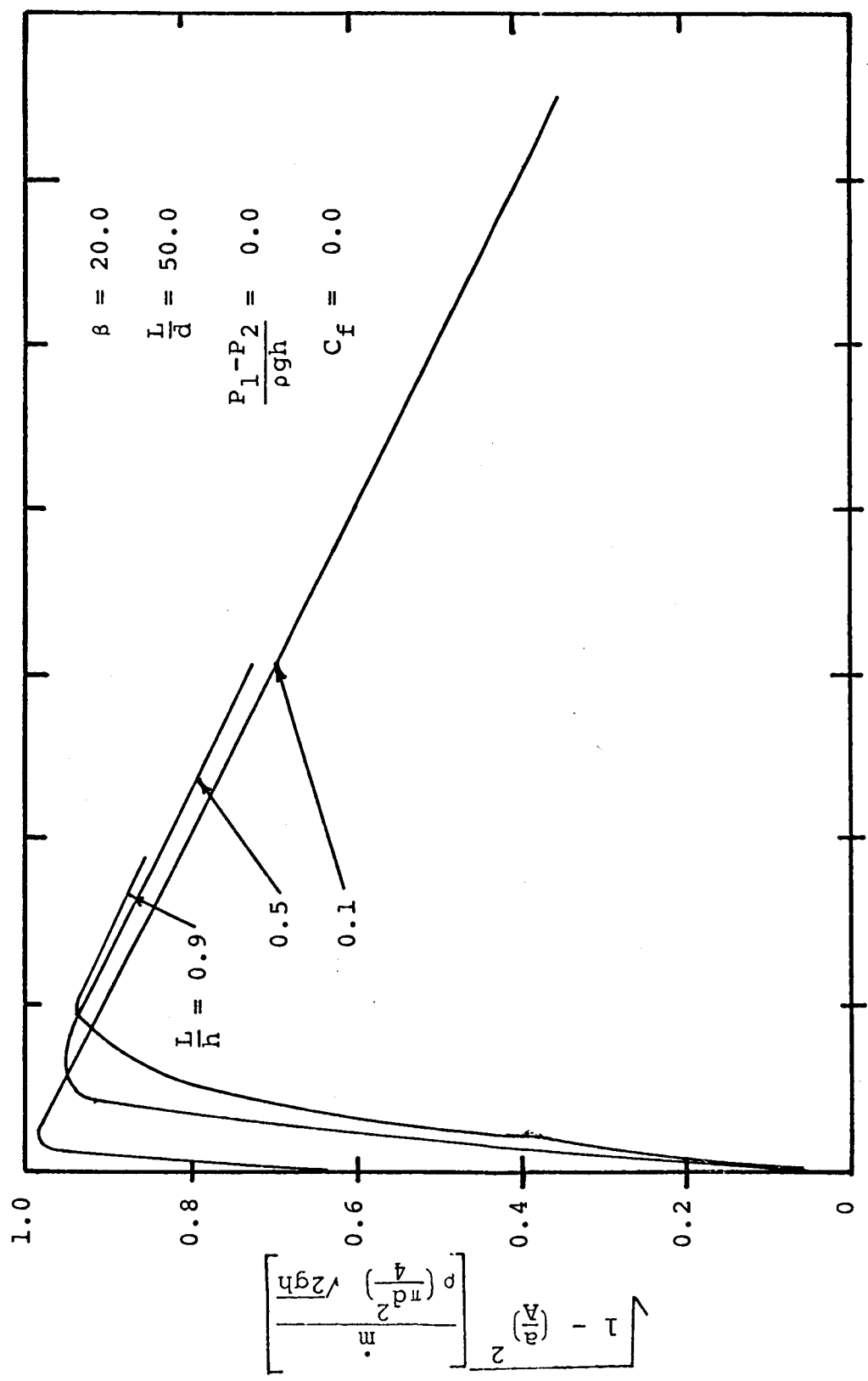

FIG. 30 VARIATION OF DIMENSIONLESS MASS FLOW RATE WITH DIMENSIONLESS TIME FOR VARIOUS VALUES OF THE PARAMETER $\frac{L}{h}$

dimensionless parameters given by the initial dimensional analysis (equations (2b) and (3b)). It should be noted that the skin friction coefficient c_f (which is ¼ of the friction factor "f" introduced in equation (27) is a function of the Reynolds number $\frac{d\sqrt{2gh}}{\nu}$. The assumption that c_f is a constant is justified in view of the fact that the variation in the discharge velocity is not too large (except for a very short period during the initial acceleration). The results are plotted so that the influence of each of the five dimensionless parameters on the variation of dimensionless liquid height and dimensionless mass flow rate with dimensionless time can be easily seen. FIGURES 21 and 22 indicate that except for small values of β (i.e., relatively large discharge areas) the variation of β has very little effect, just as in the case of the orifice discharge (FIG. 6 and 7). FIGURES 23 and 24 show the reduction in discharge times and increase in the mass flow rates with increasing pressure drop. FIGURES 25 and 26 show the retarding effect of friction. It can be noted that unless the viscous effect is large the time of discharge is always lower with a tube than with an orifice (without viscous or geometric effects). This is to be expected because the head in case of discharge through a tube is larger, and consequently, the velocity of discharge is higher than in the case of discharge through an orifice. FIGURES 27 and 28 indicate the physically reasonable trend that tubes with large diameter take less time to discharge

than tubes with relatively smaller diameter. FIGURES 29 and 30 show the effect of the length of the tube on time of discharge. As the value of L/h becomes larger, the time of discharge becomes shorter.

EXPERIMENTAL MEASUREMENTS AND COMPARISONS

In order to verify the analysis conducted in previous sections, numerous experiments were performed. The data obtained were put in non-dimensional form and compared to theoretical predictions. This served several purposes. Comparison of experimental results and theoretical predictions indicate the validity of any simplifying assumptions made, and in what flow situations these assumptions are justified. They may also indicate situations in which the analytical methods do not apply, and where further analysis is needed. Finally, they serve to verify the significance and importance of individual system parameters.

Apparatus and Procedure

The discharge containers used for experimental purposes are illustrated in FIG. 2. Two separate containers, of different diameters, were used. Both containers were equipped with discharge tubes of various lengths and diameters. Orifice type openings of several diameters were employed. This arrangement allowed each geometric parameter to be varied independently of any other geometric parameter. For instance, the discharge tube diameter was varied while all other system dimensions remained fixed. As another example, various

initial fluid heights, h, were used, while all other geometric parameters were kept constant. Numerous experimental runs were made, varying one geometric parameter for each particular series of experimental runs.

Variable external pressure drops were also used. This could be accomplished by increasing the container air supply pressure, P_1, above atmospheric pressure, or by reducing the discharge pressure, P_2, below atmospheric pressure, or by combinations of both. Tests were also conducted with no external pressure drop, for the case where $P_1 = P_2$.

Thus, it was possible to conduct experimental runs using various initial fluid geometries and external pressure drops while varying only one of these parameters for any given experimental run. Fluid properties and the gravitational field were constant in these experiments.

The objective of the experiments was to determine mass flow rate for any given combination of parameters. However, in practice, it was considered more convenient, and accurate, to measure fluid height as a function of time. The fluid height versus time measurements were then fit to curves using the method of least squares. With these curves, and their corresponding equations, mass flow rates could be computed. It was felt that this would give an accurate method of obtaining mass flow rates compared to any of the various flowmeter arrangements, and would not have the disadvantage of disturbing the discharge flow pattern.

Fluid height versus time measurements were carried out both by visual and photographic methods. The visual measurements were made by attaching graduated paper strips to the exterior of the container wall. The zero coordinate was set at the initial fluid surface, and surface heights were marked at fixed increments of time. This gave a permanent record of the fluid surface decrease as a function of time, which was converted to fluid height as a function of time.

For the more rapid discharge processes, photographic methods were used. A high speed movie camera served to photograph the discharge process. The camera operated at a fixed rate of number of frames exposed per second. The system was prepared for the experimental run, and the camera set at operating speed. At the exact instant the discharge process was initiated, the lighting system was actuated, thus fixing the initial frame at which the discharge process was started. Fluid height as a function of time was obtained from the film. This was done by counting the number of frames which were exposed during the period from the initiation of discharge until a particular fluid height of interest was reached. The number of frames exposed were then converted to elapsed time by employing the camera speed. This procedure gave fluid height as a function of time, as in the cases where visual measurements were made.

Determination and Verification of C_D Values

The fluid height versus time data were fitted with curves using the method of least squares. The resulting equation gave fluid height as a function of time. This equation could be differentiated in order to obtain instantaneous mass flow rate. The actual fluid heights and mass flow rates were then reduced to non-dimensional form.

Several assumptions were made prior to making the curve fit. The equations based on the assumption of quasi-steady flow were used. This seemed justified by the fact that the values of β for the experimental model were much greater than one. The lowest value of β encountered was eighty. Previous analysis showed that the approximation of quasi-steady flow to describe the process would result in a negligible error. The values of the discharge coefficient, C_D, were also assumed to remain constant during the discharge process. This resulted in the determination of a mean value of the discharge coefficient for the entire transient run. Previous analysis, see FIG. 17, indicated that this was a valid approximation provided the value of the Reynolds number based on the discharge opening diameter and velocity was not too low. Calculations based on the idealized flow equations predicted that the Reynolds number to be encountered in the experiments would be on the flat section of the C_D

versus Reynolds number curve shown by FIG. 17.

Subsequent comparisons of the raw data and the least squares curve, based on the assumption of quasi-steady flow and constant discharge coefficient, showed negligible deviation of individual raw data points from the least squares curve.

The equation for the instantaneous fluid height, y, as a function of time is given by

$$y = h - \frac{1}{\beta}\left[2g\ (h + \Delta P/\rho g) \right]^{\frac{1}{2}} + \frac{1}{\beta^2}\frac{gt^2}{2} \qquad (30)$$

and when the discharge coefficient, C_D, is introduced it becomes

$$y = h - \frac{C_D}{\beta}\left[2g(h + \Delta P/\rho g) \right]^{\frac{1}{2}} + \frac{C_D^2}{\beta^2}\frac{gt^2}{2} \qquad (31)$$

This equation was used, in conjunction with experimental data, to determine the values of C_D. Substitutions were made to simplify equation (31) for computational purposes. New variables were defined as follows

$$B = \frac{C_D}{\beta}\sqrt{g/2} \qquad (32)$$

and

$$S = (h + \Delta P/\rho g)^{\frac{1}{2}} \qquad (33)$$

With these terms, equation (31) is written as

$$y = h - 2SBt + B^2t^2 \qquad (34)$$

For a given initial fluid height and external pressure drop, h and s were constants. The values for instantaneous fluid height, y, and time, t, constituted the experimental data. With this information available it was possible to determine B using the method of least squares. The details of this procedure are outlined in Appendix D. When B had been determined, the value of C_D could be obtained, since it is

$$C_D = B \cdot \beta \sqrt{\frac{2}{g}} \tag{35}$$

The mass flow rate could be determined, because it is the product of the discharge area, discharge velocity, and discharge coefficient. All of these values had been determined.

$$\dot{m} = C_D \cdot a \cdot \frac{dy}{dt} \left(\frac{A}{a}\right) \tag{36}$$

After the actual instantaneous heights and the instantaneous mass flow rates had been determined, they were reduced to the appropriate non-dimensional forms as given by equations (18) and (19).

While the case of liquid discharge through an opening was studied in analyzing the possible flow situations, and thus insight gained of the discharge process, in practice, orifice flow was encountered in few experimental situations. The fluid was found to fill the discharge area for all ratios of L/d greater than 1.33 except for high values of the

discharge Reynolds number. For values of the L/d ratio greater than two, no cases of orifice flow were encountered. Thus, the primary interest in the experiments centered on the process of liquid discharge through a tube.

Values of discharge coefficient were determined for various L/d ratios from two to two hundred fifty and Reynolds numbers in the range of 1.6×10^4 to 3.5×10^5. Typical experimental values of C_D are shown superimposed on theoretical values obtained from equation (29), see FIG. 31.

Results of Surface Height Measurements

Experiments to determine instantaneous fluid heights in the container were conducted using the methods discussed previously. A series of experiments was conducted varying each geometric factor and the external pressure drop independently. These data were then reduced to non-dimensional form. The results of non-dimensional height versus time measurements are shown by FIG. 32 through FIG. 62. Individual raw data points are shown on these figures.

The fluid height versus time measurements were then fit to curves using the method of least squares. This resulted in sets of emperical equations which expressed instantaneous fluid height as a function of time. These equations were differentiated in order to determine instantaneous fluid velocities. The instantaneous mass flow rate was then computed and non-dimensionalized. The resulting curves are shown in FIG. 33 through FIG. 63.

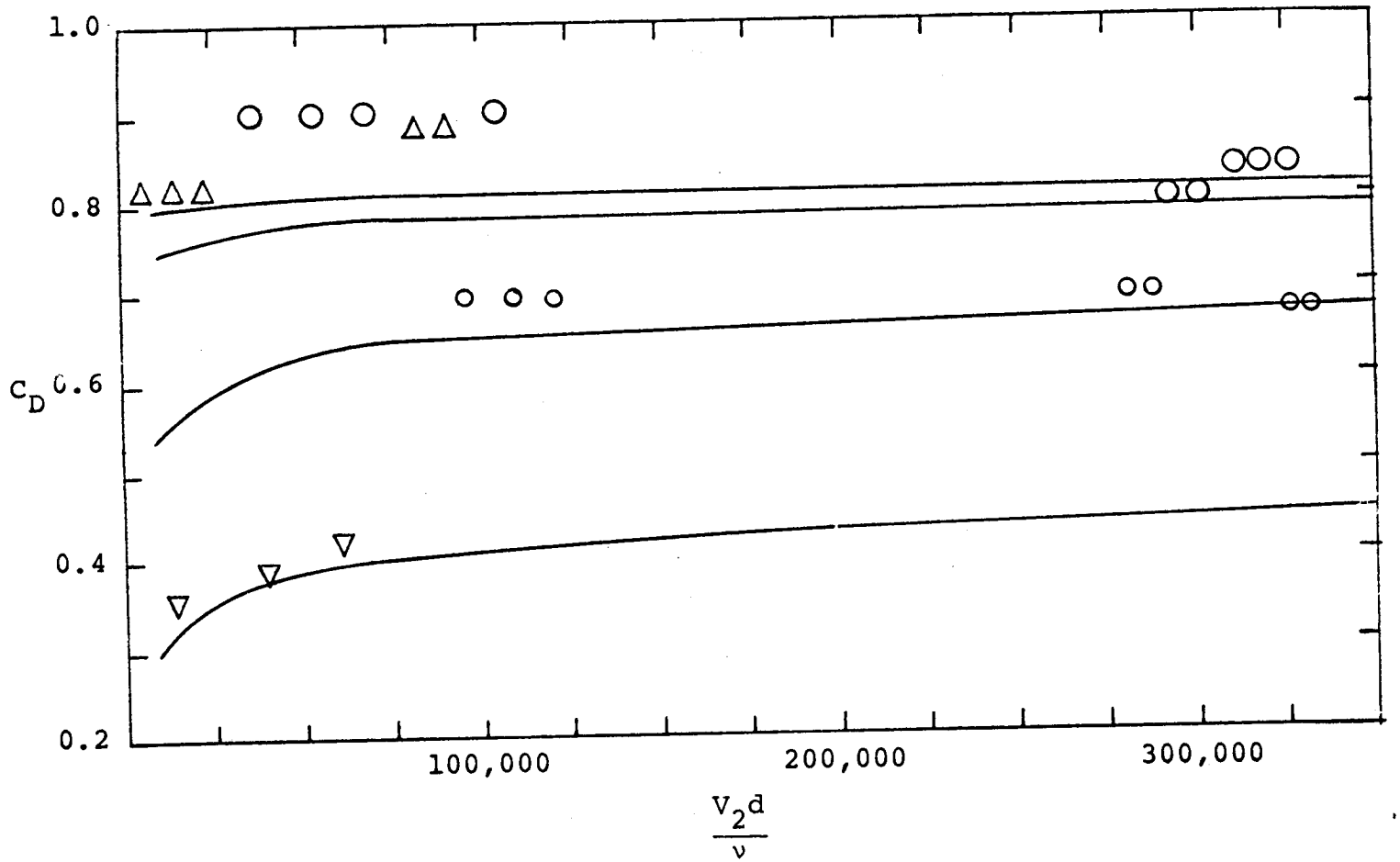

Experimental Measurements				
Symbol	O	Δ	o	∇
L/d	2.0	8.0	52.0	257.52

FIG. 31 EXPERIMENTALLY DETERMINED VALUES OF DISCHARGE COEFFICIENT FOR VARIOUS VALUES OF L/d AND REYNOLDS NUMBER. SOLID LINES ARE THEORETICAL PREDICTIONS (SEE FIG. 17).

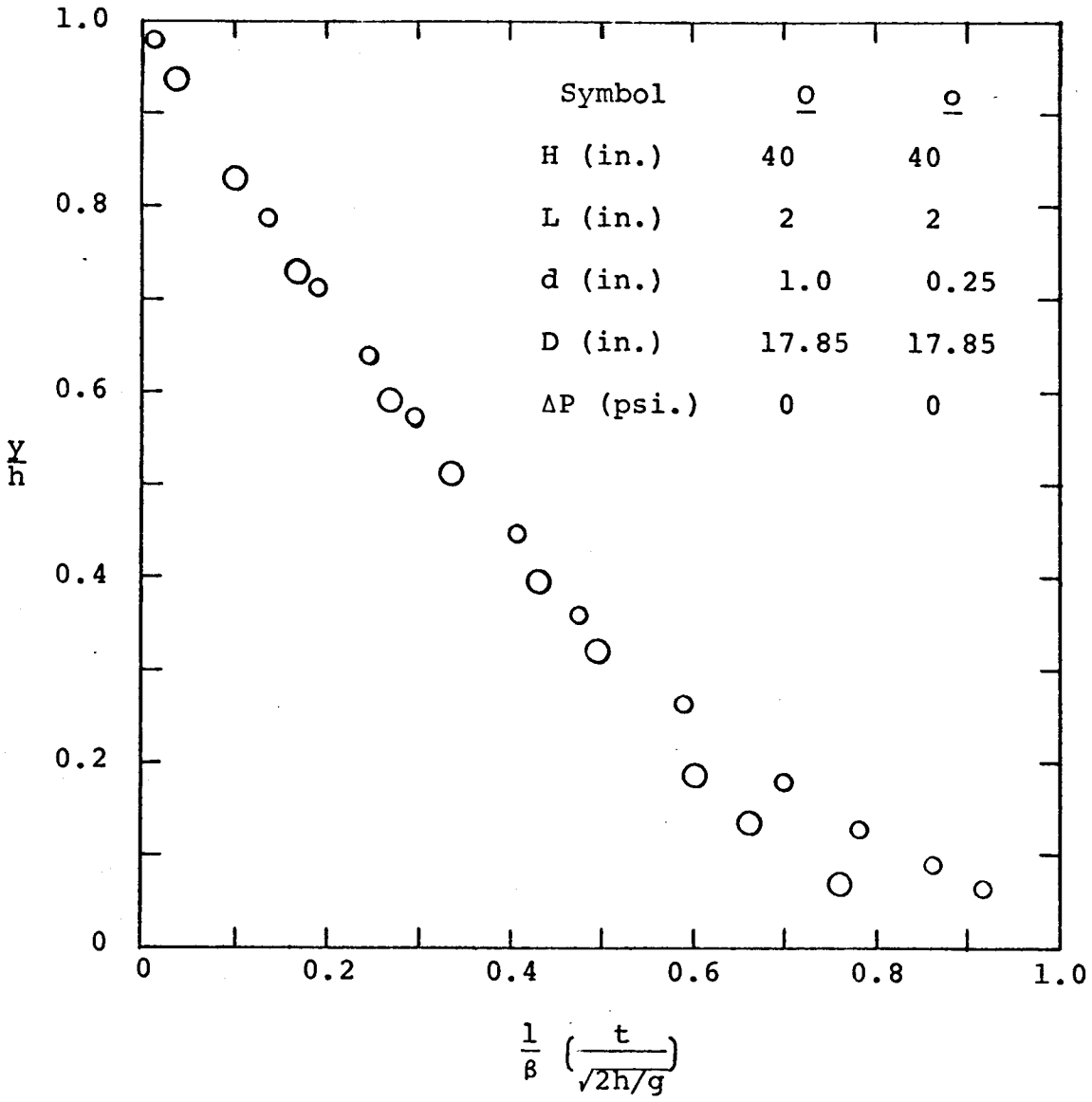

FIG. 32[1]

1. FIG. 32 through FIG. 63 are plots of experimental data. The figures represent dimensionless heights, y/h versus dimensionless times, $\frac{1}{\beta}\left(\frac{t}{\sqrt{2h/g}}\right)$, and dimensionless mass flow rates $\sqrt{1-\left(\frac{a}{A}\right)^2}\cdot\left[\frac{\dot{m}}{\rho\left(\frac{\pi d^2}{4}\right)\sqrt{2gh}}\right]$ versus dimensionless time alternately. The values of the parameters are given in the legend of each figure.

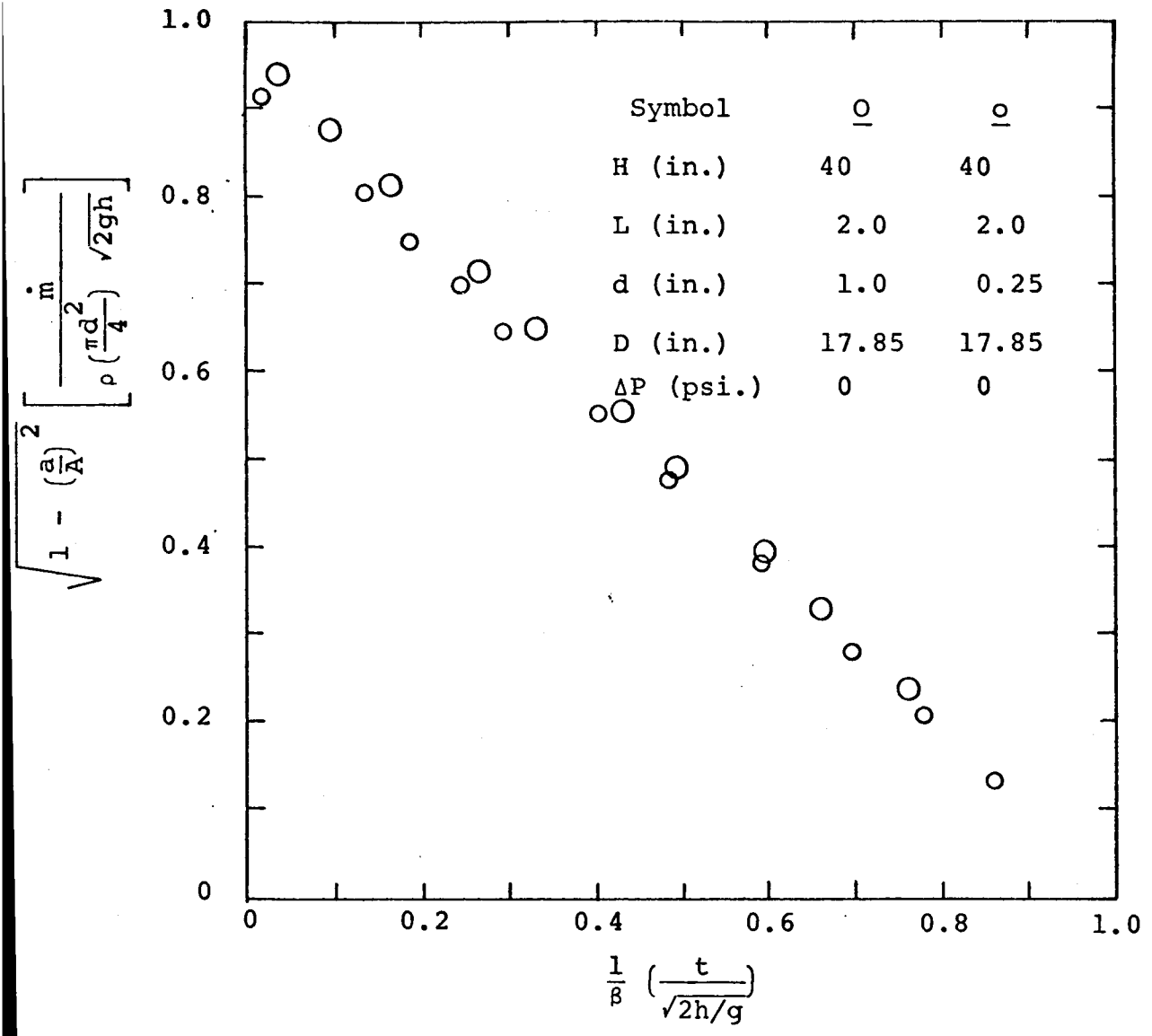
1.0
0.8
0.6
0.4
0.2
0
0
0.2
0.4
0.6
0.8
1.0
Symbol O o
H (in.) 40 40
L (in.) 2.0 2.0
d (in.) 1.0 0.25
D (in.) 17.85 17.85
ΔP (psi.) 0 0
$\frac{1}{\beta}\left(\frac{t}{\sqrt{2h/g}}\right)$
$\sqrt{1-\left(\frac{a}{A}\right)^2}\left[\frac{\dot{m}}{\rho\left(\frac{\pi d^2}{4}\right)\sqrt{2gh}}\right]$

FIG. 33

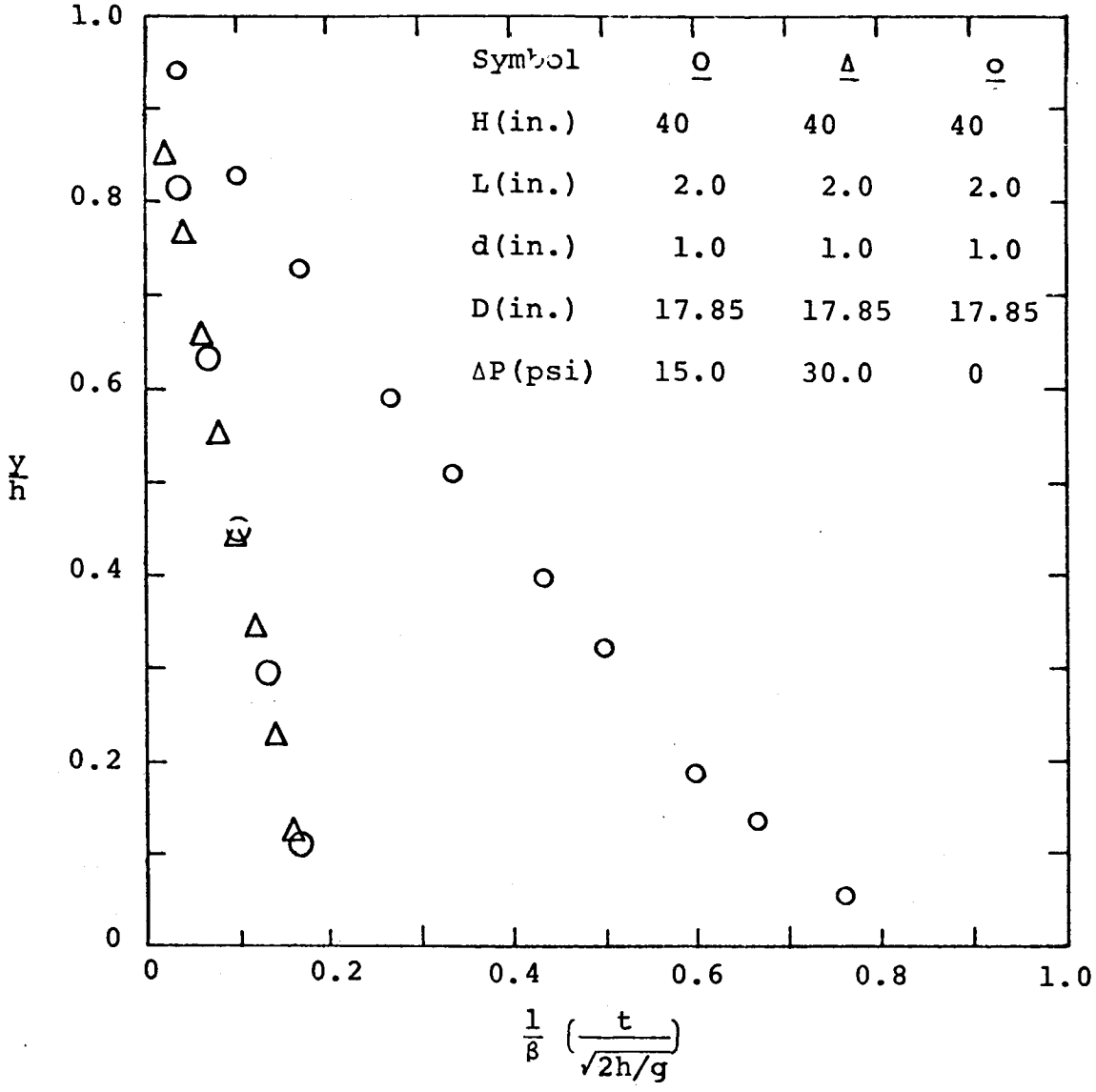
Symbol
H(in.) 40 40 40
L(in.) 2.0 2.0 2.0
d(in.) 1.0 1.0 1.0
D(in.) 17.85 17.85 17.85
ΔP(psi) 15.0 30.0 0
1.0
0.8
0.6
0.4
0.2
0
0
0.2
0.4
0.6
0.8
1.0
y/h
1/β (t/√2h/g)

FIG. 34

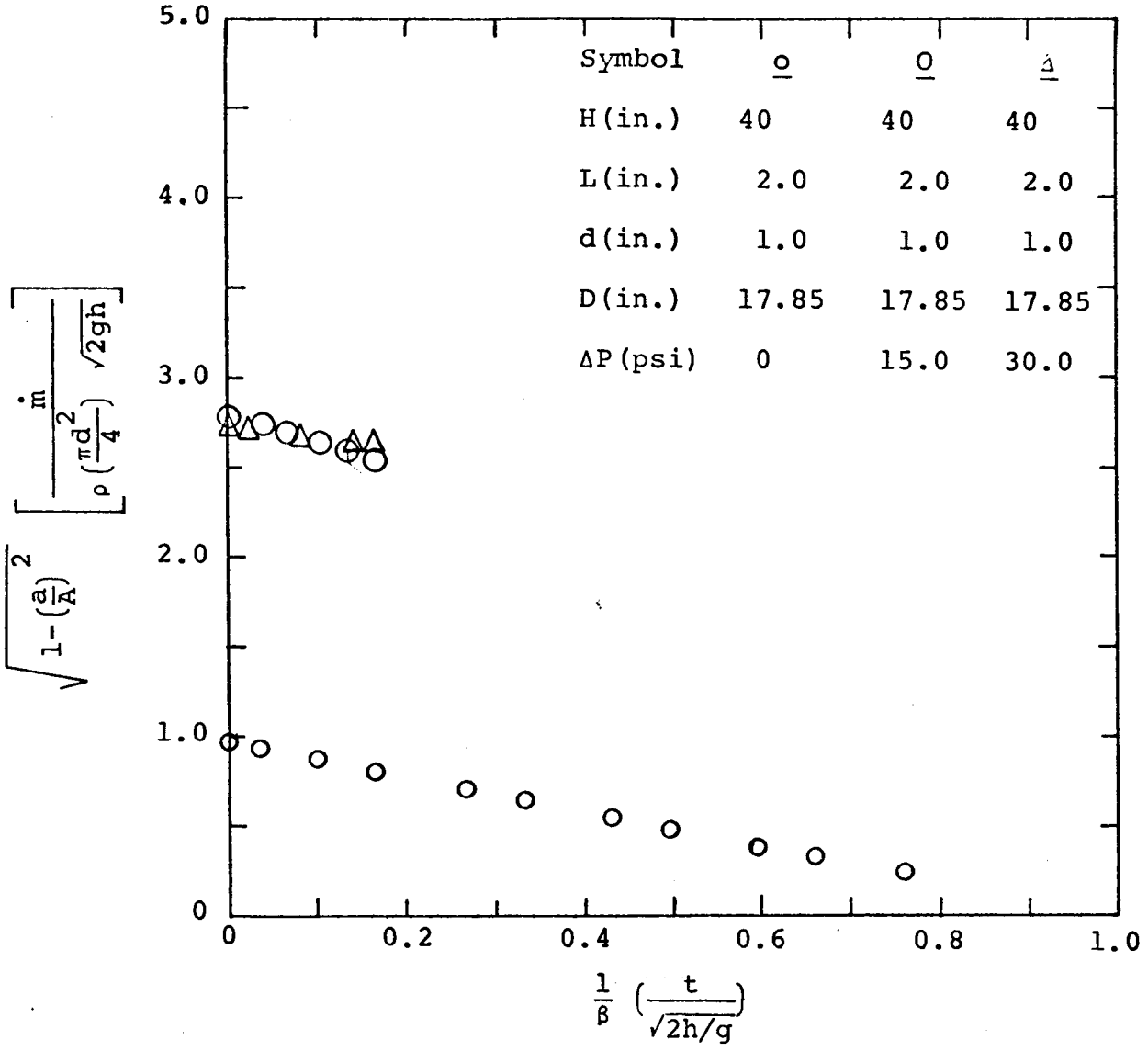
Symbol
H(in.)
L(in.)
d(in.)
D(in.)
ΔP(psi)
40
2.0
1.0
17.85
0
40
2.0
1.0
17.85
15.0
40
2.0
1.0
17.85
30.0
5.0
4.0
3.0
2.0
1.0
0
0
0.2
0.4
0.6
0.8
1.0
$\frac{\dot{m}}{\rho(\frac{\pi d^2}{4})\sqrt{2gh}}\sqrt{1-(\frac{a}{A})^2}$
$\frac{1}{\beta}\ (\frac{t}{\sqrt{2h/g}})$

FIG. 35

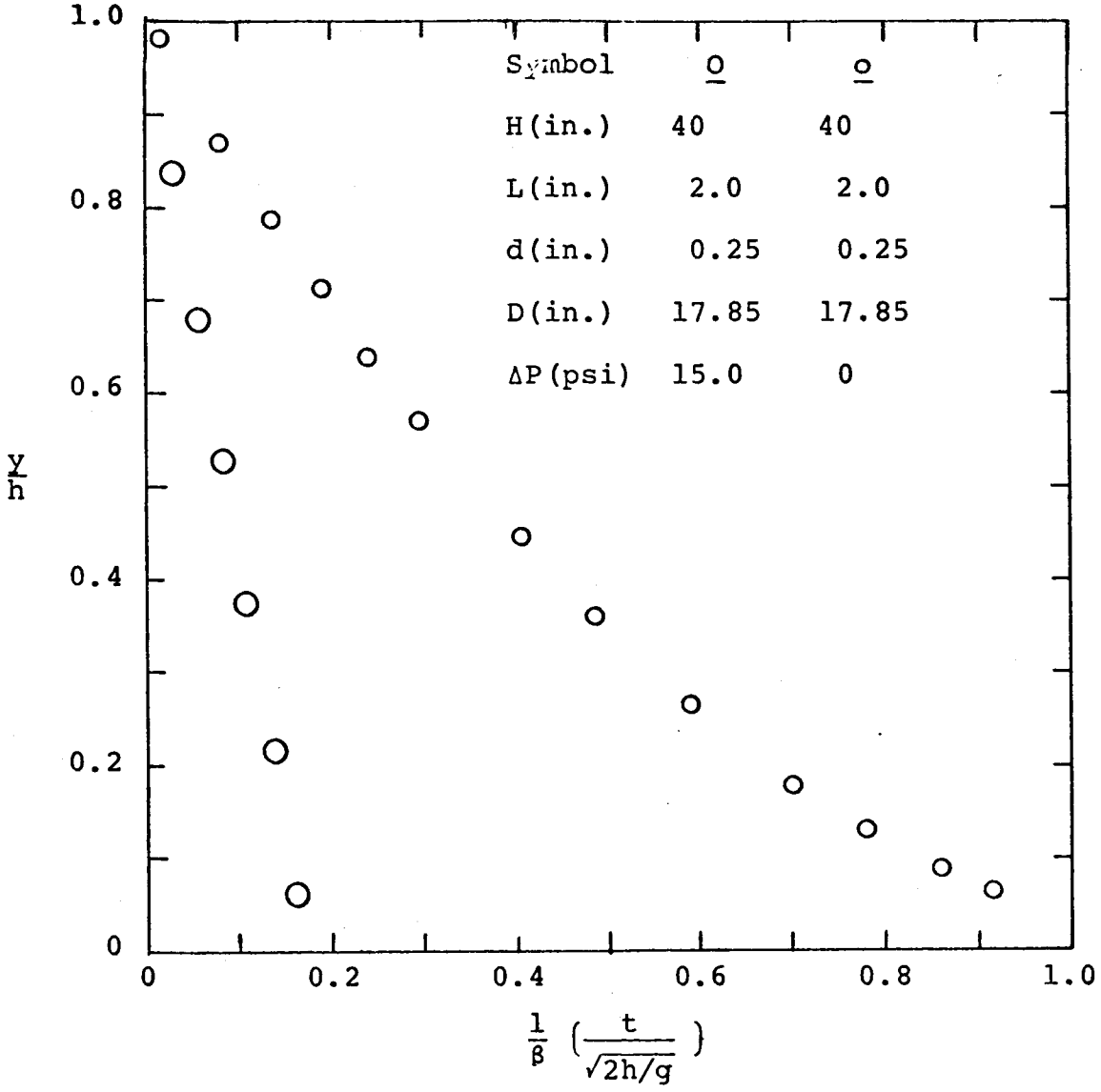
Symbol o o
H(in.) 40 40
L(in.) 2.0 2.0
d(in.) 0.25 0.25
D(in.) 17.85 17.85
ΔP(psi) 15.0 0
y/h
1.0
0.8
0.6
0.4
0.2
0
0 0.2 0.4 0.6 0.8 1.0
1/β (t/√2h/g)

FIG. 36

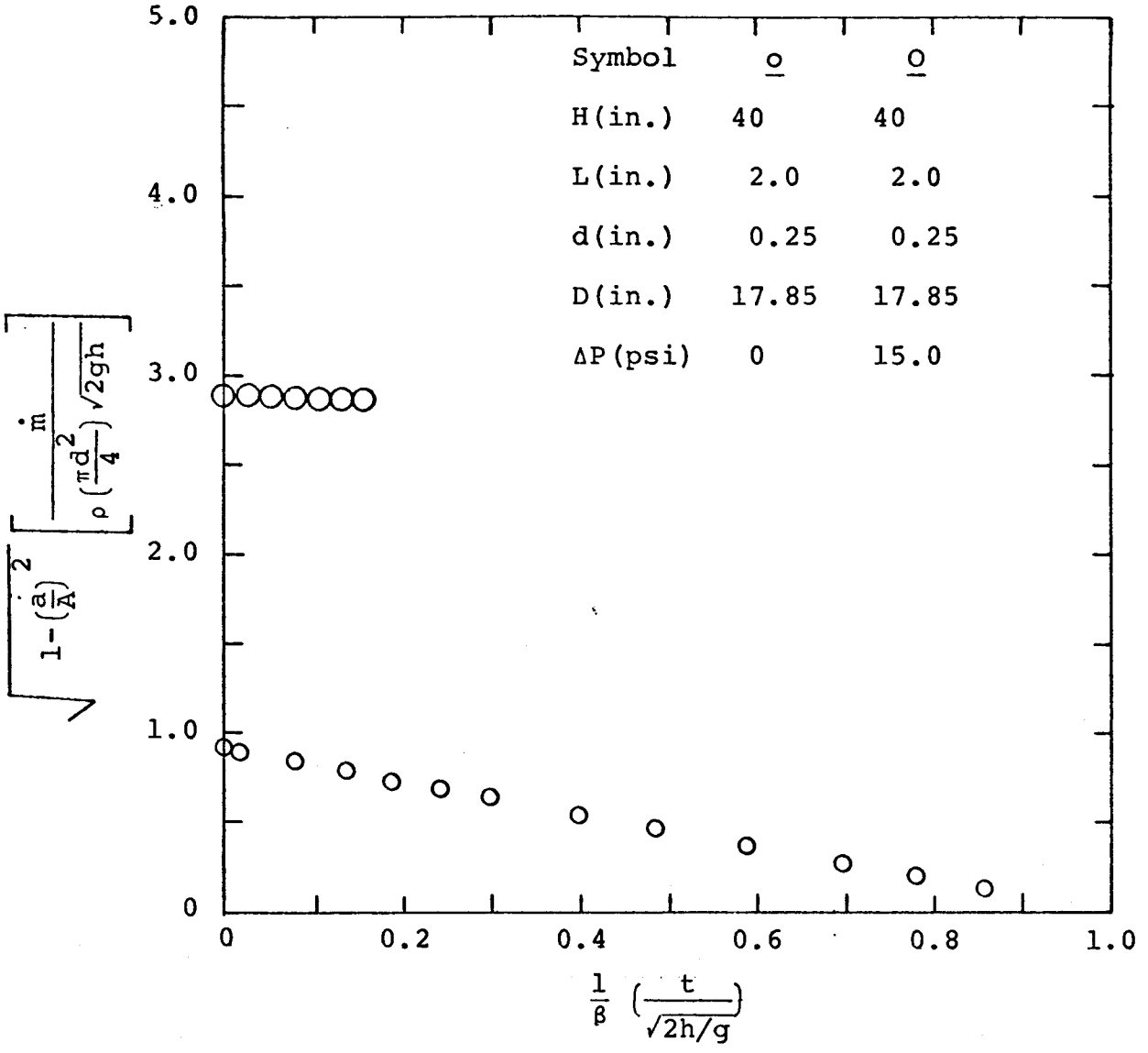
Symbol o O
H(in.) 40 40
L(in.) 2.0 2.0
d(in.) 0.25 0.25
D(in.) 17.85 17.85
ΔP(psi) 0 15.0
5.0
4.0
3.0
2.0
1.0
0
0
0.2
0.4
0.6
0.8
1.0
$\frac{\dot{m}}{\rho\left(\frac{\pi d^2}{4}\right)\sqrt{2gh}}\sqrt{1-\left(\frac{a}{A}\right)^2}$
$\frac{1}{\beta}\left(\frac{t}{\sqrt{2h/g}}\right)$

FIG. 37

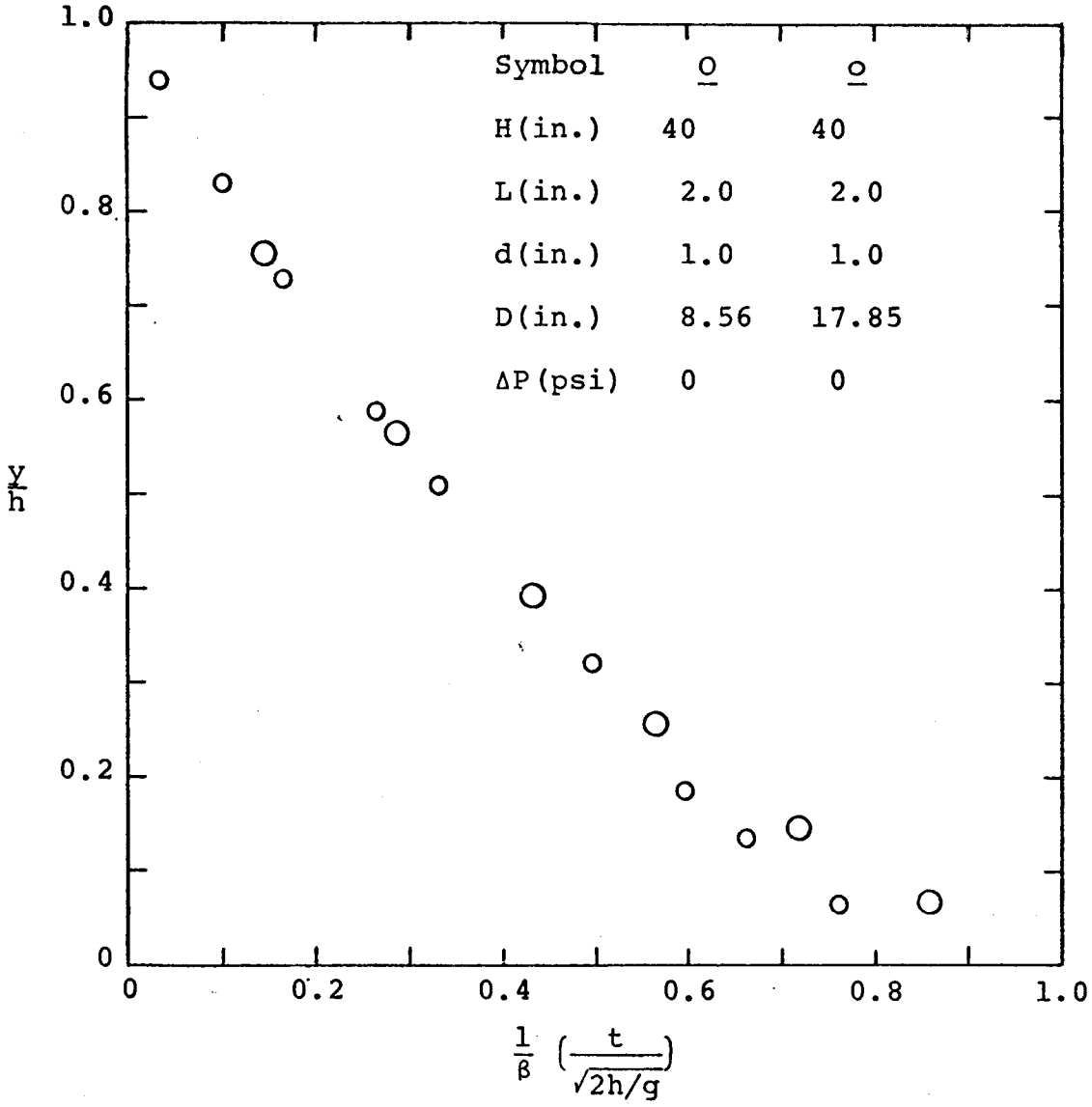
Symbol o o
H(in.) 40 40
L(in.) 2.0 2.0
d(in.) 1.0 1.0
D(in.) 8.56 17.85
ΔP(psi) 0 0
y/h
1.0
0.8
0.6
0.4
0.2
0
0 0.2 0.4 0.6 0.8 1.0
1/β (t/√2h/g)

FIG. 38

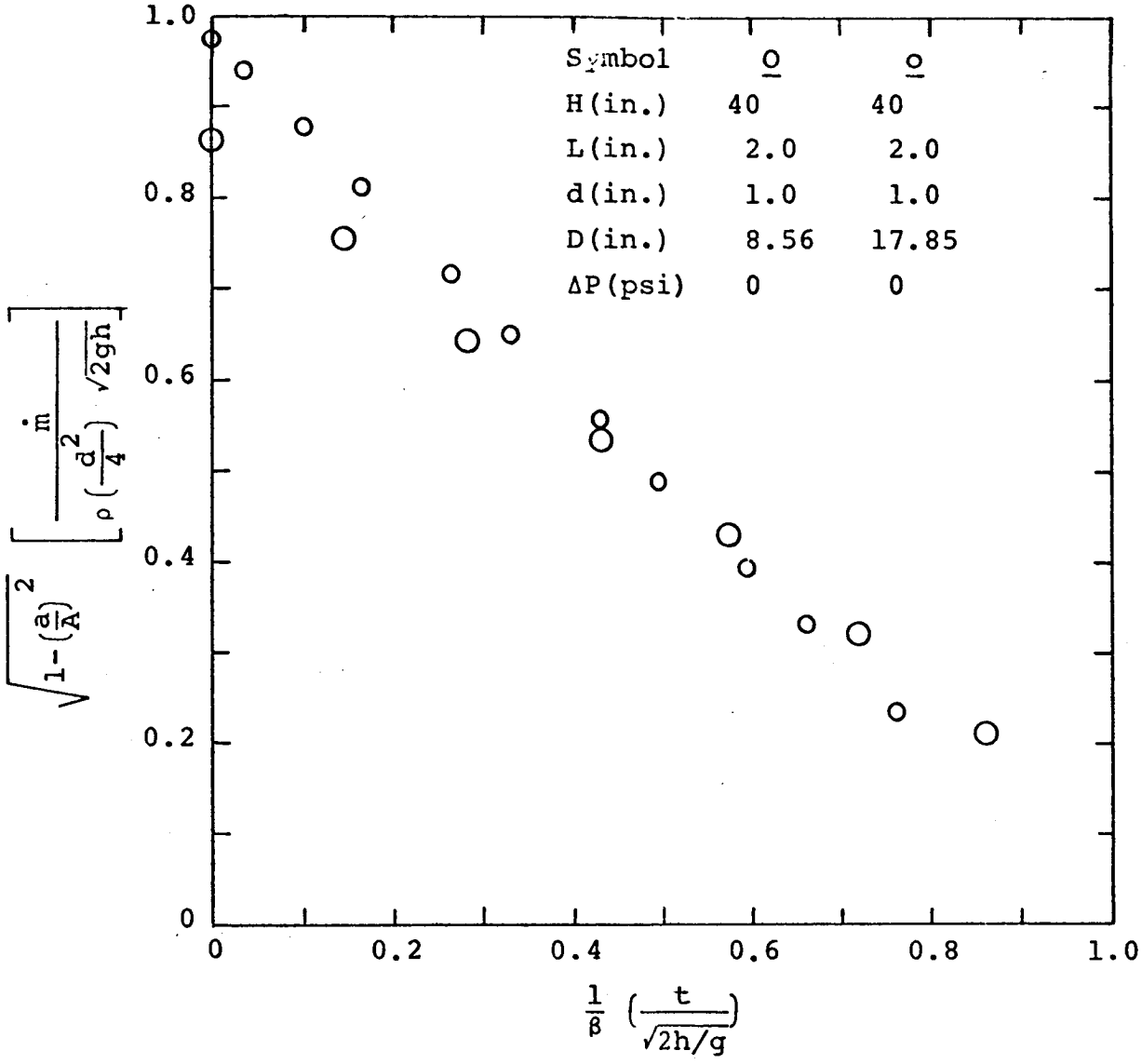
Symbol
H(in.) 40 40
L(in.) 2.0 2.0
d(in.) 1.0 1.0
D(in.) 8.56 17.85
ΔP(psi) 0 0
1.0
0.8
0.6
0.4
0.2
0
0
0.2
0.4
0.6
0.8
1.0
$\sqrt{1-(\frac{a}{A})^2}\left[\frac{\dot{m}}{\rho(\frac{d^2}{4})\sqrt{2gh}}\right]$
$\frac{1}{\beta}\left(\frac{t}{\sqrt{2h/g}}\right)$

FIG. 39

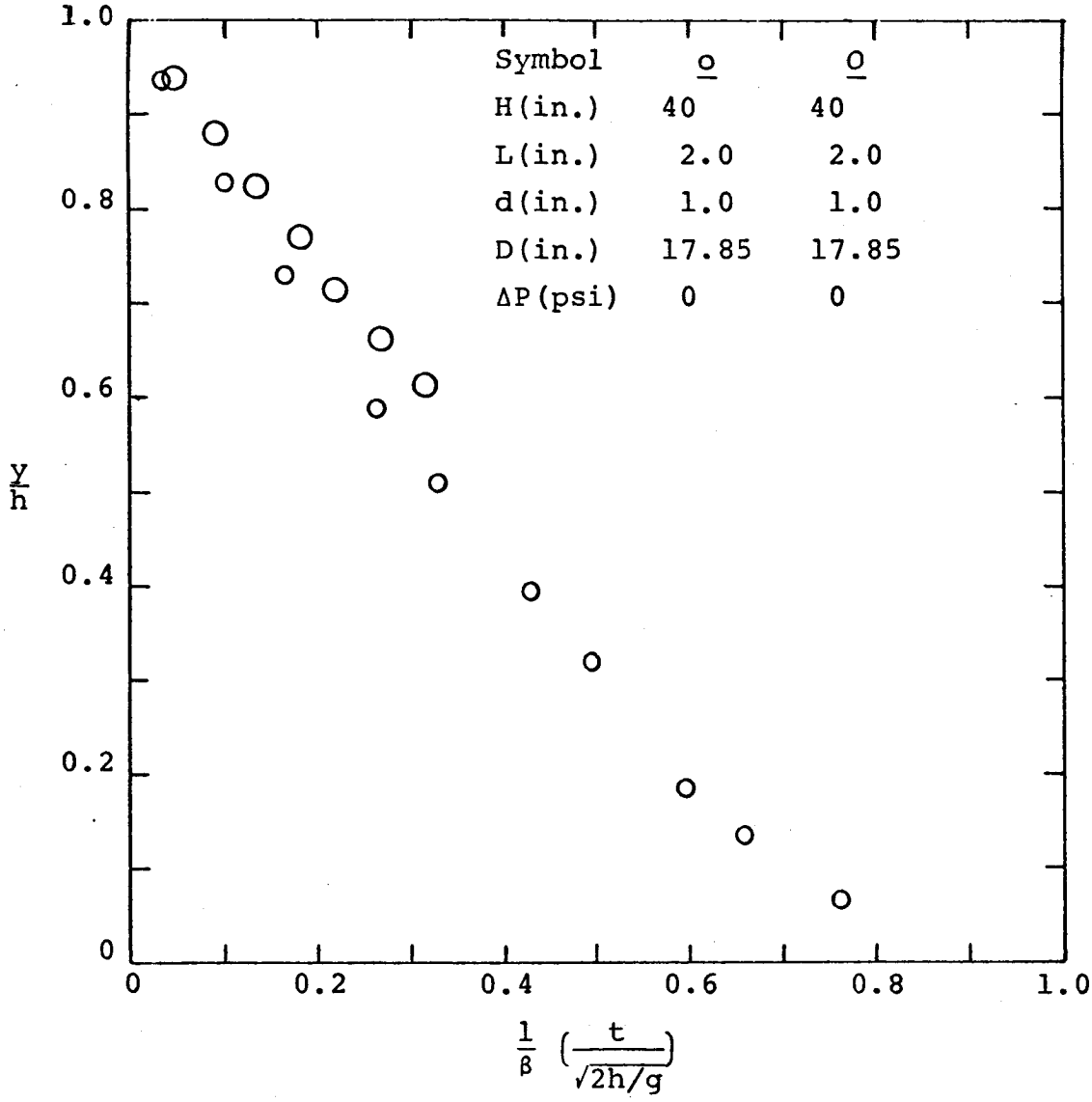
Symbol o O
H(in.) 40 40
L(in.) 2.0 2.0
d(in.) 1.0 1.0
D(in.) 17.85 17.85
ΔP(psi) 0 0
y/h
1.0
0.8
0.6
0.4
0.2
0
0
0.2
0.4
0.6
0.8
1.0
1/β (t/√2h/g)

FIG. 40

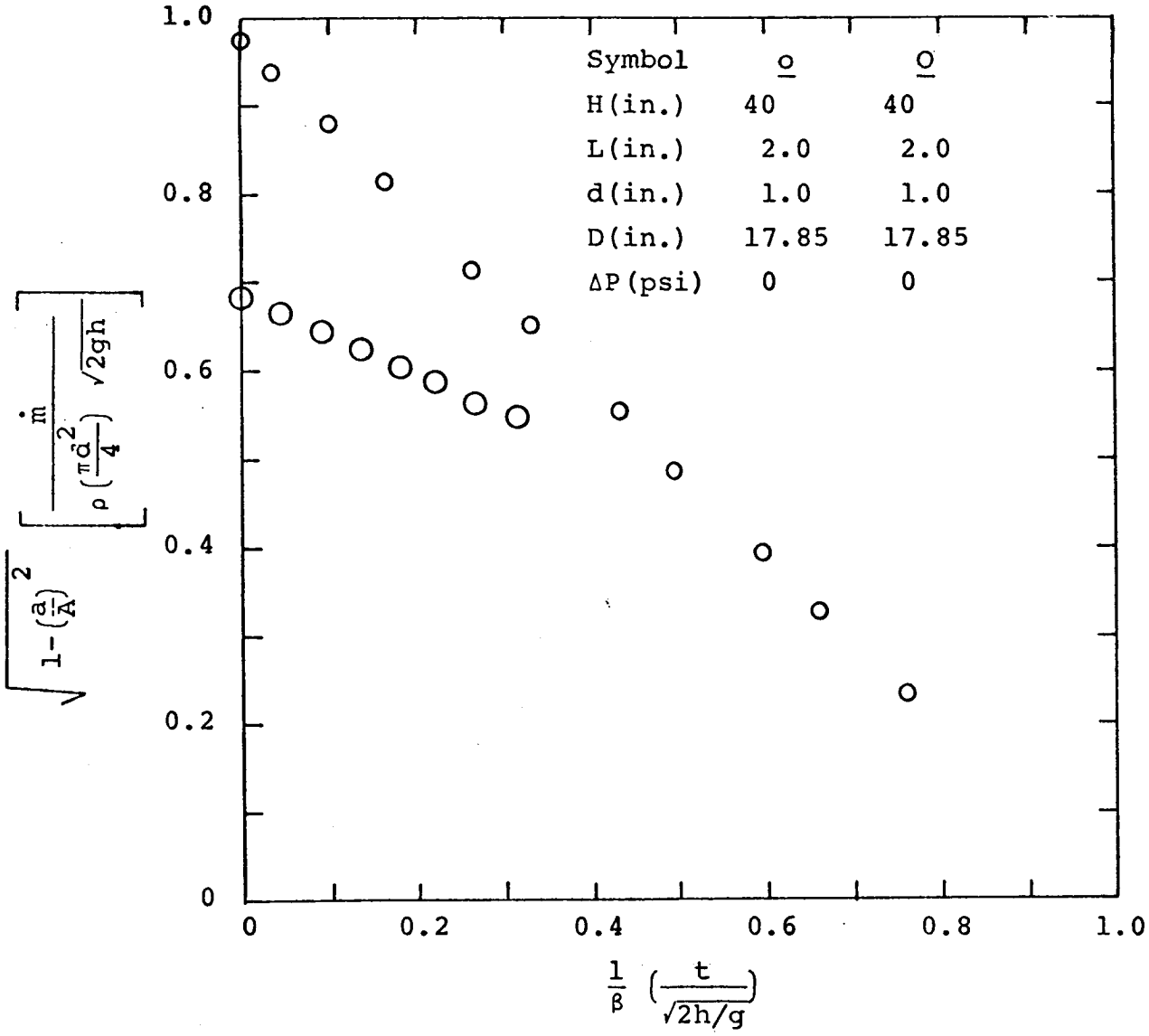
Symbol o O
H(in.) 40 40
L(in.) 2.0 2.0
d(in.) 1.0 1.0
D(in.) 17.85 17.85
ΔP(psi) 0 0
1.0
0.8
0.6
0.4
0.2
0
0 0.2 0.4 0.6 0.8 1.0
$\sqrt{1-(\frac{a}{A})^2}\left[\frac{\dot{m}}{\rho(\frac{\pi d^2}{4})\sqrt{2gh}}\right]$
$\frac{1}{\beta}\left(\frac{t}{\sqrt{2h/g}}\right)$

FIG. 41

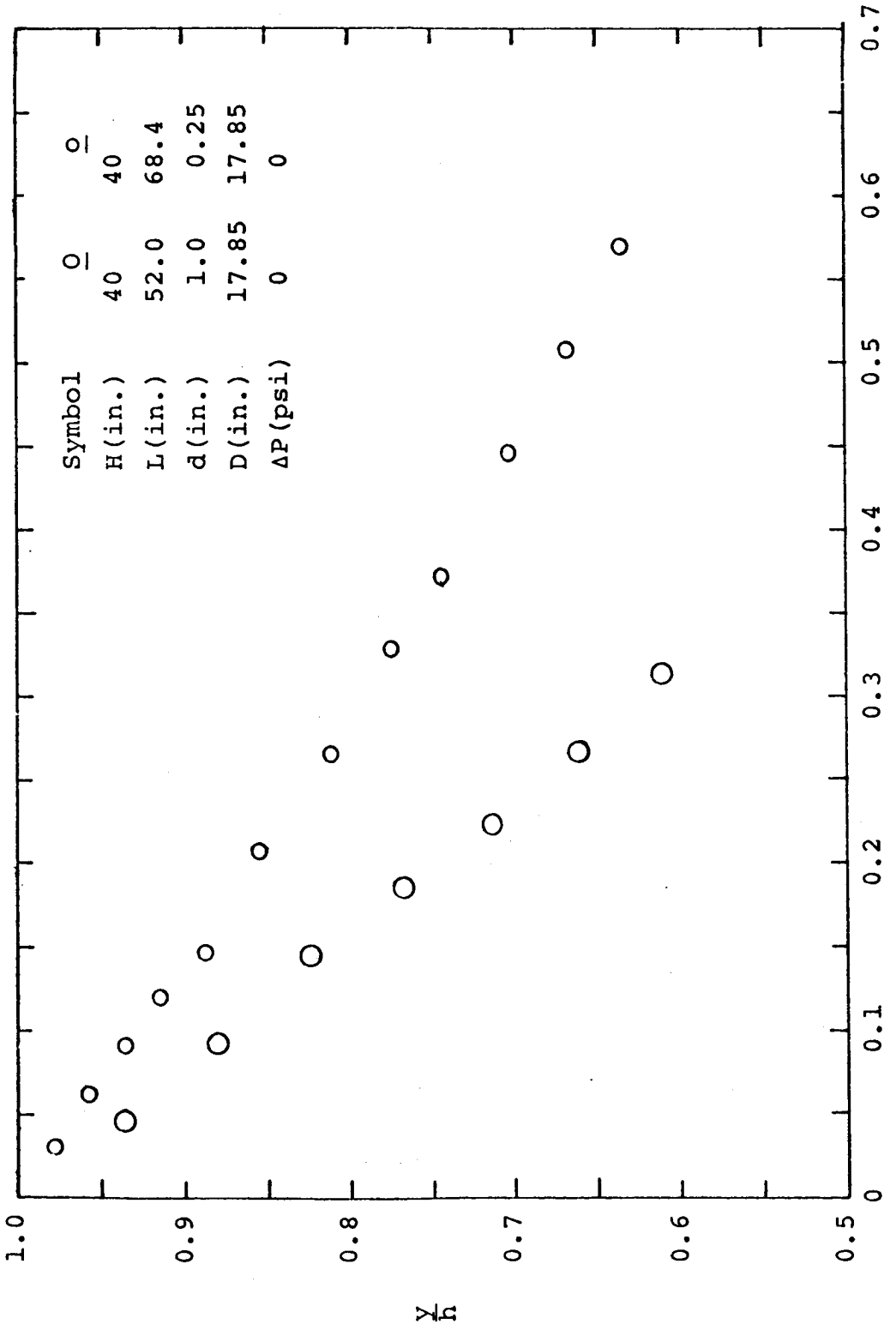
Symbol
H(in.)
L(in.)
d(in.)
D(in.)
ΔP(psi)
40
52.0
1.0
17.85
0
40
68.4
0.25
17.85
0
y/h
1.0
0.9
0.8
0.7
0.6
0.5
0
0.1
0.2
0.3
0.4
0.5
0.6
0.7
1/β (t/√(2h/g))

FIG. 42

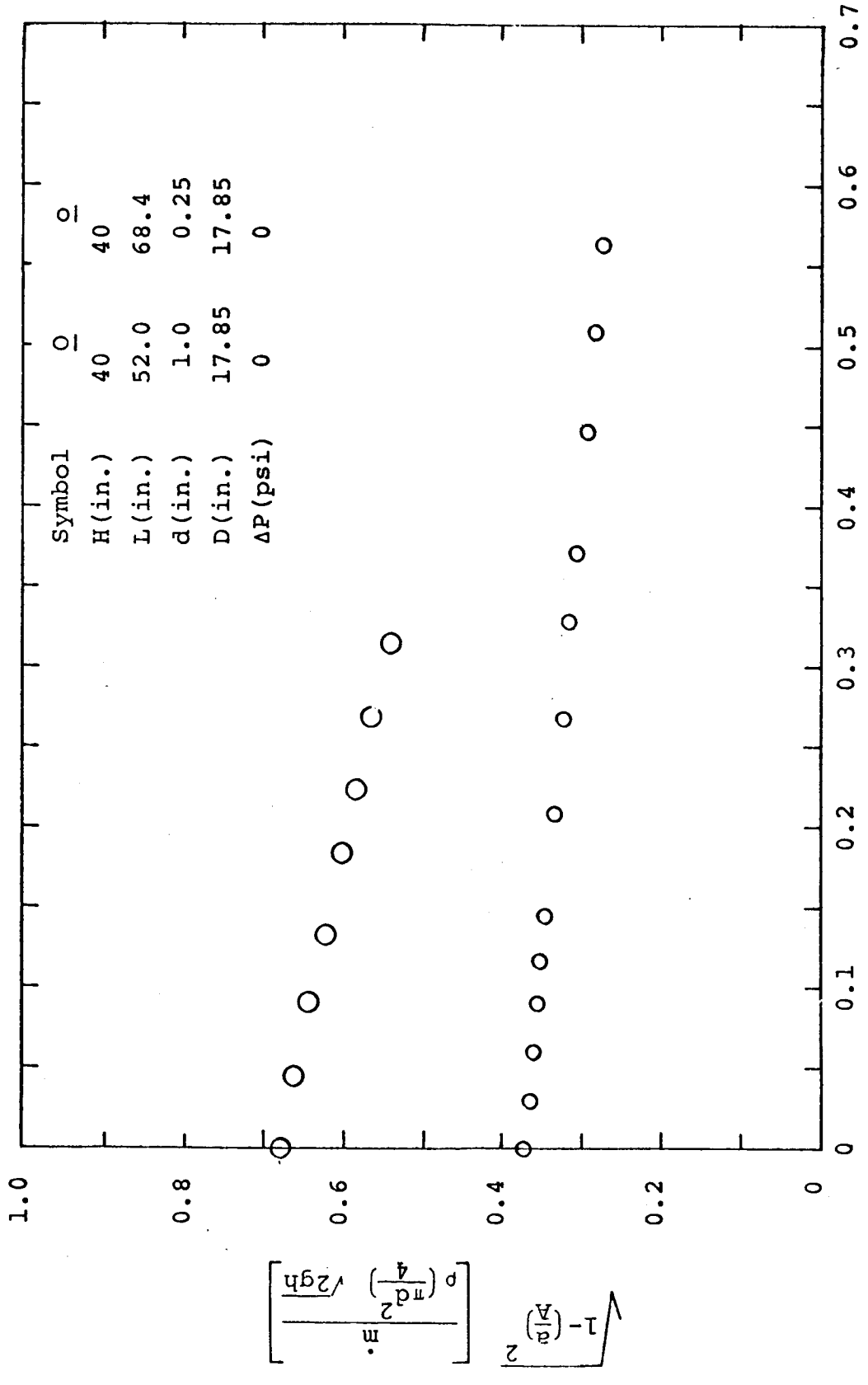
Symbol
H(in.)
L(in.)
d(in.)
D(in.)
ΔP(psi)
40
52.0
1.0
17.85
0
40
68.4
0.25
17.85
0
0
0.1
0.2
0.3
0.4
0.5
0.6
0.7
0.2
0.4
0.6
0.8
1.0

FIG. 43

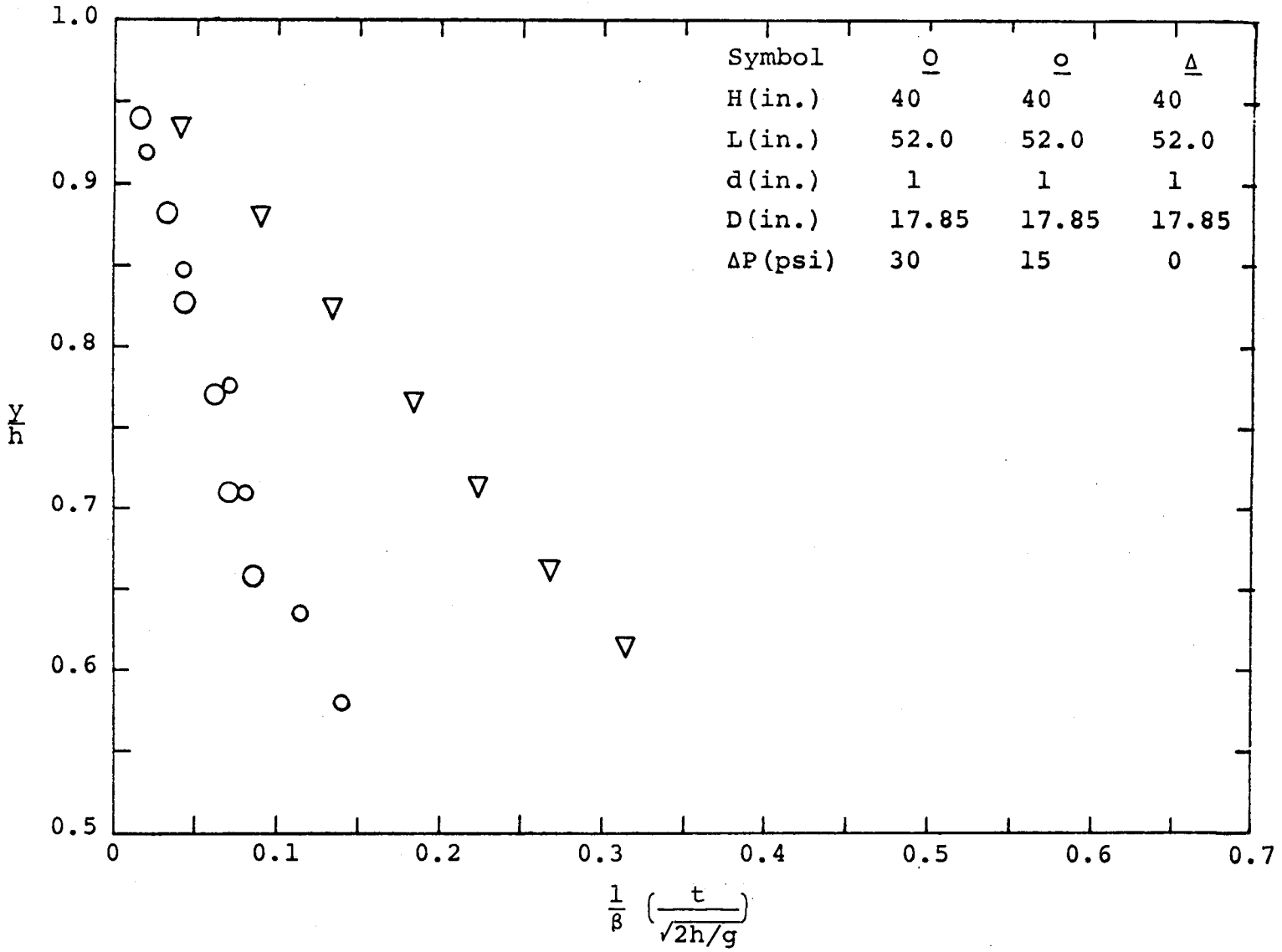
1.0
0.9
0.8
0.7
0.6
0.5
0
0.1
0.2
0.3
0.4
0.5
0.6
0.7
y/h
1/β (t/√2h/g)
Symbol
H(in.)
L(in.)
d(in.)
D(in.)
ΔP(psi)
40
52.0
1
17.85
30
40
52.0
1
17.85
15
40
52.0
1
17.85
0

FIG. 44

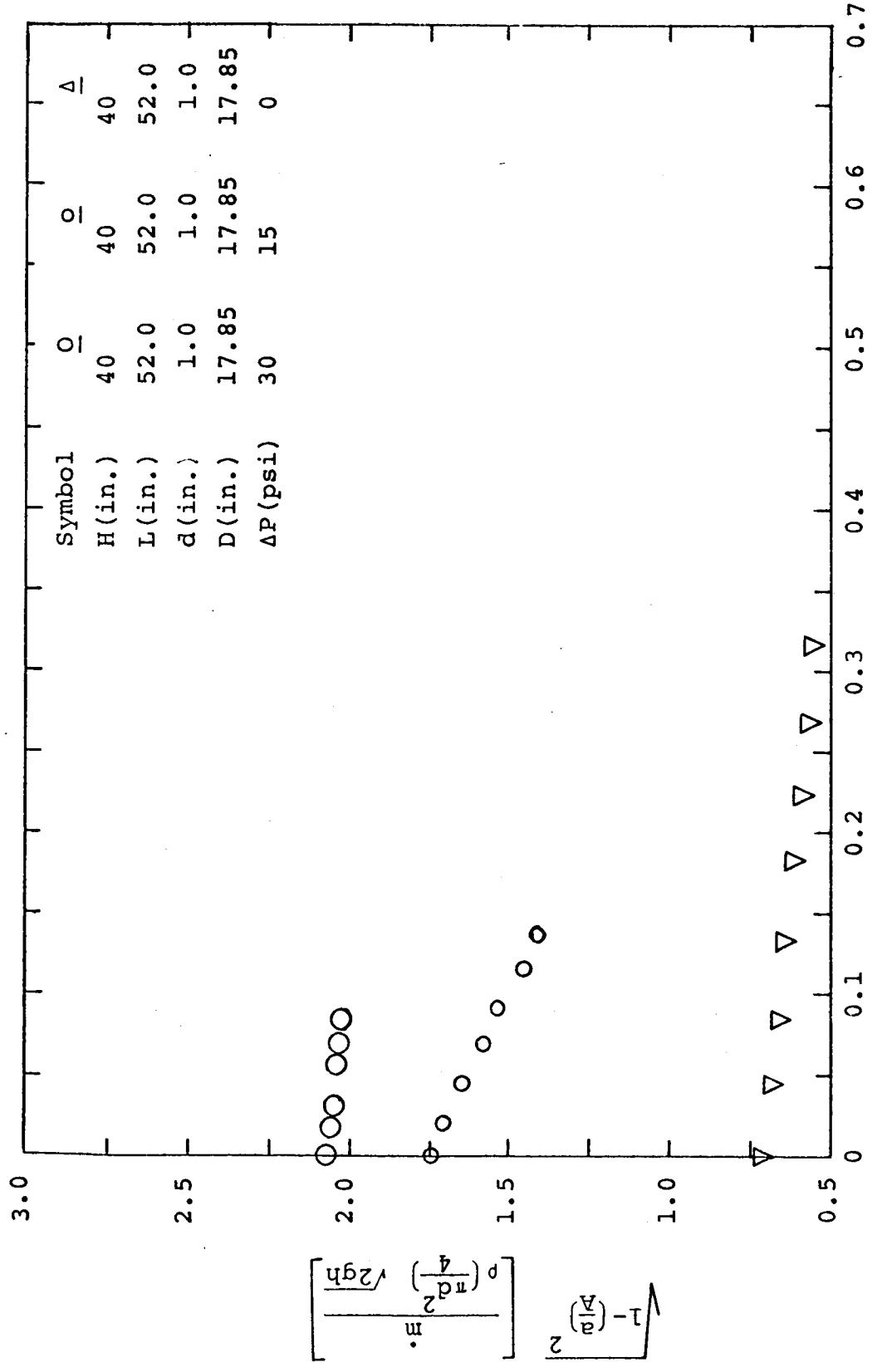
Symbol
H(in.)
L(in.)
d(in.)
D(in.)
ΔP(psi)
40
52.0
1.0
17.85
30
40
52.0
1.0
17.85
15
40
52.0
1.0
17.85
0
3.0
2.5
2.0
1.5
1.0
0.5
0
0.1
0.2
0.3
0.4
0.5
0.6
0.7
$\frac{1}{\beta}\left(\frac{t}{\sqrt{2h/g}}\right)$
$\sqrt{1-\left(\frac{a}{A_1}\right)^2}\left[\frac{\dot{m}}{\rho\left(\frac{\pi d^2}{4}\right)\sqrt{2gh}}\right]$

FIG. 45

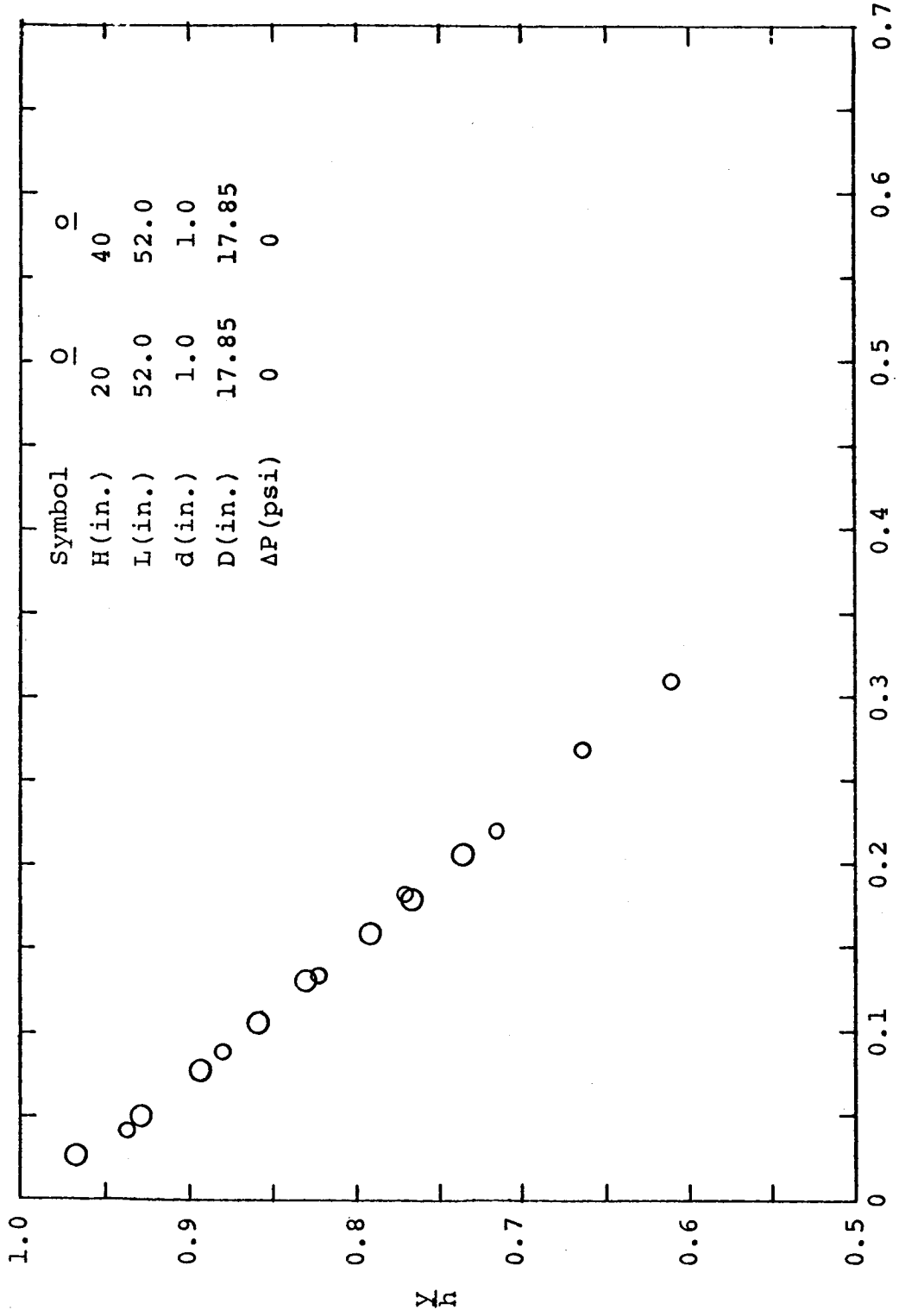
Symbol
H(in.)
L(in.)
d(in.)
D(in.)
ΔP(psi)
20
52.0
1.0
17.85
0
40
52.0
1.0
17.85
0
Y/h
1.0
0.9
0.8
0.7
0.6
0.5
0
0.1
0.2
0.3
0.4
0.5
0.6
0.7
1/β (t/√2h/g)

FIG. 46

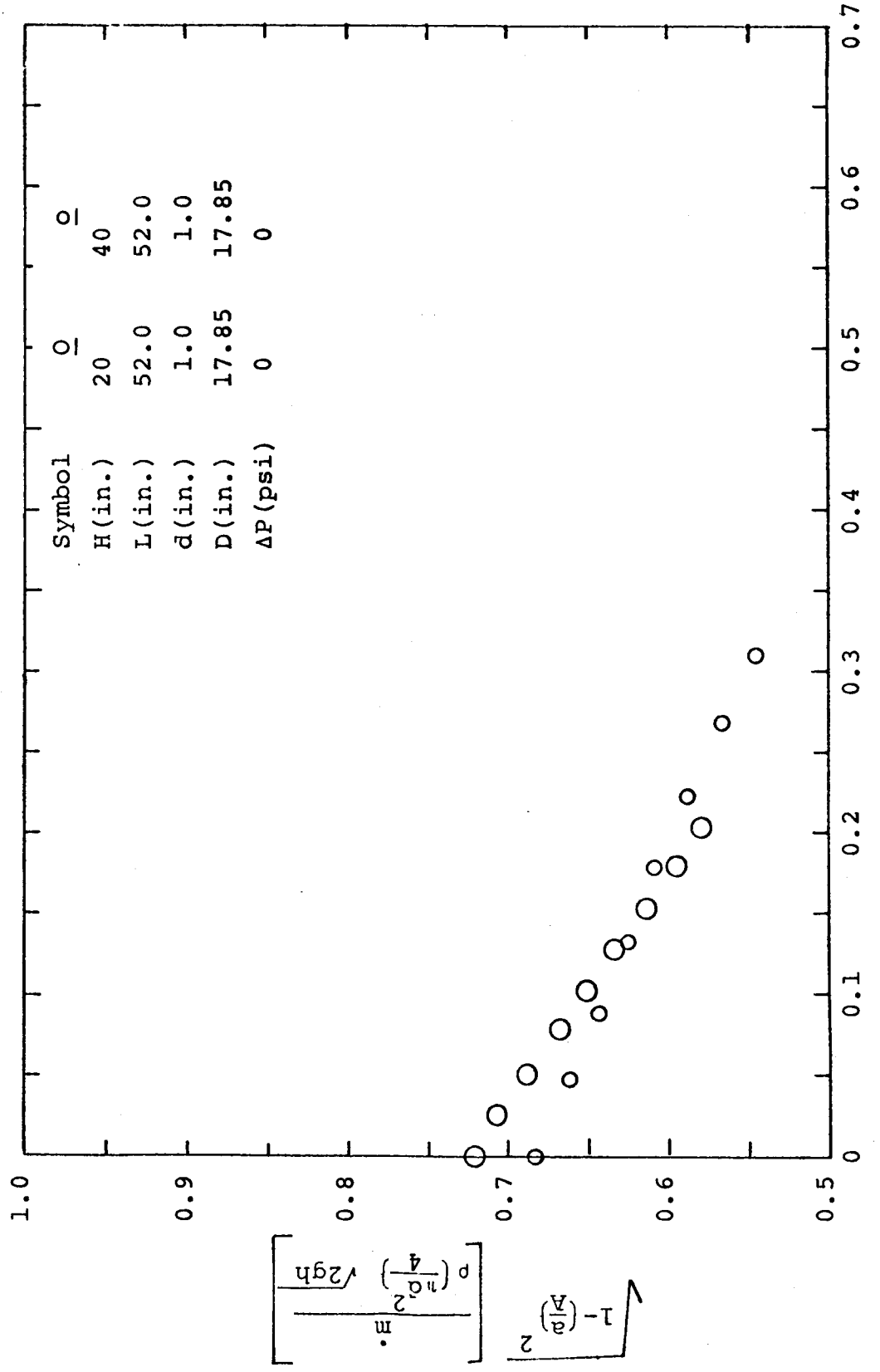
Symbol
H(in.)
L(in.)
d(in.)
D(in.)
ΔP(psi)
20
52.0
1.0
17.85
0
40
52.0
1.0
17.85
0
1.0
0.9
0.8
0.7
0.6
0.5
0
0.1
0.2
0.3
0.4
0.5
0.6
0.7
$\frac{1}{\beta}\left(\frac{t}{\sqrt{2h/g}}\right)$
$\sqrt{1-\left(\frac{a}{A}\right)^2}$
$\left[\frac{\dot{m}}{\rho\left(\frac{\pi a^2}{4}\right)\sqrt{2gh}}\right]$

FIG. 47

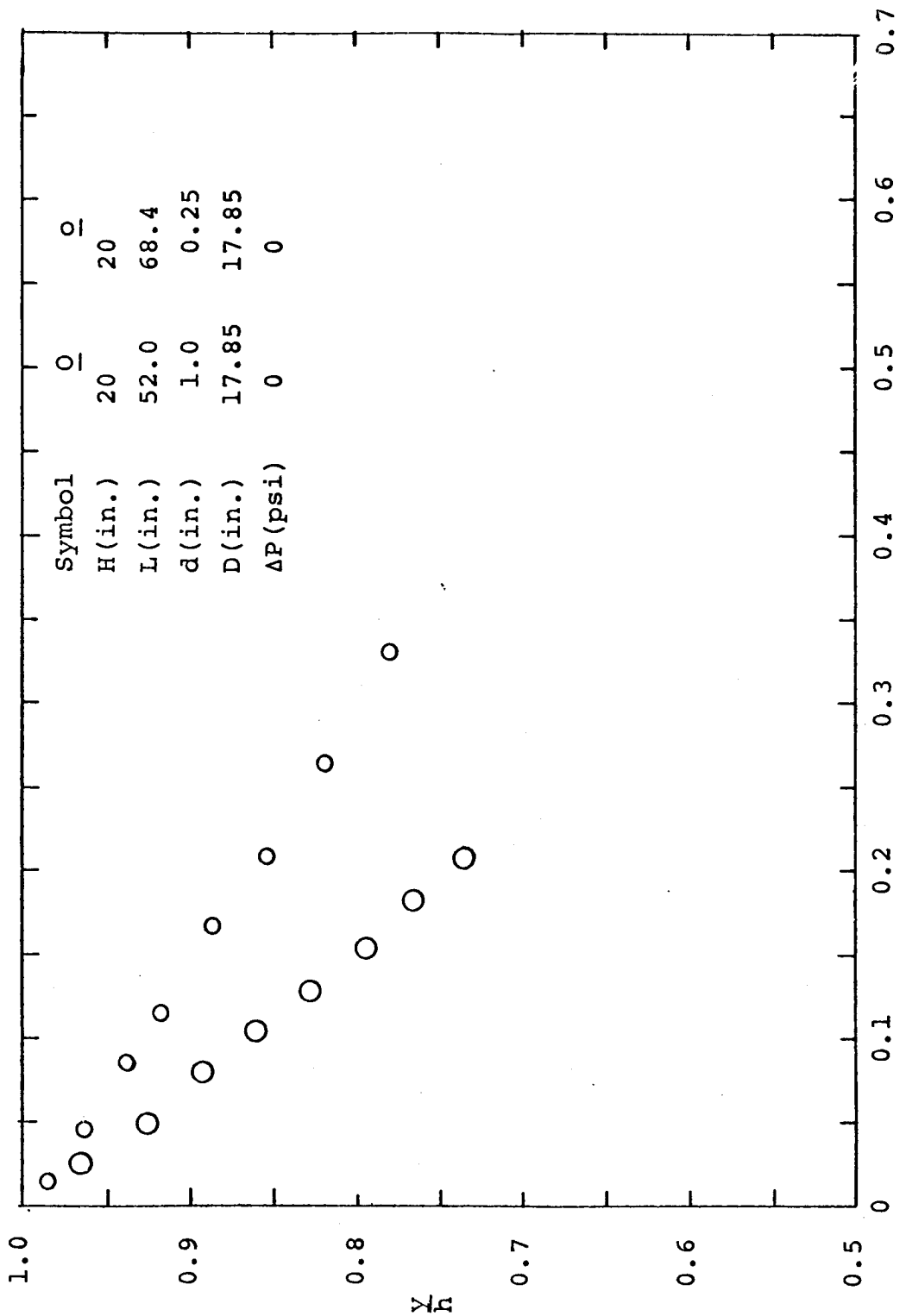
Symbol
H(in.)
L(in.)
d(in.)
D(in.)
ΔP(psi)
20
52.0
1.0
17.85
0
20
68.4
0.25
17.85
0
y/h
1.0
0.9
0.8
0.7
0.6
0.5
0
0.1
0.2
0.3
0.4
0.5
0.6
0.7
1/β (t/√2h/g)

FIG. 48

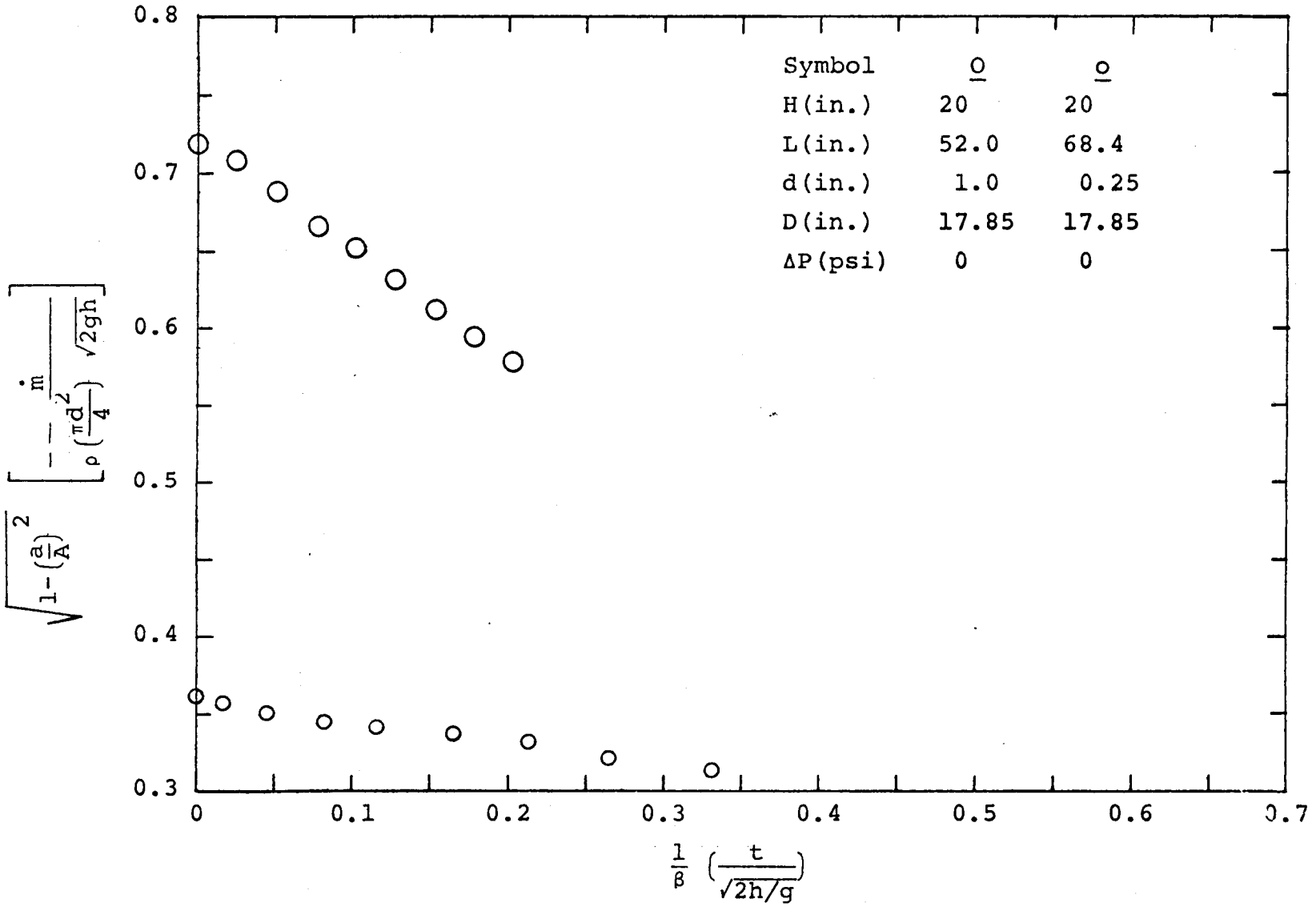
Symbol O o
H(in.) 20 20
L(in.) 52.0 68.4
d(in.) 1.0 0.25
D(in.) 17.85 17.85
ΔP(psi) 0 0
0.8
0.7
0.6
0.5
0.4
0.3
0
0.1
0.2
0.3
0.4
0.5
0.6
0.7
$\sqrt{1-\left(\frac{a}{A}\right)^2}\left[\frac{\dot{m}}{\rho\left(\frac{\pi d^2}{4}\right)\sqrt{2gh}}\right]$
$\frac{1}{\beta}\left(\frac{t}{\sqrt{2h/g}}\right)$

FIG. 49

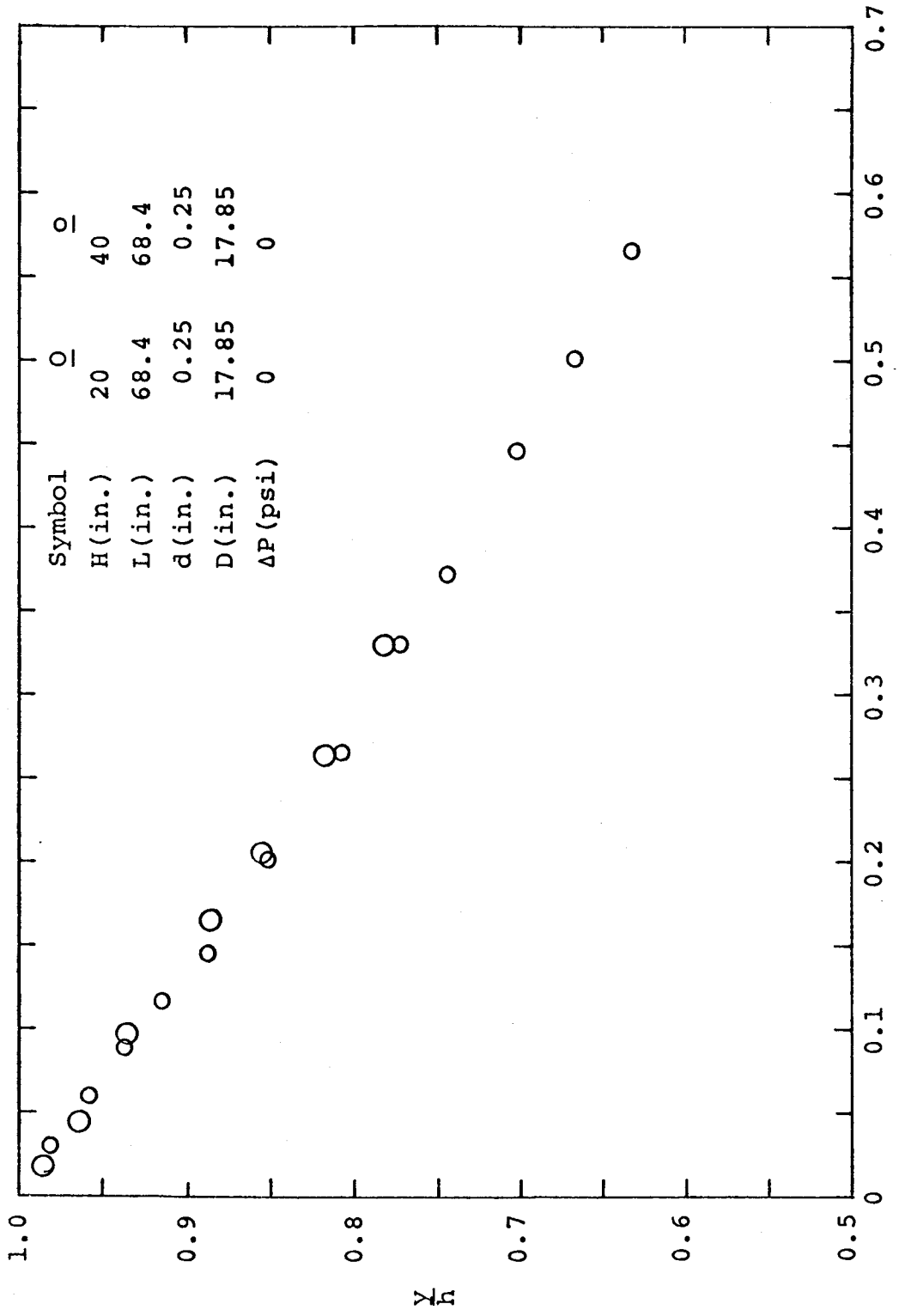
Symbol
H(in.) 20 40
L(in.) 68.4 68.4
d(in.) 0.25 0.25
D(in.) 17.85 17.85
ΔP(psi) 0 0
y/h
1.0
0.9
0.8
0.7
0.6
0.5
0
0.1
0.2
0.3
0.4
0.5
0.6
0.7
1/β (t/√2h/g)

FIG. 50

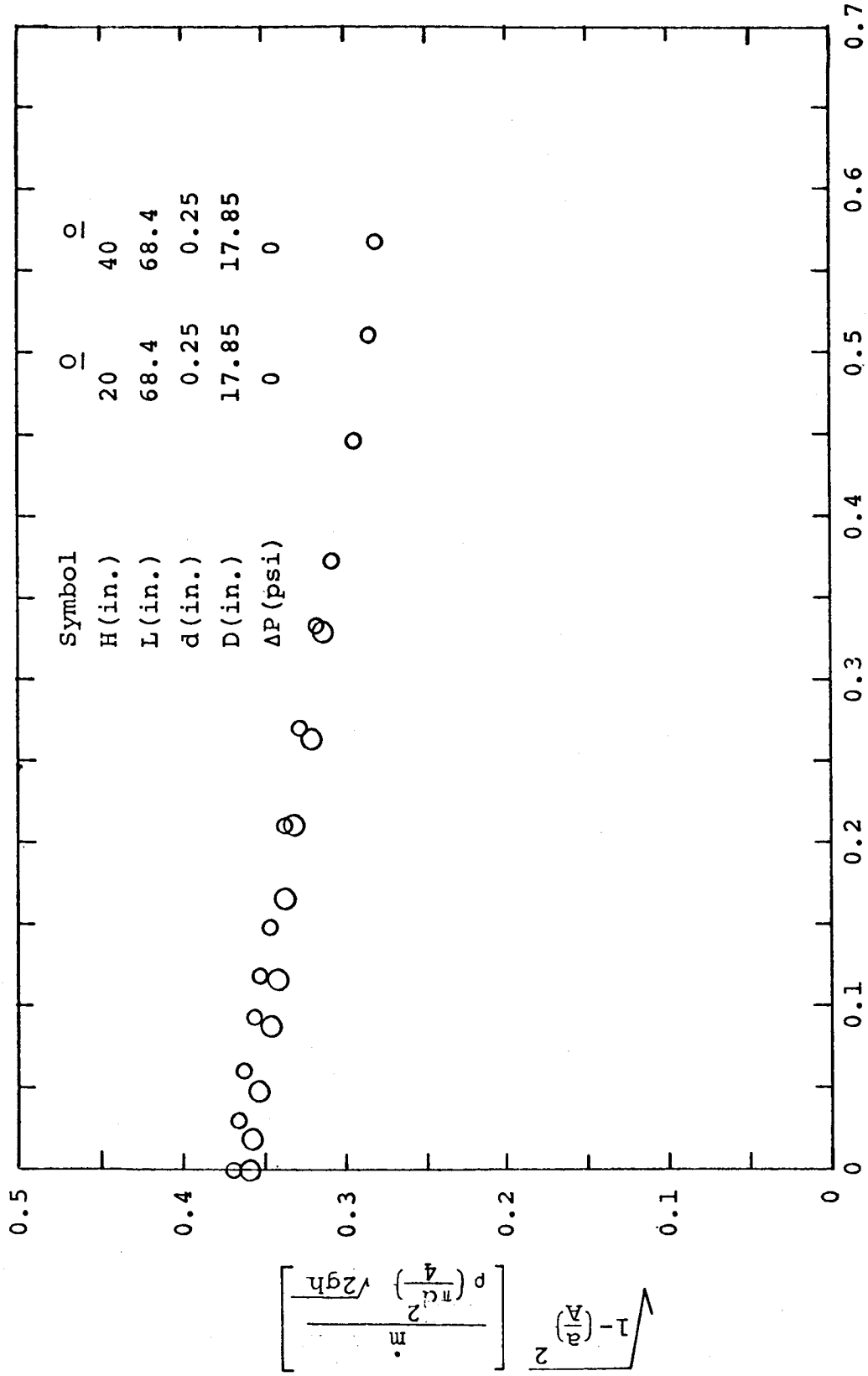

$$\frac{1}{\beta}\left(\frac{t}{\sqrt{2h/g}}\right)$$

$$\sqrt{1-\left(\frac{a}{A}\right)^2}\left[\frac{\dot{m}}{\rho\left(\frac{\pi d^2}{4}\right)\sqrt{2gh}}\right]$$

FIG. 51

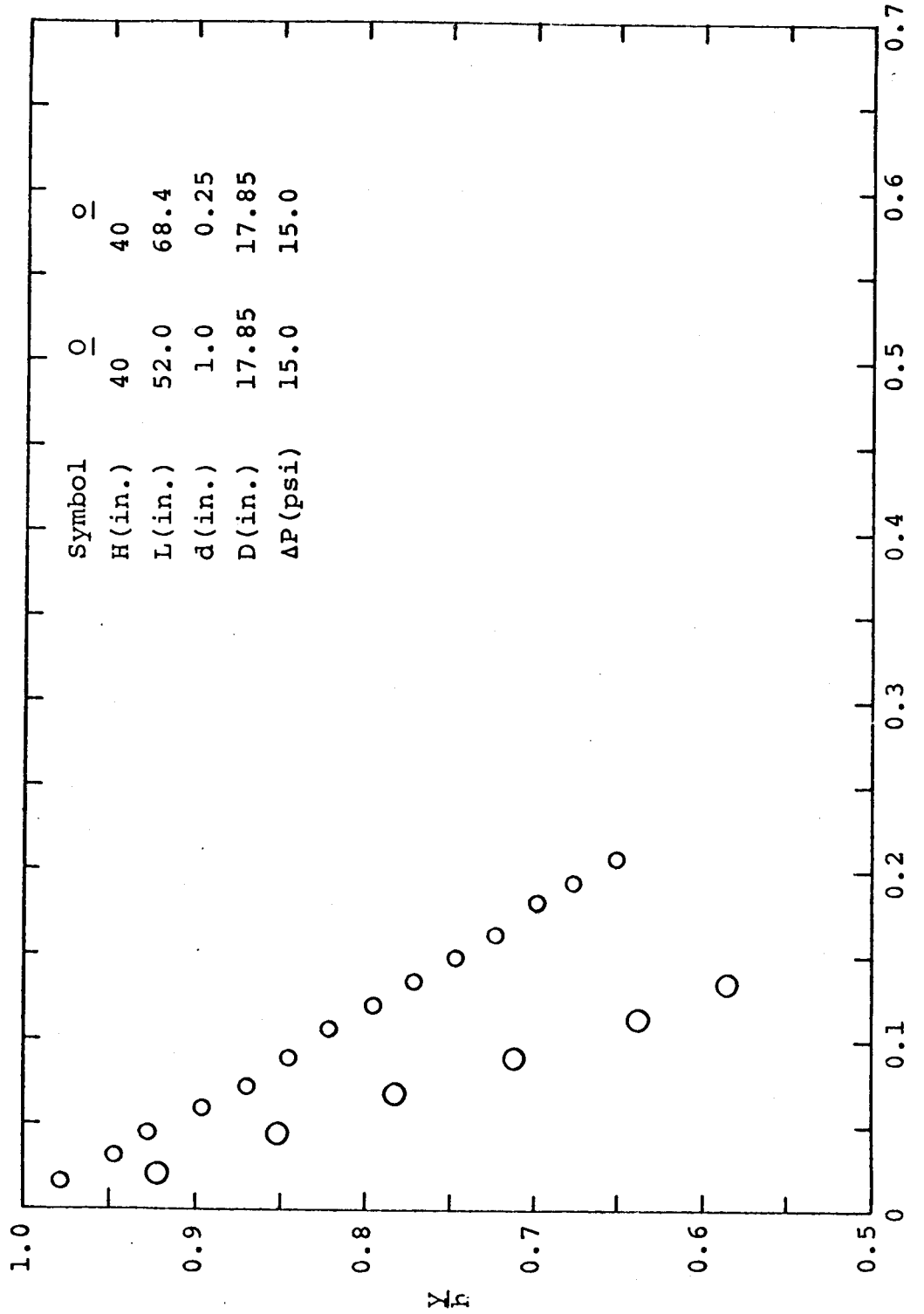
Symbol
H(in.)
L(in.)
d(in.)
D(in.)
ΔP(psi)
40
52.0
1.0
17.85
15.0
40
68.4
0.25
17.85
15.0
1.0
0.9
0.8
0.7
0.6
0.5
0
0.1
0.2
0.3
0.4
0.5
0.6
0.7
y/h
1/β (t/√(2h/g))

FIG. 52

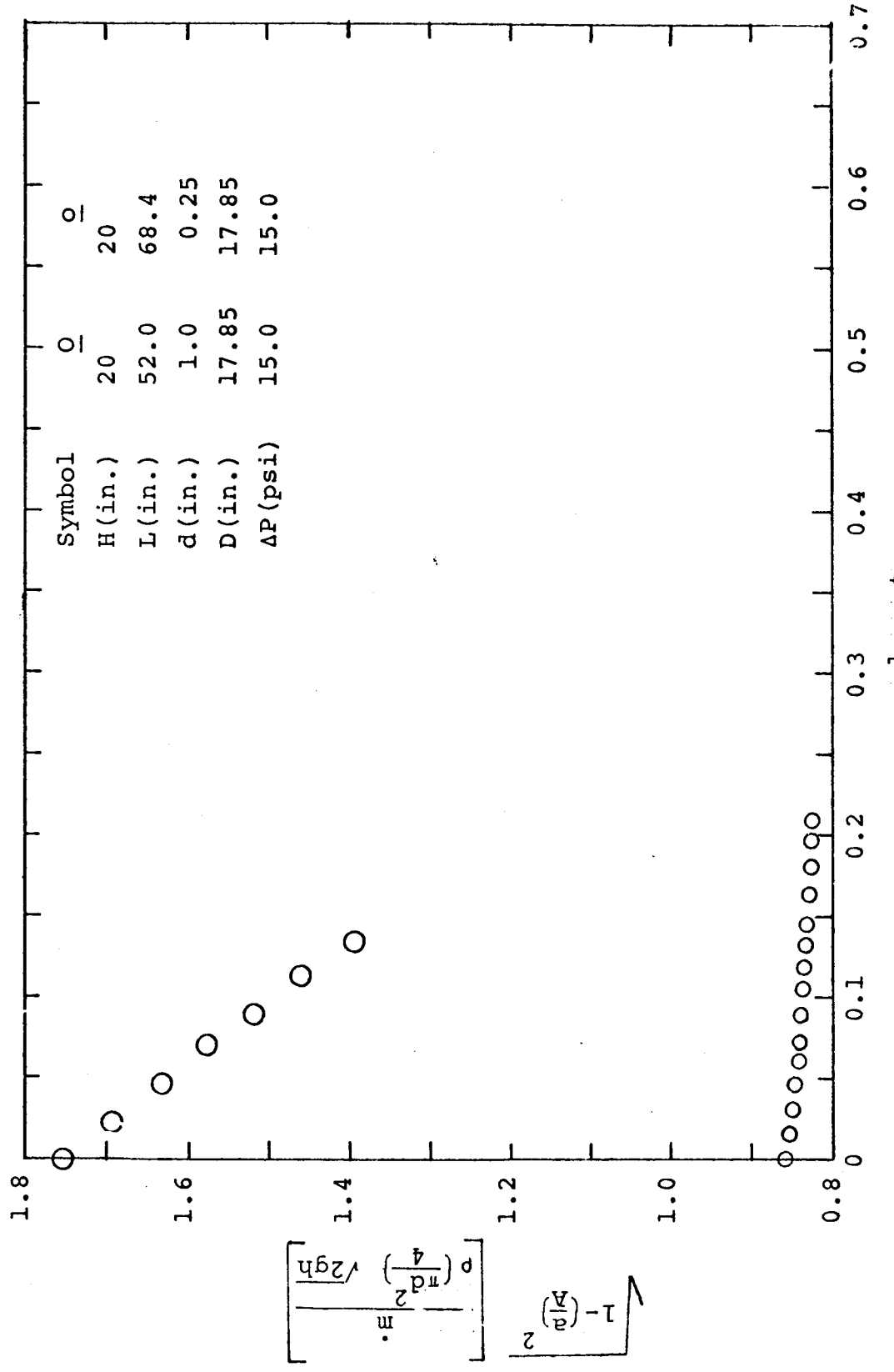
Symbol
H(in.)
L(in.)
d(in.)
D(in.)
ΔP(psi)
20
52.0
1.0
17.85
15.0
20
68.4
0.25
17.85
15.0
1.8
1.6
1.4
1.2
1.0
0.8
0
0.1
0.2
0.3
0.4
0.5
0.6
0.7
$\frac{1}{\beta}\left(\frac{t}{\sqrt{2h/g}}\right)$
$\sqrt{1-\left(\frac{a}{A}\right)^2}\ \frac{\dot{m}}{\rho\left(\frac{\pi d^2}{4}\right)\sqrt{2gh}}$

FIG. 53

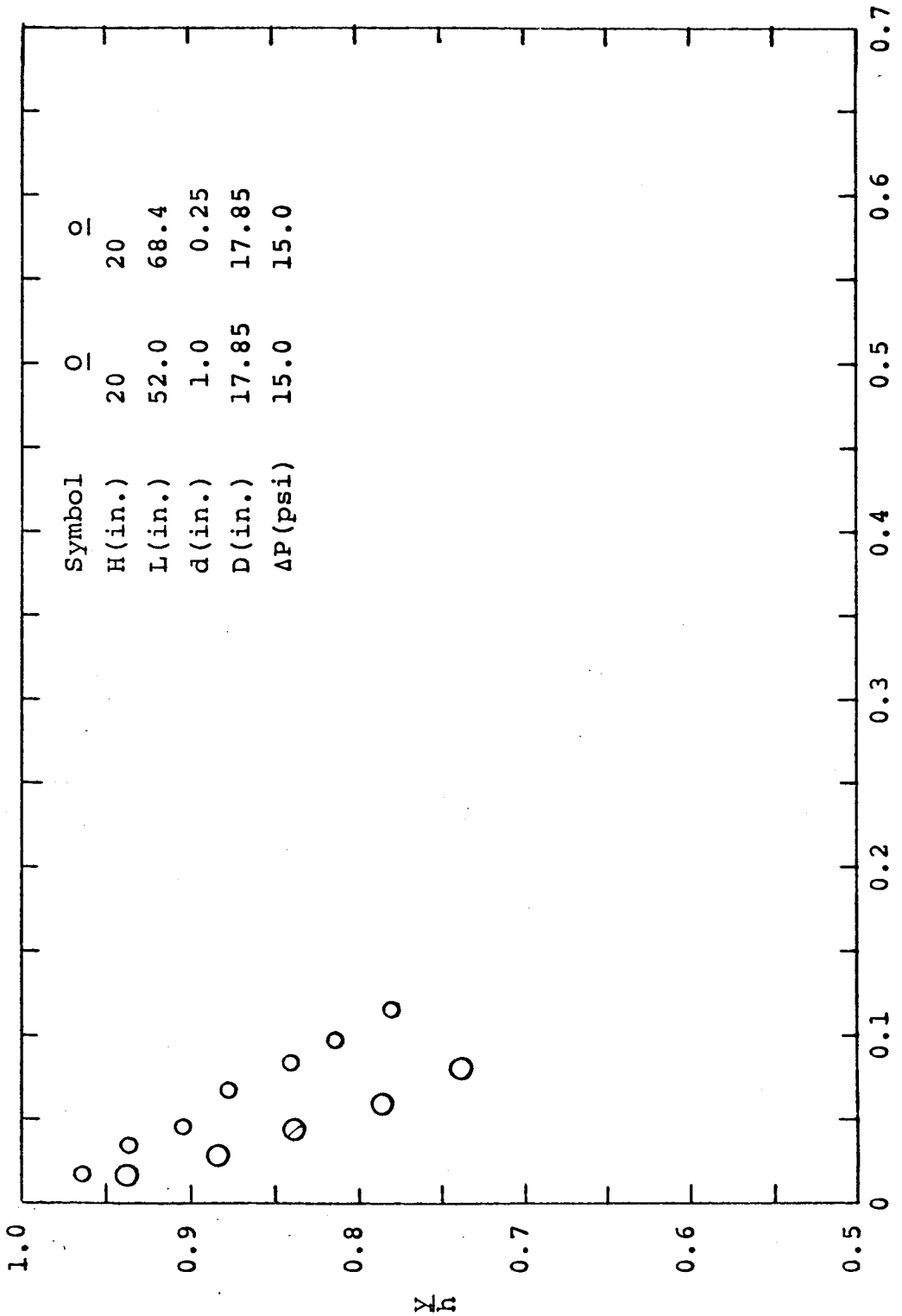
Symbol
H(in.)
L(in.)
d(in.)
D(in.)
ΔP(psi)
20
52.0
1.0
17.85
15.0
20
68.4
0.25
17.85
15.0
Y/h
1.0
0.9
0.8
0.7
0.6
0.5
0
0.1
0.2
0.3
0.4
0.5
0.6
0.7
1/β (t/√2h/g)

FIG. 54

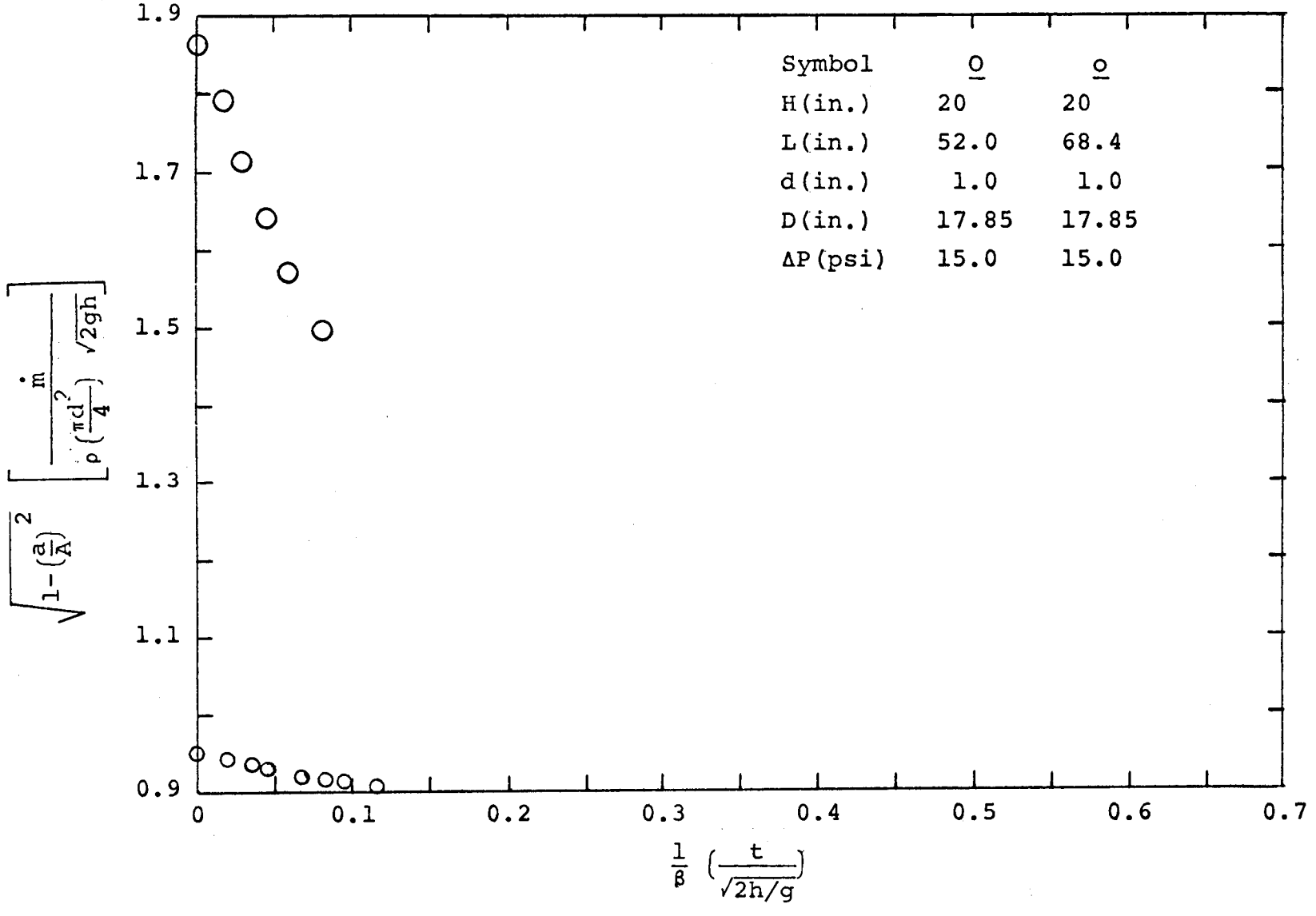
1.9
1.7
1.5
1.3
1.1
0.9
0
0.1
0.2
0.3
0.4
0.5
0.6
0.7
Symbol O o
H(in.) 20 20
L(in.) 52.0 68.4
d(in.) 1.0 1.0
D(in.) 17.85 17.85
ΔP(psi) 15.0 15.0
$\frac{\dot{m}}{\rho(\frac{\pi d^2}{4})\sqrt{2gh}}\Big]\Big/\sqrt{1-(\frac{a}{A})^2}$
$\frac{1}{\beta}\ (\frac{t}{\sqrt{2h/g}})$

FIG. 55

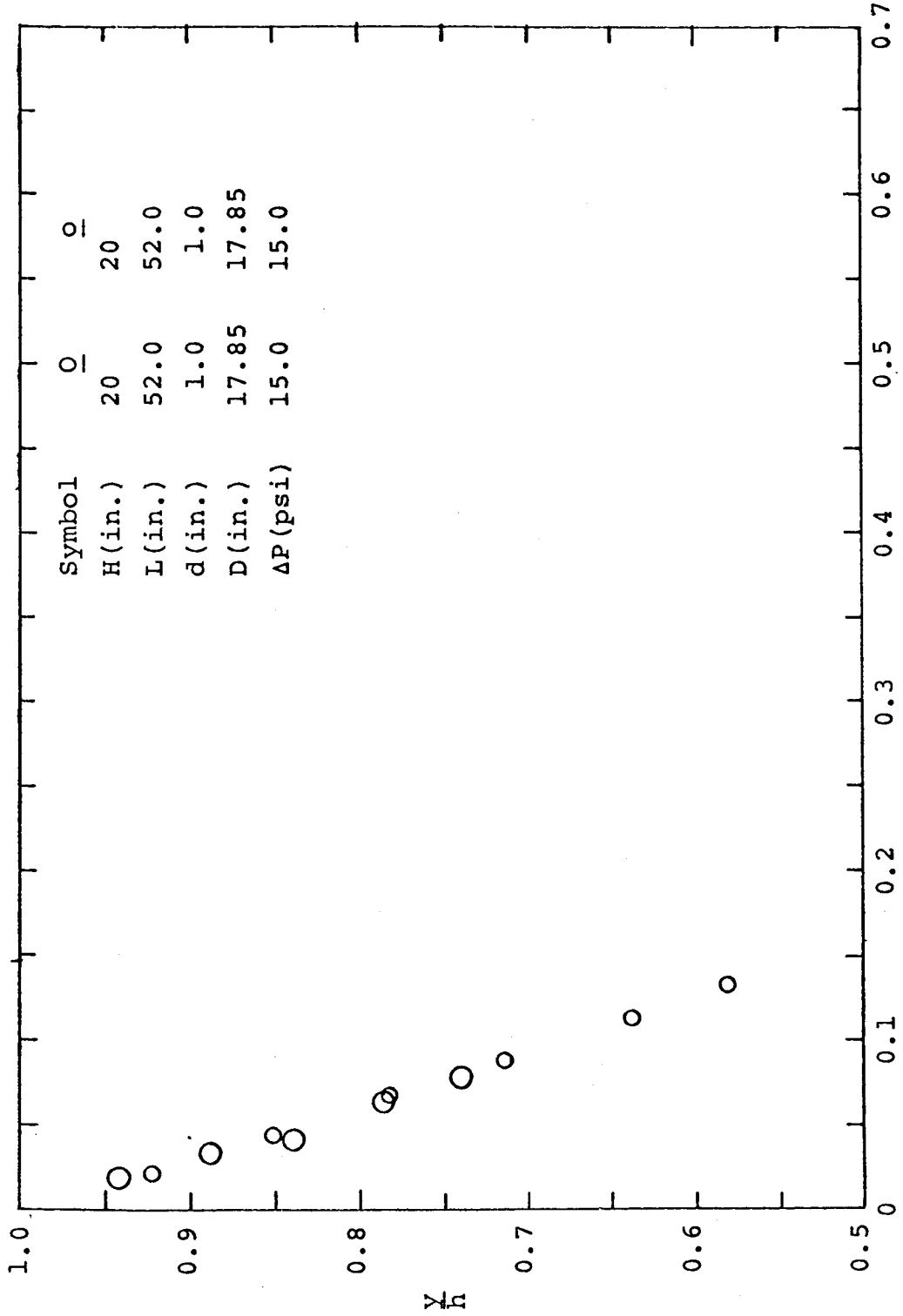
Symbol
H(in.)
L(in.)
d(in.)
D(in.)
ΔP(psi)
20
52.0
1.0
17.85
15.0
20
52.0
1.0
17.85
15.0
y/h
1.0
0.9
0.8
0.7
0.6
0.5
0
0.1
0.2
0.3
0.4
0.5
0.6
0.7
1/β (t/√(2h/g))

FIG. 56

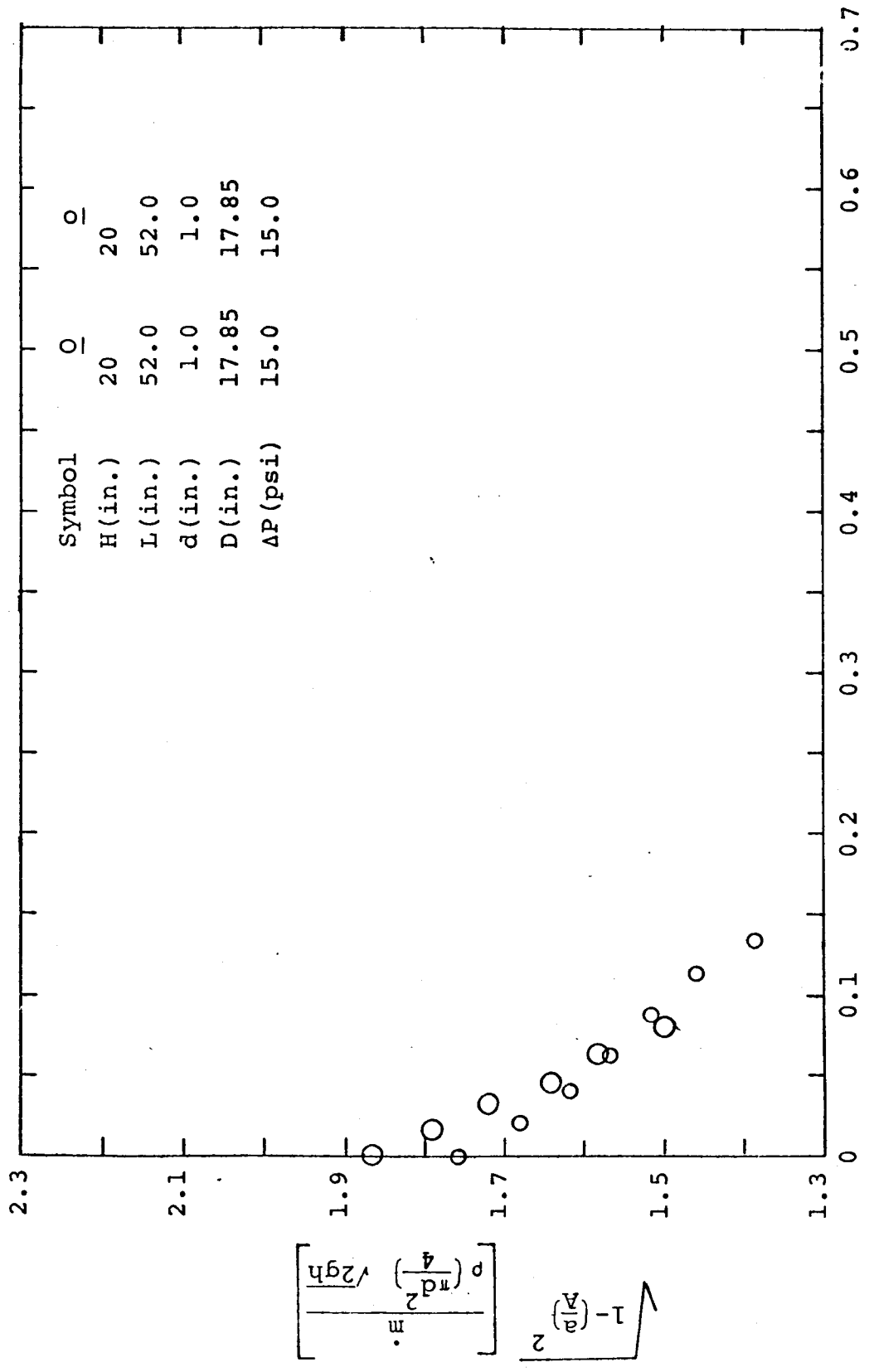
Symbol
H(in.)
L(in.)
d(in.)
D(in.)
ΔP(psi)
20
52.0
1.0
17.85
15.0
20
52.0
1.0
17.85
15.0
2.3
2.1
1.9
1.7
1.5
1.3
0
0.1
0.2
0.3
0.4
0.5
0.6
0.7
$\frac{1}{\beta}\left(\frac{t}{\sqrt{2h/g}}\right)$
$\sqrt{1-\left(\frac{a}{A}\right)^2}\left[\frac{\dot{m}}{\rho\left(\frac{\pi d^2}{4}\right)\sqrt{2gh}}\right]$

FIG. 57

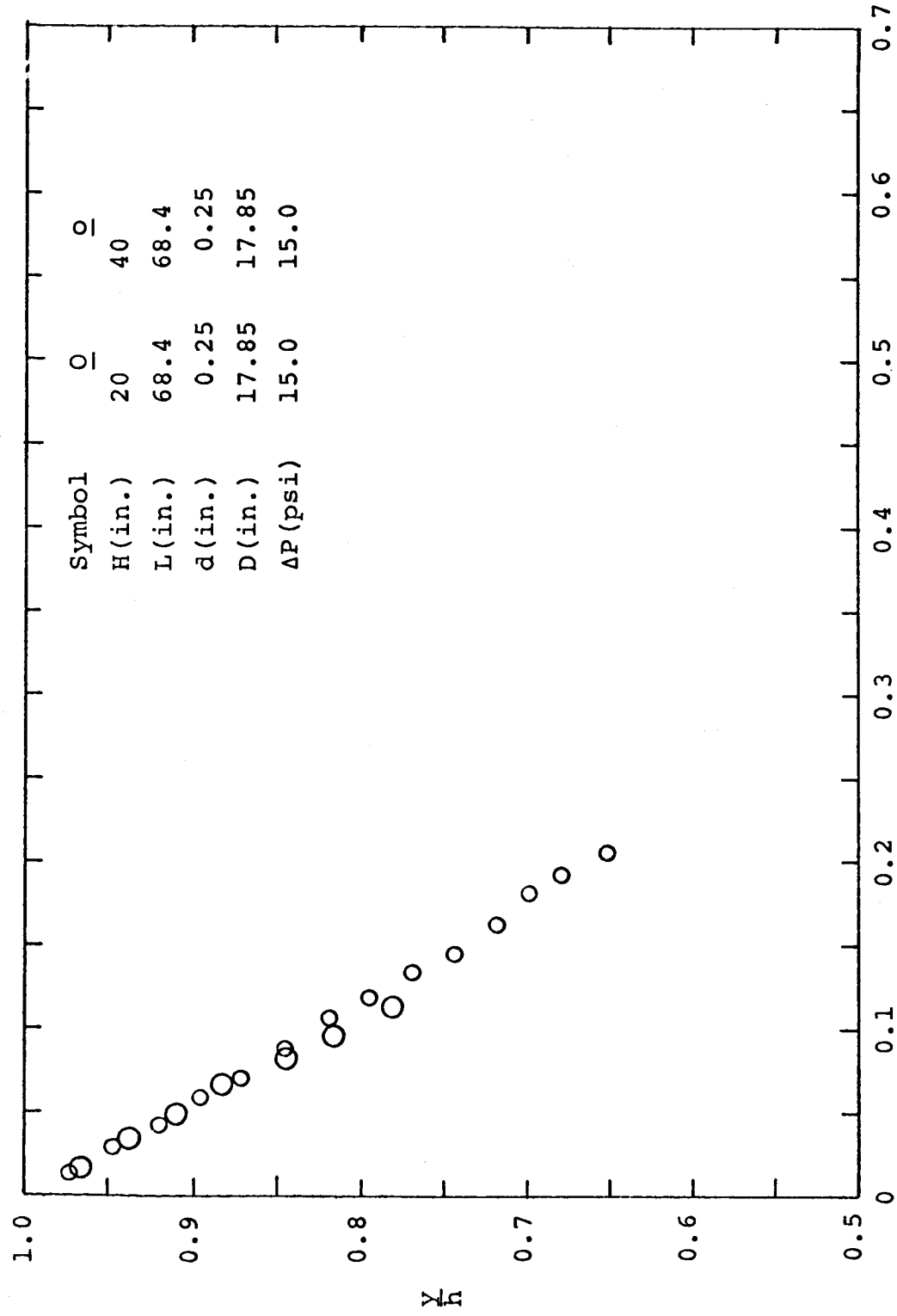
Symbol
H(in.)
L(in.)
d(in.)
D(in.)
ΔP(psi)
20
68.4
0.25
17.85
15.0
40
68.4
0.25
17.85
15.0
Y/h
1.0
0.9
0.8
0.7
0.6
0.5
0
0.1
0.2
0.3
0.4
0.5
0.6
0.7
1/β (t/√2h/g)

FIG. 58

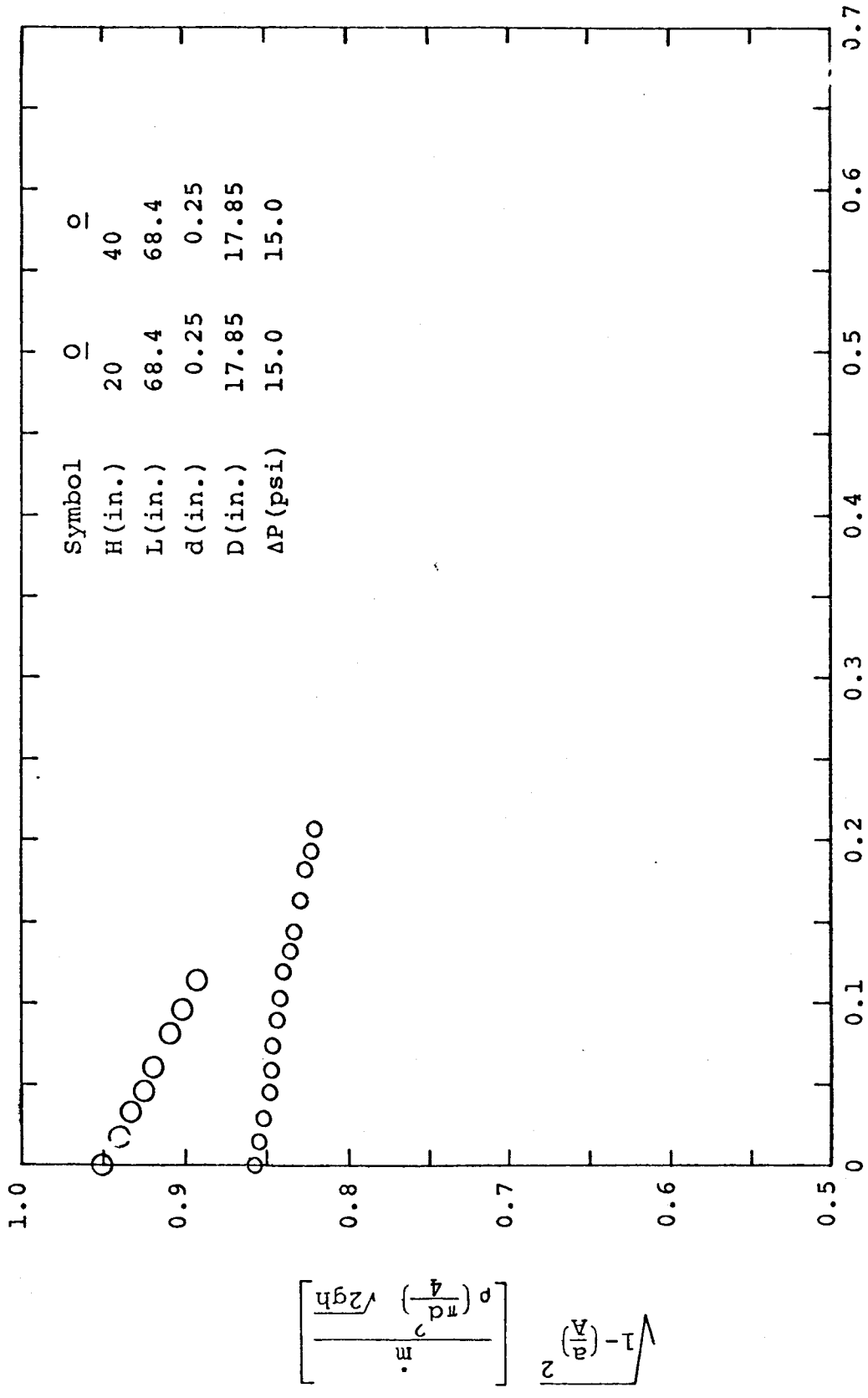
Symbol O O
H(in.) 20 40
L(in.) 68.4 68.4
d(in.) 0.25 0.25
D(in.) 17.85 17.85
ΔP(psi) 15.0 15.0
1.0
0.9
0.8
0.7
0.6
0.5
0
0.1
0.2
0.3
0.4
0.5
0.6
0.7
$\frac{1}{\beta}\left(\frac{t}{\sqrt{2h/g}}\right)$
$\sqrt{1-\left(\frac{a}{A}\right)^2}\ \left[\frac{\dot{m}}{\rho\left(\frac{\pi d}{4}\right)^2\sqrt{2gh}}\right]$

FIG. 59

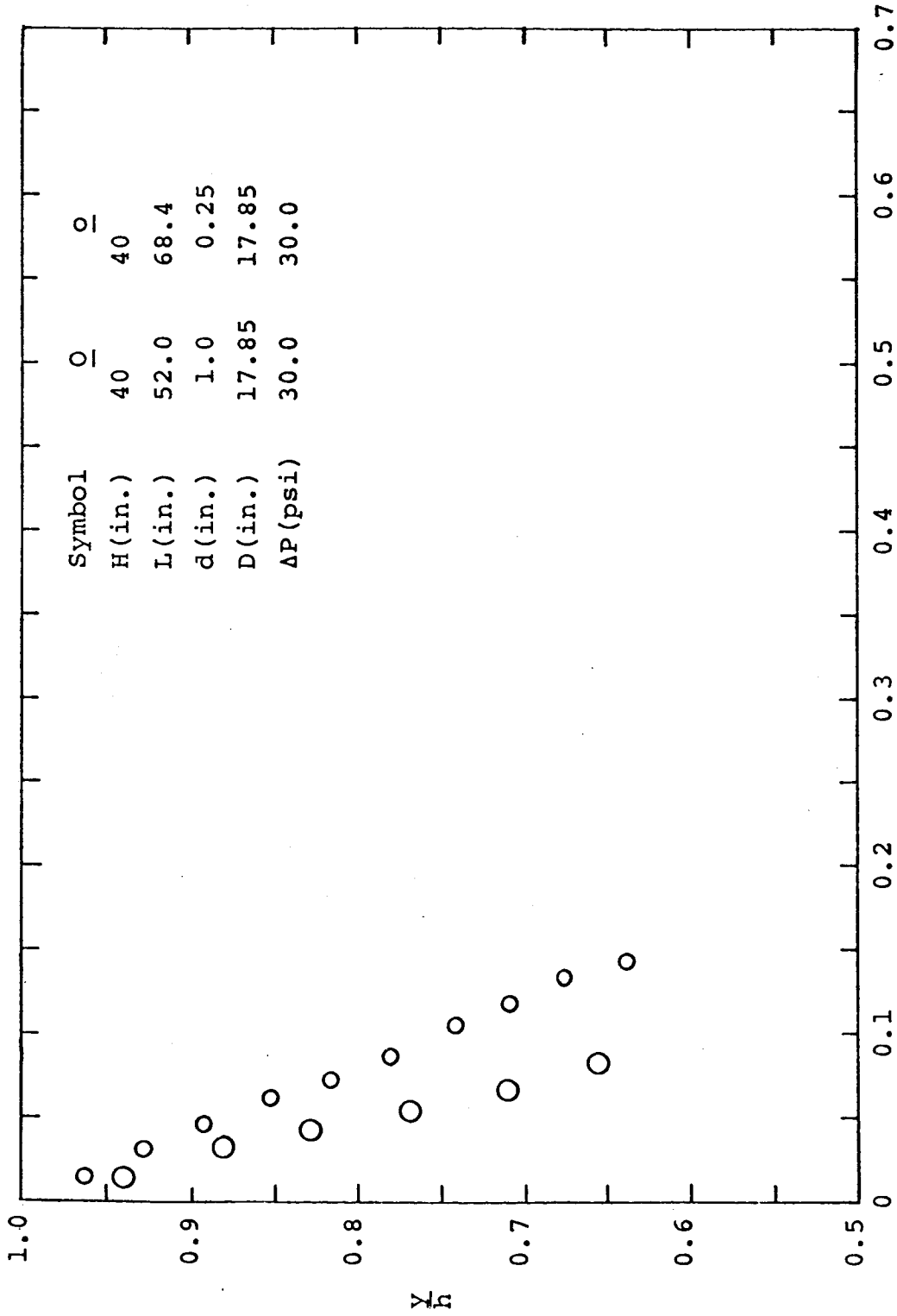
Symbol O O
H(in.) 40 40
L(in.) 52.0 68.4
d(in.) 1.0 0.25
D(in.) 17.85 17.85
ΔP(psi) 30.0 30.0
1.0
0.9
0.8
0.7
0.6
0.5
0
0.1
0.2
0.3
0.4
0.5
0.6
0.7
$\frac{y}{h}$
$\frac{1}{\beta}\left(\frac{t}{\sqrt{2h/g}}\right)$

FIG. 60

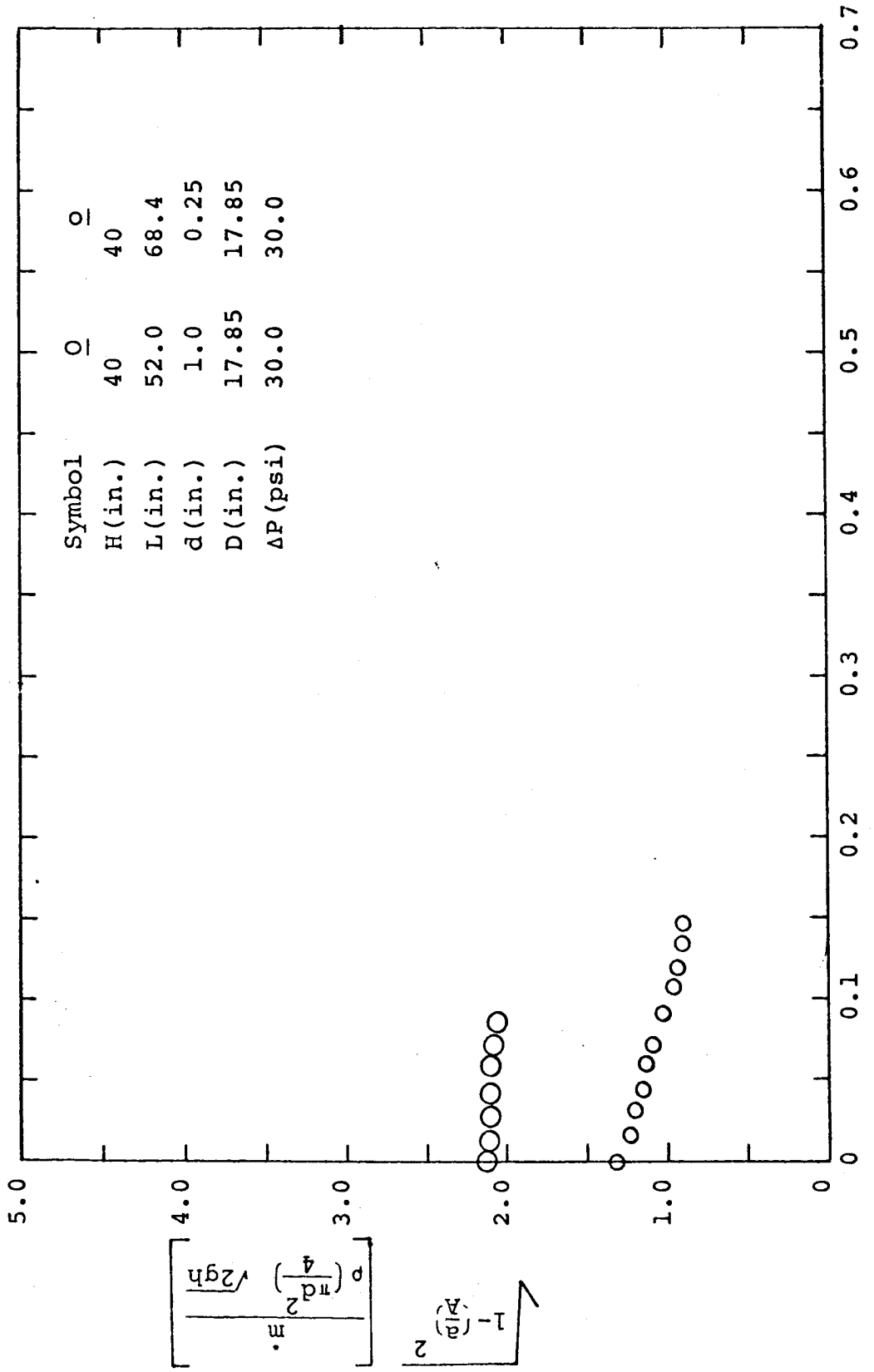
Symbol O O
H(in.) 40 40
L(in.) 52.0 68.4
d(in.) 1.0 0.25
D(in.) 17.85 17.85
ΔP(psi) 30.0 30.0
0
0.1
0.2
0.3
0.4
0.5
0.6
0.7
1.0
2.0
3.0
4.0
5.0
$\frac{1}{\beta}\left(\frac{t}{\sqrt{2h/g}}\right)$
$\sqrt{1-\left(\frac{a}{A}\right)^2}$
$\left[\frac{\dot{m}}{\rho\left(\frac{\pi d^2}{4}\right)\sqrt{2gh}}\right]$

FIG. 61

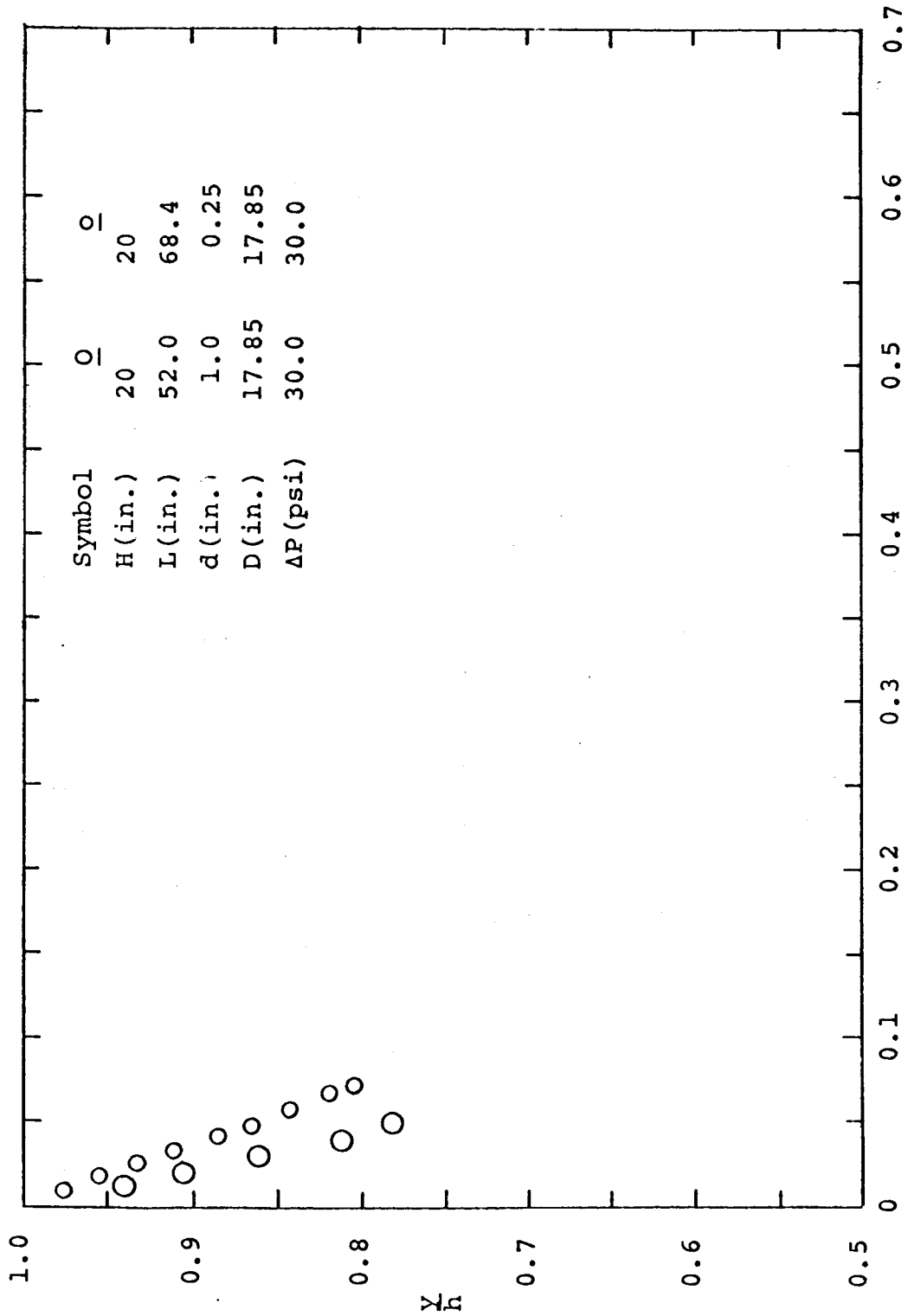
Symbol O O
H(in.) 20 20
L(in.) 52.0 68.4
d(in.) 1.0 0.25
D(in.) 17.85 17.85
ΔP(psi) 30.0 30.0
Y/h
1.0
0.9
0.8
0.7
0.6
0.5
0
0.1
0.2
0.3
0.4
0.5
0.6
0.7
1/β (t/√2h/g)

FIG. 62

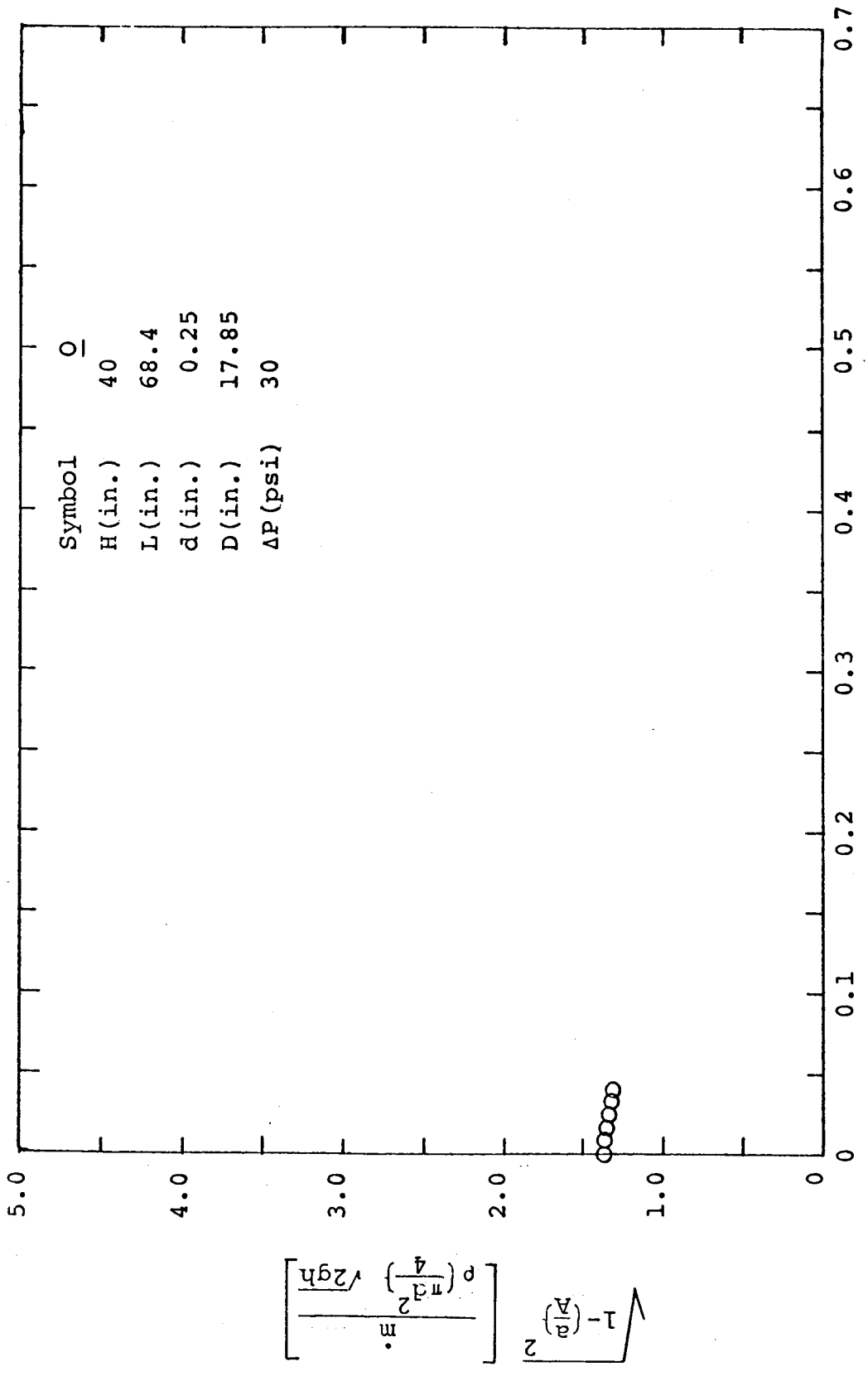
Symbol O
H(in.) 40
L(in.) 68.4
d(in.) 0.25
D(in.) 17.85
ΔP(psi) 30
5.0
4.0
3.0
2.0
1.0
0
0.1
0.2
0.3
0.4
0.5
0.6
0.7
$\sqrt{1-\left(\frac{a}{A_1}\right)^2}\left[\frac{\dot{m}}{\rho\left(\frac{\pi d^2}{4}\right)\sqrt{2gh}}\right]$
$\frac{1}{\beta}\left(\frac{t}{\sqrt{2h/g}}\right)$

FIG. 63

CRITERIA FOR TWO-PHASE FLUID FLOW IN ABSENCE OF HEAT TRANSFER

During high speed discharge of liquid propellant tanks, localized low pressure areas are caused by both geometric factors and fluid flow conditions. Such environments may generate two-phase fluid conditions that seriously affect the transfer rates in the propellant system.

An investigation into the physical aspects of the two-phase inception in the absence of heat transfer leads to the formulation of a parameter which can be used to predict the phenomenon of cavitation. This parameter, the cavitation index σ, is first verified experimentally as a test of the basic physical theory, and then it is applied in the form of the non-dimensional parameters derived for the discharge of a propellant tank in the absence of two phase flow. In such a way, the basic similarity transformations are used as an indication of the susceptibility of a given discharge system to cavitation.

This report is mainly concerned with the extension of the basic cavitation parameter to the similarity parameters of the discharge systems and the subsequent applications.

SURVEY OF LITERATURE

Cavitation has been widely investigated with respect to practical problems such as pump impellers and hydrofoil shapes. Each analysis was centered on the parameters specifically applicable to the problem such as blade pressure coefficients for impeller type pumps and pressure-reduction coefficients for airfoil profiles. The team of Hall and Wislicenus (Ref. 20) published a general but complete study on scale factors affecting the similarity conditions of any liquid flow.

Starting from Thoma's law of similarity, σ_H is given by

$$\sigma_H = \frac{H_{sv}}{H} = \text{const.} \tag{37}$$

where H is the total head of the machine and H_{sv} is the total suction head above vapor pressure, the basic requirements of a similarity analysis are discussed. After the cavitation number σ,

$$\sigma = \frac{P_o - P_v}{1/2\ \rho V_o^2} \tag{38}$$

they discuss the Reynolds number characterized by the ratio of the inertia and viscous forces, the Froude number giving the ratio of the inertia and gravitational forces, and the Mach number for compressibility and note that different sets

of conditions are necessary for each parameter to be maintained constant. Considerations of surface irregularities, relative roughness, dissolved gas concentration and local effects are also discussed.

Hall notes a distinction between the appearance of cavitation under a diminishing pressure and the dissappearance of cavitation under increasing pressure (Ref.21). Thus defined are the incipient and desinent cavitation numbers respectively.

σ_i = incipient cavitation no.

σ_d = desinent cavitation no.

$\sigma_d \geq \sigma_i$ as shown by Hall.

Kermeen (Ref.22) and Hall and Treaster (Ref.23) came to similar conclusions concerning the significance of the previous history of the fluid with incipient and desinent cavitation. In a more specific sense, Kamiyama (Ref.25) concluded that the longer the region of minimum pressure to which a fluid was subjected, the easier became cavitation inception.

The existence of the dual cavitation numbers prompted researchers to investigate what effects dissolved gas content, surface roughness, surface tension and the flow history of the liquid had on cavitation. Hall and Treaster (Ref.23) associated the incipient and desinent cavitation as a hysterisis effect with a measurable cavitation-delay time. Unfortunately the complexities of the problem allowed for only an explanatory investigation of this effect.

A study by Kamiyama yielded data for cavitation in pipe bends with the possibility of direct application to propellant lines. Generally, a head loss coefficient defined for non-cavitating flow as

$$\xi = \frac{P_1 - P_2 + \gamma h_d}{1/2\ \rho V_o^2} = \text{loss coefficient} \qquad (39)$$

and a similarly defined loss coefficient, ξ_c, under cavitating conditions were taken as a ratio:

$$\beta = \xi_c/\xi \qquad (40)$$

The parameter β did not appreciably increase as long as the cavity did not develope over 0.8 - 1.0 times a defined channel width. This indicates the relative amount of cavitation in a propellant line which would not seriously affect the flow. Also listed were experimental values for a critical cavitation number which corresponded to a choked condition in the apparatus.

Local heat transfer properties affecting cavitation were discussed by Stahl, et al., (Ref.26) for the specific problem of a centrifugal pump. The results and analysis can be generalized for any cavitation problem and are noted under a later part of this report.

In summary, it can be said that the numerous investigations have given sufficient background to apply the theory of cavitation in a similarity analysis of the discharge of fluids from propellant tanks.

PHYSICAL EFFECTS

Cavitation is defined as the formation of vapor and gas filled voids in a liquid due to a local pressure reduction resulting from flow dynamics. Potential flow theory of a pure liquid indicates that minimum pressure will occur on a boundary for some given value of the ratio,

$$\frac{P_o - P_{minimum}}{1/2\ \rho V_o^2}$$

The quantity P_o is a reference static pressure and V_o is a reference velocity usually taken at the same point where P_o is obtained.

For a liquid which cannot support a tension, cavitation can be assumed when the minimum pressure equals the vapor pressure. Thus the cavitation number, σ, is defined as

$$\sigma = \frac{P_o - P_{vap}}{1/2\ \rho V_o^2} \tag{41}$$

Classical similarity theory indicates that the conditions of cavitation in similar systems will be identical if the systems have the same value of the cavitation number. Although this theory holds true in a general sense, some departures have been noted.

Consideration of the surface tension of the liquid leads to a modification of the assumption that cavitation appears as soon as the local pressure reaches the vapor pressure of the liquid. For a single spherical bubble, thermodynamic equilibrium requires that

$$\pi r^2 \left(P_v - P_\ell\right) = 2\pi r\alpha \tag{42}$$

where α is the surface tension of the liquid. Thus the pressure difference becomes,

$$P_v - P_\ell = \frac{2\alpha}{r} \tag{43}$$

This requires that the pressure inside the bubble must be greater than that of the liquid for the bubble to exist. Since a basic assumption is that of thermal equilibrium, the liquid must be superheated to allow the vapor bubble to achieve equilibrium. The magnitude of the super-heat is dependent on the size of the bubble within the liquid.

From the form of the equation, (43), it is obvious that as the radius becomes smaller a larger degree of super-heat is required. This leads to the conclusion that for cavitation, the presence of gas bubbles dissolved within the liquid serve as the nuclei of the subsequent vapor bubble formation. Without the initial nuclei, estimates indicate that tensions in the range from 500 to 10,000 atmospheres must exist for cavitation to occur.

A further refinement of the nuclei theory involves consideration of the gas partial pressure inside the nuclei. Thus the previous equation of equilibrium becomes

$$P_g + P_v - P_\ell = \frac{2\alpha}{r} \tag{44}$$

where P_g is the gas partial pressure. This term will be significant only at cavitation inception when the nuclei is beginning to expand. For a constant mass of gas in a nuclei at constant temperature,

$$P_g = K/r^3 \tag{45}$$

$$\text{so that } P_\ell - P_v = \frac{K}{r^3} - \frac{2\alpha}{r} \tag{46}$$

For a minimum value,

$$P_\ell - P_v = P_{min}$$

a critical radius

$$r = r_{min} = \left(\frac{3K}{2\alpha}\right)^{\frac{1}{2}} \tag{47}$$

$$\text{or} \qquad r_{min} = \frac{-4\alpha}{3\left(P_\ell - P_v\right)} \tag{48}$$

is defined which is necessary for cavitation inception. The negative sign indicates that the critical pressure is below the vapor pressure.

The theory of gas bubbles acting as cavitation nuclei can also be extended to include pockets of undissolved gas trapped in flows or crevices of a solid which can be micoscopic in size. For this reason it appears that the concentration of cavitation nuclei per unit volume may be important only in regions not near a solid boundary where crevices and other surface irregularities cannot act as cavitation nuclei. Gilmore and Plesset have shown that in regions far from a flow boundary, the concentration of nuclei is a significant variable only when every nucleus acts as a cavitation center; that is, when impurities and the gas bubbles are low in volumetric concentration (Ref. 34).

Local heat transfer effects cannot be neglected during the boiling process of cavitation. The latent heat of vaporization must come from the liquid.

The necessary flow of heat can take place only when the liquid temperature is above that corresponding to the saturation temperature at the corresponding pressure of the region of cavitation. This consideration requires, as did the surface tension consideration, that a certain degree of superheat is required for cavitation.

Let this amount of superheat $\equiv \Delta T$.

Thus $\Delta h_f = c_p \Delta T$ is available for vaporization of the liquid (c_p = specific heat of liquid).

If it is assumed that thermal equilibrium is restored, a heat-balance, written for a unit mass of liquid flowing,

becomes

$$\Delta h_f = \frac{m_g}{m_f} h_{fg} \tag{49}$$

$$\Delta h_f = \frac{V_g}{V_f} \frac{v_f}{v_g} h_{fg} \tag{50}$$

let $$\Gamma = \frac{V_g}{V_f} \equiv \text{relative vapor ratio} \tag{51}$$

thus $$\Gamma = \frac{v_g}{v_f} \frac{c_p \Delta T}{h_{fg}} \tag{52}$$

The following parameters are derived for a given control volume:

h_f = enthalpy of the liquid

h_{fg} = heat of evaporation

m_g = mass of vapor generated

m_f = mass of liquid

v_g = specific volume of vapor

v_f = specific volume of liquie

V_g = total volume of vapor

V_f = total volume of liquid

A look at the steam tables provides an insight into the physical significance of the superheat.

T	P_{vap}	V_g	h_{fg}	h_f
59.3	0.25	1235.3	1060.3	27.36
64.5	0.30	1039.5	1057.4	32.52
201.96	12.0	32.40	976.6	109.96
202.16	12.05	32.28	976.5	169.76
400.95	250	1.8438	825.1	376.00
400.97	250.05	1.8435	835.08	376.02
635.82	2000	0.1878	463.4	671.7

The observations are listed below:

1. For a given fluid bulk temperature of 59.3°F, a local pressure depression of 0.05 PSI yields a superheat of 5.2°F.

2. The same pressure depression of 0.05 PSI at a bulk fluid temperature of 201.96°F will give a superheat ΔT of only 0.2°F; and at a bulk fluid temperature of 250°F the same pressure depression yields a superheat of only 0.02°F.

3. The difference in enthalpy of water per degree F is essentially the same at 59.3, 201.96, and 400.95°F.

4. The specific volume of the vapor at 59.3°F is 38 times larger than v_g at 201.96°F and 670 times larger than v_g at 400.95°F.

Therefore, for the same pressure depression more heat is available for vaporization at lower temperatures, and the specific volume decrease at increasing temperatures indicates that the process of cavitation is much more severe at temperatures far below the critical temperature than near the critical temperature of the liquid.

ANALYSIS

The following assumptions are made:

1. The liquid is incompressible.
2. Surface tension and viscosity effects are negligible.
3. The partial pressure of the gas in the dissolved gas bubbles has no effect on the cavitation.
4. Sufficient cavitation nuclei are available such that the concentration is not a limiting parameter.
5. Cavitation occurs when the local pressure reaches the vapor pressure of the liquid.

The classical similarity theory states that the cavitation conditions will be similar in two "similar" systems with "similar" flows if the cavitation number,

$$\sigma = \frac{P_o - P_v}{1/2\rho V_o^2}, \text{ is the same.}$$

The previous analysis for the discharge of the propellant tanks yielded, among others, the following dimensionless groups.

$$\frac{\dot{m}}{\rho \frac{\pi d^2}{4} \sqrt{2gh}}, \quad \text{mass flow rate} = \pi_1$$

$$\frac{\Delta P/\rho g}{h}, \quad \text{ratio of pressure head to initial hydrostatic head} = \pi_2$$

$$\frac{d\sqrt{2gh}}{\nu}, \quad \text{characteristic Reynolds no.} = \pi_3$$

Combining these groups with the system analysis yields cavitation number described for the type of discharge system being investigated. Thus

$$\sigma = \frac{\pi_2 - \pi_{2v}}{\pi_1^2} \tag{53}$$

where π_{2v} is defined with the vapor pressure.

The cavitation number σ plotted against a Reynolds number on logarithmic coordinates yields a straight line relationship when downstream conditions remain constant. For the discharge system, this corresponds to a constant back pressure. Placing the Reynolds number in the form of the non-dimensional parameters yields

$$Re = \frac{\rho V d}{\mu} = \pi_1 \pi_3 \tag{54}$$

Thus the usual parameters for describing cavitation are shown in the particular dimensionless relationships for the discharge of propellant tanks. Similarity states that they should describe conditions accurately until the inception of two phase flow.

EXPERIMENTAL MEASUREMENTS AND COMPARISONS

A schematic diagram of the experimental facility is shown in FIG. 64a. Instantaneous pressure readings taken at stations 0 and 1 permitted calculation of σ and Reynolds number values.

From the relation,

$$\frac{1}{2g}\rho V_1^2 = P_o + \rho z_o - P_1 \tag{55}$$

the cavitation number is

$$\sigma = \frac{P_1 - P_{vap}}{P_o + \rho z_o - P_1} \tag{56}$$

The geometry of the system yields,

$$Re_1 = \frac{\rho V_1 D_1}{\mu} \tag{57}$$

or

$$Re = \frac{\rho D_1}{\mu}\left[\frac{2g}{\rho}\left(P_o + \rho z_o - P_1\right)\right]^{1/2} \tag{58}$$

where D_1 = diameter of pipe at station 1.

The obtained values of σ and Re are tabulated in comparison with the theoretical values. Data for two different geometries are listed on page 122.

In FIG. 65 a photograph of the test section is given. FIGURE 66 contains a close-up photograph showing the onset of cavitation along the wall for the double round geometry.

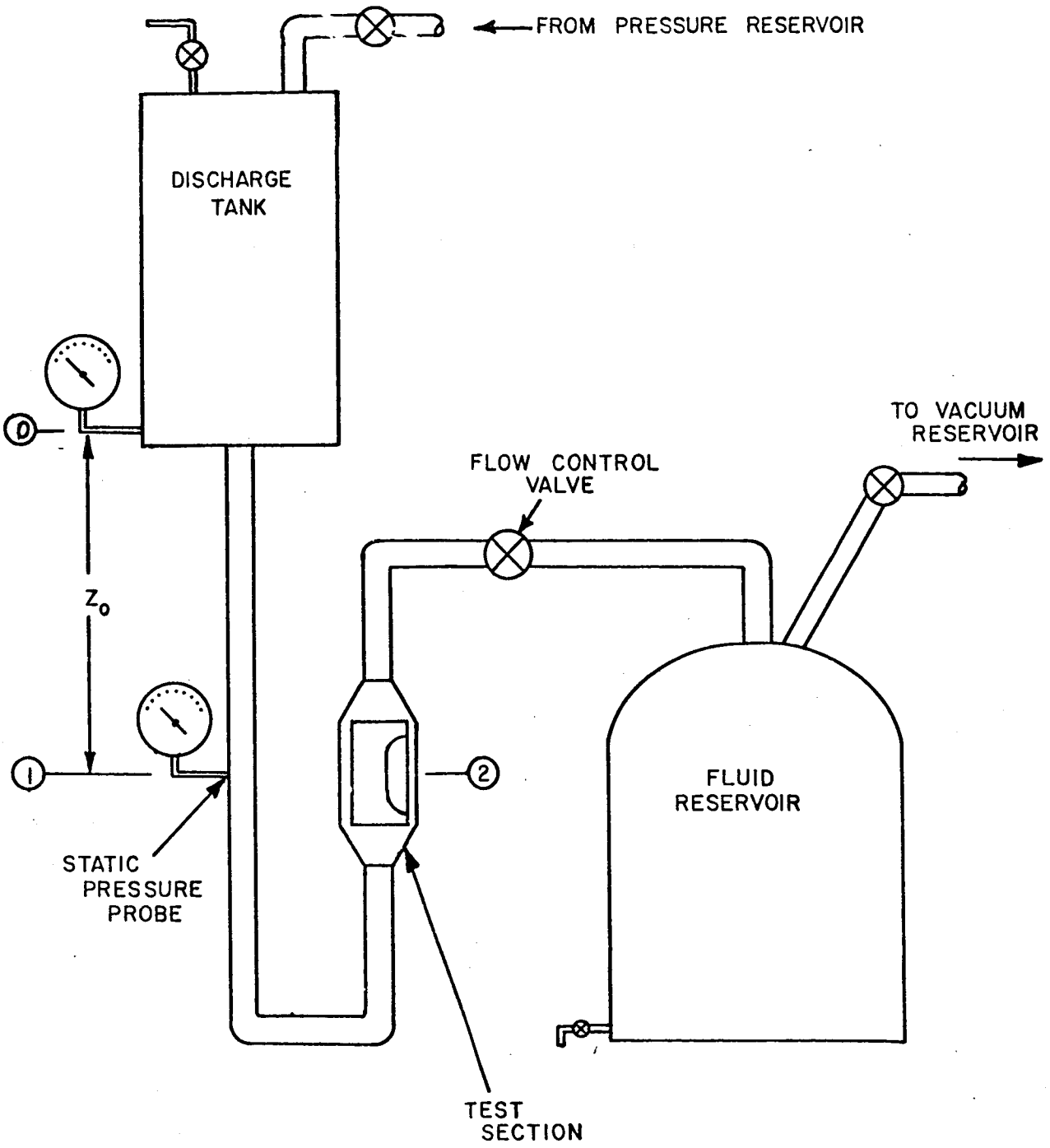

FIGURE 64a SCHEMATIC DIAGRAM OF CAVITATION EXPERIMENTAL FACILITY

TABLE OF VALUES, DOUBLE ROUND
TEST GEOMETRY

Re	$\sigma_{Theoretical}$	$\sigma_{Experimental}$
290,000	6.36	6.39
284,000	7.35	6.40
274,800	6.50	6.59
277,600	6.75	6.72
272,400	6.71	6.75
301,200	6.89	6.87
295,200	6.96	6.95
295,200	6.75	6.74
304,800	6.26	6.64
298,400	6.63	6.64
290,400	6.80	6.86
298,400	6.83	6.86
298,400	6.57	6.61
290,400	6.77	6.85

TABLE OF VALUES, RECTANGULAR
(SHARP EDGE) GEOMETRY

Re	$\sigma_{Theoretical}$	$\sigma_{Experimental}$
188,400	20.4	13.6
182,000	20.4	13.5
175,000	23.5	15.7
185,600	20.3	13.5
176,000	21.9	14.6
176,000	23.2	15.4
185,600	20.2	13.6
185,600	19.7	13.2
185,600	19.2	12.8
175,600	23.7	15.4
185,600	20.0	13.9
185,600	19.5	13.1
176,000	21.4	14.4

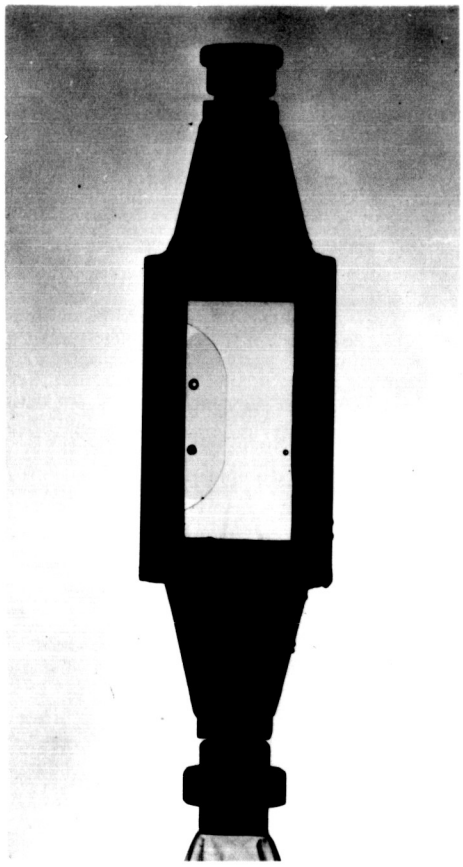

FIG. 64b TEST SECTION

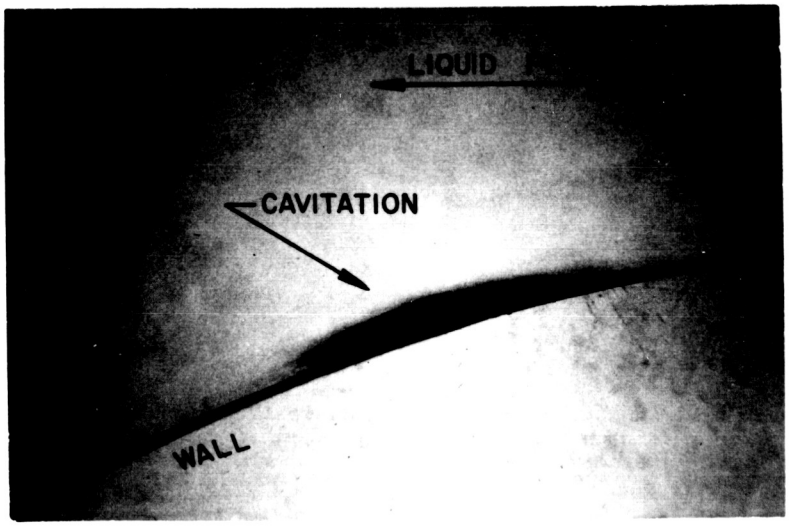

FIG. 64c ONSET OF CAVITATION

The close agreement between theoretical and experimental values of σ for the double round shape indicates the cavitation parameter can predict the onset of cavitation for systems where the Bernoulli equation assumptions are maintained. The spread between the σ values for the sharp edged shape shows that the analysis cannot be used accurately for such situations.

Similarly, considerations were listed which permitted the development of the cavitation number and the Reynolds number in non-dimensional parameters describing the discharge system up to the inception of two-phase flow.

The description of physical effects showed that the closer a liquid is to its critical temperature, the less effective are the conditions aiding cavitation inception. It has also been noted that the longer the liquid is exposed to low pressures of magnitude approximating the vapor pressure, the easier becomes cavitation inception when the liquid pressure equals the saturation pressure.

HEAT TRANSFER SIMILARITY IN STRATIFYING FLUIDS IN THE ABSENCE OF PRIMARY FLOW

The discharge of a fluid which is initially stationary within a vessel has been described in a preceeding section. The discharge rate, $\dot{m}$, was explained to be a function of fluid properties, such as density, ρ, viscosity, μ, etc. The analysis of gravity and pressure driven liquid discharge was simplified by the assumptions of constant properties and temperature.

For a small body of fluid contained in a vessel with a small temperature gradient across the container walls the constant bulk temperature assumption is justified. However, when the volume of the fluid and the temperature gradient become large, the bulk temperature will not be the same at different locations in the fluid. A non-uniform temperature distribution is caused by the temperature gradients inducing heat transfer through the walls of the vessel. The heat transfer induces stratification within the body of the stationary fluid, thus, setting up horizontal layers of fluid with different densities and temperatures. The purpose of this investigation is to study the stratification process as it occurs within a fluid contained in a vessel. Before carrying out the analysis, the stratification process will be described in steps as they occur. This step by step operation is illustrated in FIG. 65.

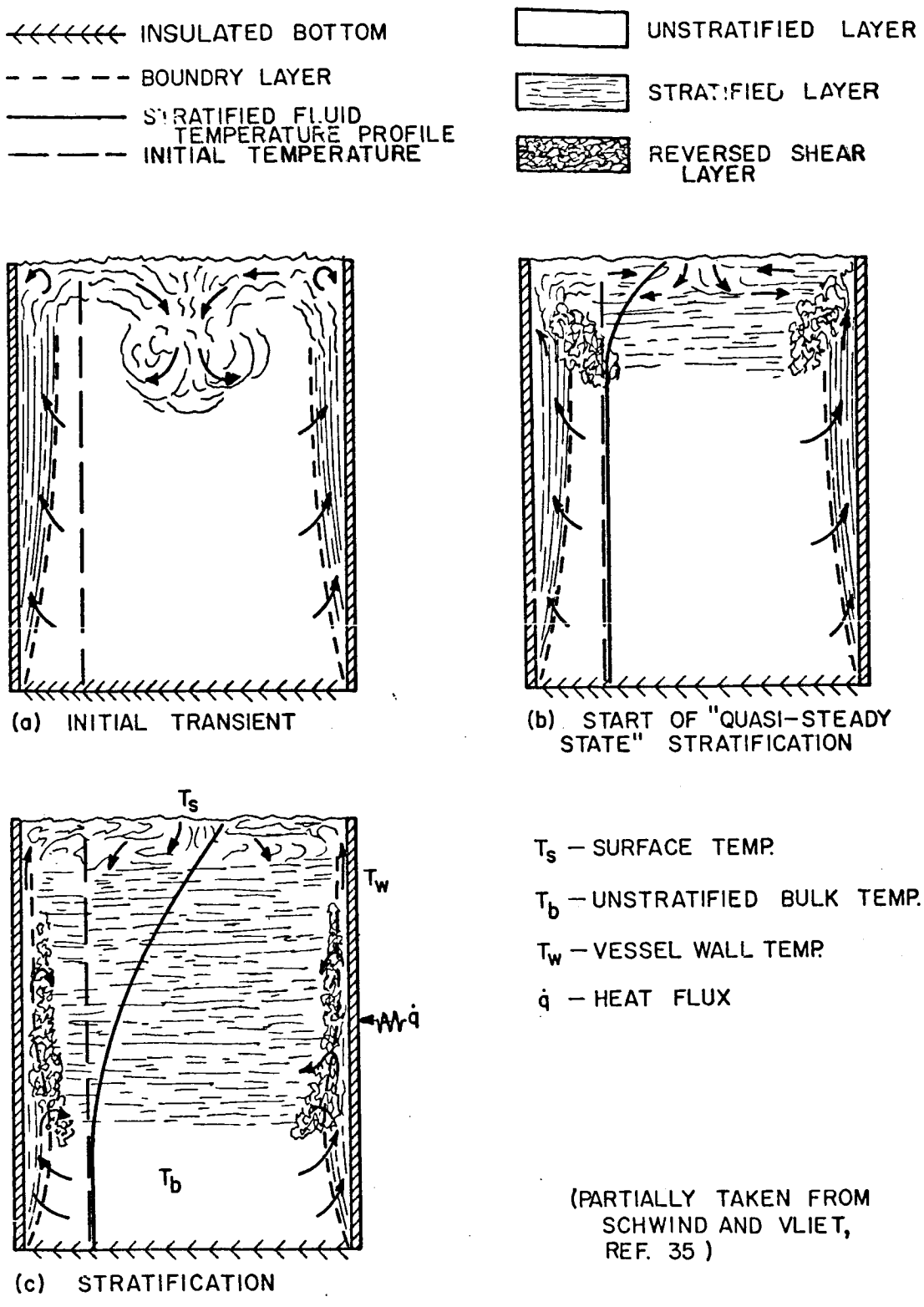

FIGURE 65 STAGES OF STRATIFICATION PROCESS

The temperature within the stratified layers is higher than the bulk temperature in the fluid below them. The difference in temperature is dependent upon the gradient across the walls of the vessel. That is, the higher the gradient, the larger the temperature difference between the stratified layers and the fluid not yet stratified.

In the preceding analysis of liquid discharge the assumption of constant properties and temperature was made. In case of discharge of a stratified liquid the analysis has to be modified to account for the variable properties resulting in a change of the mass flow rate of discharge. In order to include the effect of stratification upon liquid discharge a prior knowledge of the stratification process in a fluid in absence of primary flow is essential.

The procedure to be followed in the analysis starts with the determination of the dimensionless parameters governing the stratification process. The dimensional analysis will be supplemented by an approximate mathematical analysis which yields an equation relating the growth of the stratified layer to the elapsed time. Experiments will be carried out subsequently to check the validity of the analytical results. The experimental apparatus was completed while this report was being prepared.

It is appropriate at this point to discuss the process of stratification in detail.

For stratification to occur in a fluid, it must be receiving heat. In the analysis the fluid receives heat by free convection from the vessel walls, which are maintained at a constant temperature. A free convection boundary layer exists in the fluid along the walls. The fluid heated within the boundary layer is subjected to a density change and rises along the wall. At the same time, fluid is moved into the boundary layer and rises as it absorbs heat from the wall. As this heated fluid leaves the boundary layer it moves along the surface to the center of the vessel where it meets the heated fluid coming from the opposite wall. Upon meeting, they form a plume moving downward into the bulk of the fluid. The downward motion is soon arrested and reversed by buoyancy effects. The warmer fluid in the plume then moves upward and spreads outward to form a nearly uniform layer called the stratified layer, as (a) and (b) of FIG. 65 show. Simultaneously, a reverse shear layer is occurring, as shown by the darkened area impinging on the boundary layer. The vorticity within this layer tends to induce downward motion in the rising fluid and across the fluid bulk under the stratified layer. As the process proceeds, the reverse shear layer becomes less pronounced since the stratified layer overcomes it by its growth. Likewise, the part of the boundary layer congruent with the stratified layer becomes very thin, as shown in FIG.65 (c). The process continues until the whole body of fluid becomes uniform in temperature.

SURVEY OF LITERATURE

The stratification process has been studied by a number of investigators. An experimental investigation of the stratification of a cryogenic fluid contained in a vessel was carried out by Scott, et al., (Ref. 31). It was found that the presence of a good heat conducting material eliminated the stratification tendencies of liquid helium contained in a nonventing Dewar vessel. Because of its practical importance it is desirable to obtain a mathematical model of the phenomenon. Such a model enables one to predict the details of stratification for a fluid contained in a vessel.

A method of solving the exact equations for the motion of the fluid particles would be quite complex. A technique in which the bulk of the fluid is considered rather than each individual fluid particle is much easier to comprehend. Anderson, et al., (Ref. 32) gave a general mathematical method for the analysis of the stratification in a contained fluid. The vessel walls in this case were heated by radiation. An exact method has been developed for specific conditions. Barakat (Ref. 30) presents this method for the description of the flow patterns during the stratification process abstaining from simplifying assumptions.

Ruder (Ref.29) discovered that the temperature profile in the stratified layer is similar in shape to a Gaussian probability distribution function when the fluid is under pressure. Tellep and Harper (Ref. 28), using a cylindrical container, analyzed the stratification of a liquid receiving a constant heat flux from the surroundings.

Exact methods, as well as approximate methods, have been obtained. However, an analysis which deals with a constant wall temperature situation was not available. Therefore, the investigation reported here was initiated, its aim being to obtain a general relation between the growth of the stratified layer and elapsed time.

DIMENSIONAL ANALYSIS

The results of the dimensional analysis for the stratification process, carried out in Appendix E, are discussed in this section. The system is illustrated in FIG. 66. The depth of the stratified layer Δ is dependent on:

1. the elapsed time t
2. the physical properties of the fluid such as density ρ, viscosity μ, conductivity k, specific heat c, and thermal coefficient of expansion β.
3. gravitational field g
4. the heat transfer rate which is directly related to the temperature gradient $(T_w - T_b)$
5. the dimensions of the vessel such as the height H, the perimeter P, and the area of cross-section A_s.

Thus, expressing the growth Δ mathematically,

$$\Delta = f\ (k,\ \rho,\ c,\ t,\ g,\ \beta,\ (T_w - T_b),\ H,\ \mu,\ P,\ A_s) \quad (59)$$

The four basic dimensions needed to describe the above parameters are mass, M, length, L, time, T, and temperature, θ.

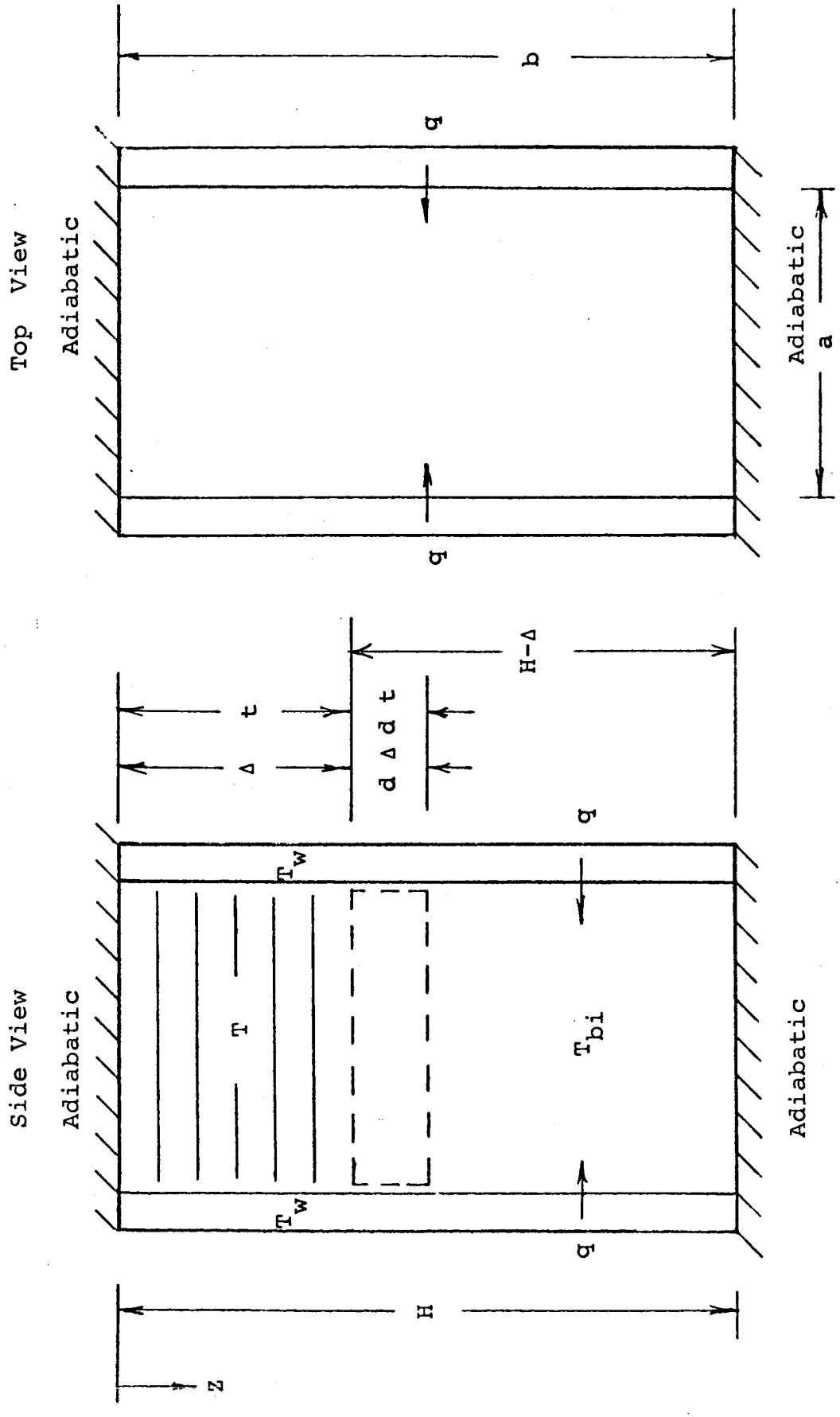

FIG. 66 PHYSICAL MODEL OF STRATIFICATION GROWTH

The parameters are listed below with their corresponding dimensions.

Symbol	Parameter	Dimension
Δ	depth of stratified layer	L
k	thermal conductivity	$MLT^{-3}\theta^{-1}$
ρ	density	ML^{-3}
c	specific heat	$L^2T^{-2}\theta^{-1}$
t	time	T
g	gravitational field	LT^{-2}
β	coefficient of thermal expansion	θ^{-1}
(T_w-T_b)	wall temperature gradient	θ
H	height of stationary fluid	L
μ	dynamic viscosity	$ML^{-1}T^{-1}$
P	heated perimeter	L
A_s	cross-sectional area of fluid	L^2

Using Buckingham's π - Theorem (see Appendix E) the following dimensionless groups were obtained.

$\frac{\Delta}{H}$, dimensionless stratified layer thickness

$\frac{P}{H}$ and $\frac{A_s}{H^2}$, geometry of container

$\frac{t}{\sqrt{H/g}}$, dimensionless time

$\frac{g\rho^2\beta(T_w - T_b)\ H^3}{\mu^2}$, Grashof Number

$\frac{\mu c}{k}$, Prandtl Number

$\frac{gH}{c\ (T_w - T_b)}$, ratio of potential energy to thermal energy

$\frac{\rho c^{3/2}\ (T_w - T_b)^{1/2}\ H}{k}$, dimensionless diffusion of thermal energy

Thus, no less than seven dimensionless groups influence the stratification process. This fact serves as a guide for the analysis to follow.

ANALYSIS

It has been explained that an analysis based on the motion of individual particles would be quite complicated. A simpler method, which considers the bulk fluid is devised. The aim of the analysis is to obtain a mathematical relation which will give the thickness of the stratified layer, Δ, as a function of time, t. Figure 66 shows the physical model and the nomenclature. The detailed analysis is presented in Appendix F. Both turbulent and laminar boundary layers are considered. If the assumption is made that the heated container walls contribute to the heating of the fluid only where stratification has not yet occurred, then the growth of the stratified layer is given by:

For turbulent boundary layer,

$$\frac{\Delta}{H} = 1 - \exp.\ [-0.042\ (Gr\ Pr)^{2/5}\ \theta] \qquad (60)$$

For laminar boundary layer,

$$\frac{\Delta}{H} = 1 - \exp.\ [-1.11\ (Gr\ Pr)^{1/4}\ \theta] \qquad (61)$$

The resulting heat transfer rates and the times required for the completion of the stratification process for any given situation represent the lower and upper bounds respectively.

In obtaining these equations, it was assumed that a boundary layer does not exist between the wall and the stratified layer, and that the heat transfer in this region could be neglected. Physically, however, the boundary layer diminishes but does not vanish, and heat transfer is never zero in this region. In fact, heat transfer at varying rates occurs over the entire wall.

The dimensionless stratification thickness, $\frac{\Delta}{H}$, is plotted as a function of dimensionless time, θ, for different values of the product (Gr Pr) in FIG. 67

The results of a numerical example where the dimensionless stratification thickness, $\frac{\Delta}{H}$, is shown versus the real time, t, in FIG. 68.

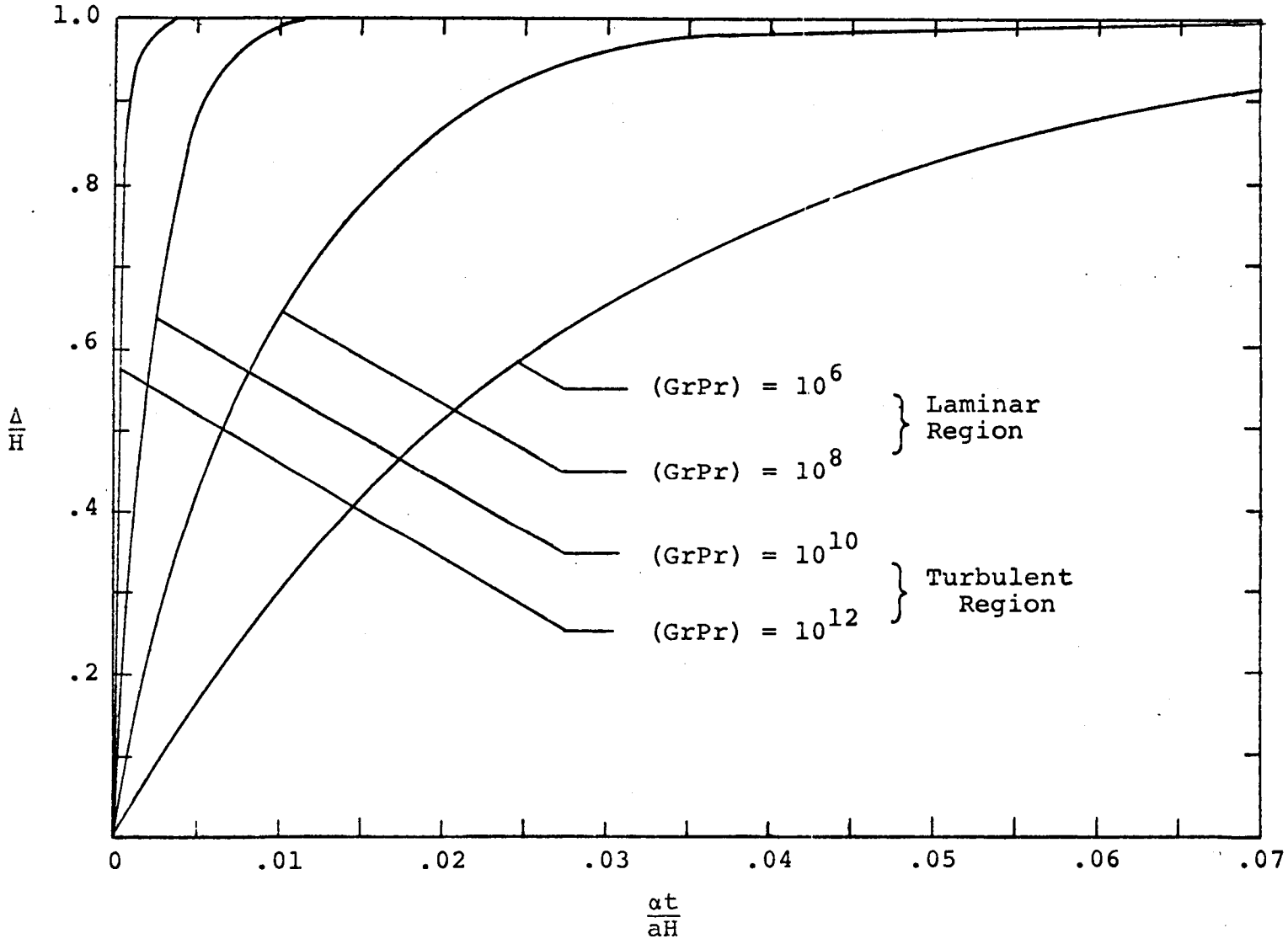

FIG. 67 DIMENSIONLESS STRATIFICATION THICKNESS, $\frac{\Delta}{H}$, VERSUS DIMENSIONLESS TIME, $\frac{\alpha t}{aH}$, FOR DIFFERENT VALUES OF THE PARAMETER (GrPr)

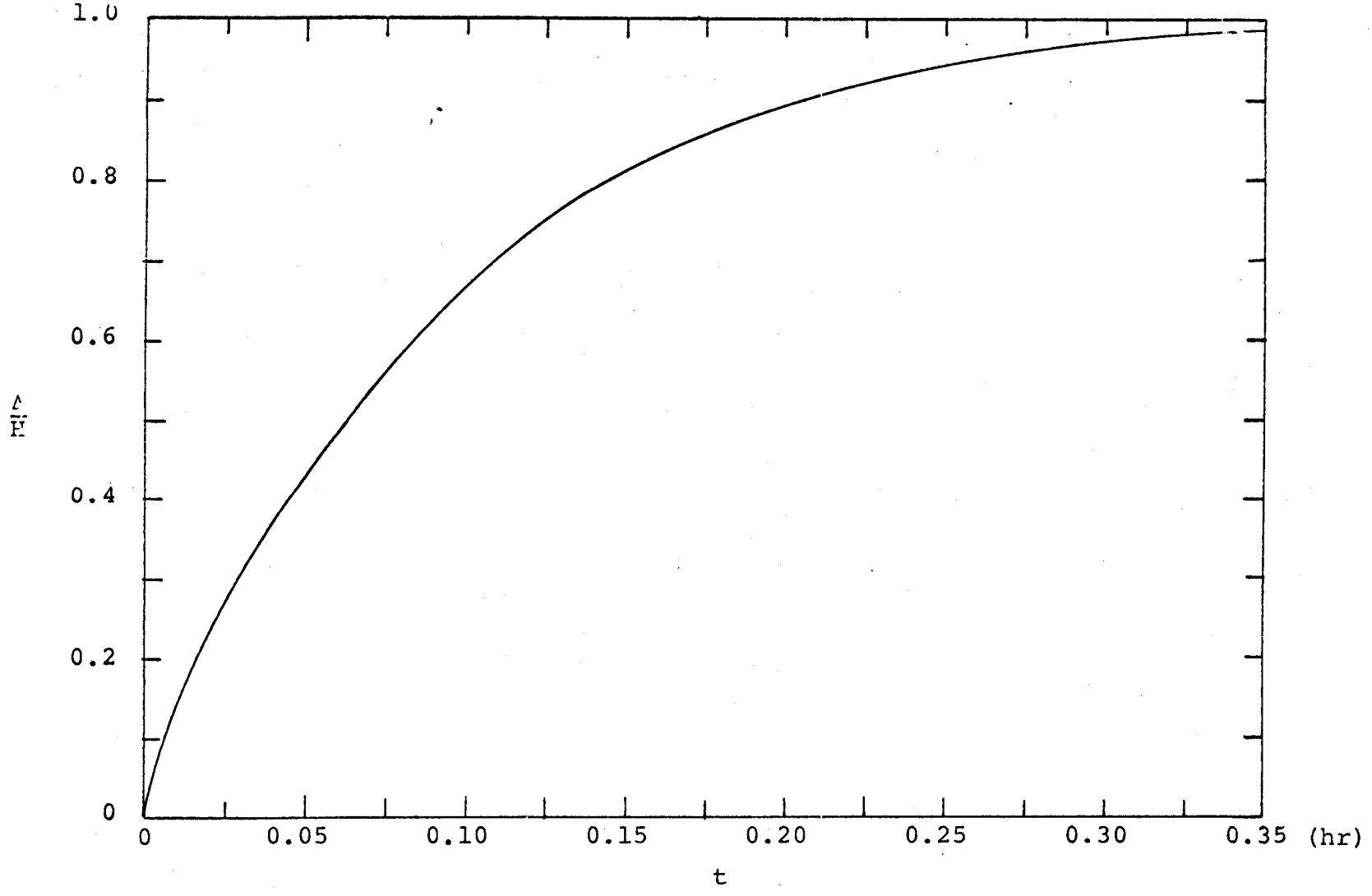

FIG. 68 DIMENSIONLESS STRATIFICATION THICKNESS, $\frac{\Delta}{H}$, VERSUS THE REAL TIME, t, FOR (GrPr) $= 1.32 \times 10^{10}$

SUMMARY

In this final section the major conclusions resulting from the first year of contract effort are given. In addition, recommendations for further research, which evolved during the course of the investigations, are outlined briefly.

CONCLUSIONS

Three major areas were selected for study in this investigation. These areas are:

(A) Single phase flow during discharge of liquids

(B) Two phase flow in the absence of heat transfer

(C) Fluid flow and energy transport in a confined liquid subjected to heat transfer

In each of the above areas, research was organized in accordance with the following pattern:

1. Literature review and evaluation
2. Investigation of physical effects, dimensional analysis, and mathematical analysis
3. Experimental verification

The literature review revealed the lack of a comprehensive study on single and two phase fluid flow in the absence and presence of heat transfer. The existing literature was evaluated and was employed to guide the research described in this report.

The physical effects associated with each of the processes studied are described in the text. The similarity parameters characterizing the relative magnitudes of these effects were obtained. Mathematical analyses based on

simplified physical models yielded concise solutions in most of the cases treated. In the remaining cases digital computer solutions were generated. All of these mathematical solutions were plotted in terms of the similarity parameters obtained previously by means of dimensional analysis.

Simultaneously with the analytical investigation experiments were carried out for purposes of verification of the analytical results. Experimental results from the discharge study are given in FIGS. 31 through 63 and can be compared with the analytical results presented in FIGS. 4 through 30. Experimentally observed cavitation numbers are compared with the corresponding analytically derived values for a range of Reynolds numbers (page 122). An experimental apparatus has been constructed for verifying the analytical stratification solutions. Experimental stratification data were obtained as this report was being completed.

RECOMMENDATIONS

The following recommendations are suggested for the completion of the present simularity study:

1) Graphical correlation of analytical and experimental discharge results, and development of semi-empirical correlations for engineering purposes.
2) Mapping of the limits of validity of the single phase discharge results by means of the criteria established for two phase flow.
3) Study of discharge of liquids over wide ranges of temperature, and also for cryogenic fluids.
4) Analytical and experimental investigation of local fluid pressures and velocities during transient discharge.
5) Improvement of stratification analysis and obtaining of verifying experimental data.
6) Study of discharge of a fluid which is stratified due to heat transfer.

LIST OF REFERENCES

1. S. S. Penner:
"Similarity Analysis for Chemical Reactors and the Scaling of Liquid Fuel Rocket Engines," CALTECH, JPL TR No. 8, Nov. 1954.

2. H. Rouse and S. Ince:
"History of Hydraulics," Iowa Inst. of Hydraulic Research, State University of Iowa, 1957.

3. E. H. Lewitt:
"Hydraulics and the Mechanics of Fluids," Sir Isaac Pitman and Sons, Ltd., London, 8th Ed., 1949.

4. V. L. Streeter:
"Fluid Mechanics," Chapters 3, 5, and 9, McGraw-Hill Book Co., Inc., New York, N.Y., 2nd Ed., 1958.

5. R. M. Sabersky and A. J. Acosta:
"Fluid Flow, A First Course in Fluid Mechanics," Chapter 3, MacMillan Co., New York, N.Y., 1964.

6. J. Allen:
"Scale Models in Hydraulic Engineering," Longmans, Green & Co., London, 1947.

7. P. W. Bridgman:
"Dimensional Analysis," Chapter IV, Yale University Press, New Haven, 1931.

8. L. I. Sedov:
"Similarity and Dimensional Methods in Mechanics," Chapter 2, Academic Press, New York, N.Y., 1959.

9. R. C. Parkhurst and D. W. Holder:
"Wind-Tunnel Technique," Chapter 9, Sir Isaac Pitman & Sons, Ltd., 1952.

10. A. Pope:
"Wind-Tunnel Testing," Chapter 7, John Wiley & Sons, Inc., New York, N.Y., 2nd Ed., 1954.

11. L. J. Flanigan and A. A. Putnam:
"The Uses of Fluid Dynamic Modeling Techniques," Battelle Technical Review 13, No. 2. pp. 2-7, Feb. 1966.

12. A. A. Ezra:
"Scaling Laws and Similitude Requirements for Valid Scale Model Work," A Paper presented at a colloquium on "Use of Models and Scaling in Shock and Vibrations," ASME Winter Annual Meeting, Philadelphia, Pa., Nov. 19, 1963, pp. 57-64.

13. W. H. Roudebush and D. A. Mandell:
"Analytical Investigation of Some Important Problems in the Pressurized Liquid Hydrogen Tank Outflow Problem," In "Proceedings of the Conference on Propellant Tank Pressurization and Stratification," 1, pp. 2-27. George C. Marshall Space Flight Center, Huntsville, Alabama. Jan. 1965.

14. M. E. Nein and J. F. Thomson, Jr.:
"Experimental and Analytical Studies of Cryogenic Propellant Tank Pressurization," In "Proceedings of the Conference on Propellant Tank Pressurization and Stratification," 1, pp. 29-54. George C. Marshall Space Flight Center, Huntsville, Alabama. Jan. 1965.

15. J. A. Clark:
"A Review of Pressurization, Stratification and Interfacial Phenomena," Paper S-1, Presented at 1964 Cryogenic Engineering Conference, Philadelphia, Pa. (International Advances in Cryogenic Engineering 10, pt. 2, pp. 259-283, Plenum Press, New York, N.Y., 1965.)

16. P. Fischer:
"Ähnlichkeitsbedingungen fur Strömungsvorgänge mit Gleichzeitigem Warmeübergang,"ZAMM 43, pp. T122-125, Sonderheft 1963.

17. H. Rouse:
"Fluid Mechanics for Hydraulic Engineers," pp. 258-261, Dover Publications, Inc., New York, N. Y., 1961.

18. J. K. Vennard:
"Elementary Fluid Mechanics," pp. 300-308, John Wiley and Sons, Inc., New York.

19. R. E. Gaskell:
"Engineering Mathematics," pp. 250-251, Holt, Rinehart, and Winston, Inc., New York, 1958.

20. William J. Holl and George F. Wislicenus:
"Scale Effects on Cavitation," pp. 385-389, Jour. of Basic Engr., September, 1961.

21. J. W. Hall:
"An Effect of Air Content on the Occurrence of Cavitation," ASME Paper No. 60-Hyd-8, March, 1960.

22. R. W. Kermeen:
"Some Observations of Cavitation on Hemispherical Head Models," Report E-35.1, Hydrodynamics Laboratory, Cal. Inst. of Tech.

23. J. W. Hall and A. L. Treaster:
"Cavitation Hysterisis," Jour. of Basic Engr., pp. 199-212, March, 1966.

24. R. Oshima:
"Theory of Scale Effects on Cavitation Inception on Axially Symetric Bodies," Jour. of Basic Engr., pp. 379-384, September, 1966.

25. S. Kamiyama:
"Cavitation Tests in Pipe Bends," Trans. of ASME, pp. 252-260, March 1966.

26. H. A. Stahl, A. J. Stepanoff, and N. J. Phillipsburg:
"Thermodynamic Aspects of Cavitation in Centrifugal Pumps," Trans. of ASME, pp. 1691-1693, November, 1956.

27. J. H. Keenan and F. G. Keys:
"Thermodynamic Properties of Steam," John Wiley and Sons, Inc., New York, 1936.

28. D. M. Tellep and E. Harper:
"Approximate Analysis of Propellant Stratification," AIAA Journal, Vol. 1, No. 8, pp. 1953-1956, August, 1963.

29. J. M. Ruder:
"Stratification in a Pressurized Container with Sidewall Heating," AIAA Journal, Vol. 2, pp. 135-137, January, 1964.

30. H. Z. Barakat:
"Transient Laminar Free-Convection Heat and Mass Transfer in Two-Dimensional Closed Containers Containing Distributed Heat Source," ASME Publication, 65-WA/HT-28, July, 1965.

31. L. E. Scott, R. Robbins, D. Mann, and B. Birmingham:
"Temperature Stratification in a Nonventing Liquid Helium Dewar," Journal of Research of the National Bureau of Standards, Vol. 64C, No. 1, pp. 19-23, January - March, 1960.

32. B. H. Anderson, S. Huntley, and D. Connolly:
"Propellant Heating Studies with Wall and Nuclear Heating," ASME Pbulication, 64-WA/AV-8, September, 1964.

33. F. Kreith:
"Principles of Heat Transfer," International Textbook Co., Scranton, Pa., 1958.

34. F. R. Gilmore, and M. S. Plesset:
"Scaling Laws for Incipient Cavitation Noise," Hydrodynamics Lab., Cal. Inst. of Tech., Report No. 26-1, April 3, 1950.

35. R. G. Schwind and G. C. Vleit:
"Observations and Interpretations of Natural Convection and Stratification in Vessels," Proc. of the 1964 Heat Transfer and Fluid Mechanics Institute, Stanford University Press, 1964, pp. 51-68.

36. W. H. Adams:
"Heat Transmission," Third Edition, McGraw-Hill Book Company, Inc., 1954, pp. 130-133.

37. V. L. Streeter:
"Fluid Dynamics," McGraw-Hill Book Company, Inc., 1948, pp. 64-67.

APPENDIX A

Dimensional Analysis of Liquid Discharge

Equation (1), modified to account for variations in geometry, is written as

$$\dot{m} = f(\rho, g, \Delta P, \nu, h, t, D, d, L) \qquad (A1)$$

The variables are listed below, along with their dimensions in terms of mass (M), length (L), and time (T).

Symbol	Parameter	Dimensions
$\dot{m}$	mass flow rate	MT^{-1}
ρ	density	ML^{-3}
g	gravitational constant	LT^{-2}
ΔP	pressure drop	$ML^{-1}T^{-2}$
ν	kinematic viscosity	$L^{2}T^{-1}$
h	initial fluid height	L
t	time	T
D	container diameter	L
d	discharge diameter	L
L	discharge tube length	L

The variables (gh), ρ, and d are chosen as repeated variables (Ref. 36). These are combined with each of the other variables separately to form dimensionless groups. In

order for each group to be dimensionless, the exponents a, b, and c must have specific values as indicated in the following table.

Dimensionless group	Dimensions M	L	T
$\dot{m}(gh^a\rho^b d^c$	(b+1)	(-2a-3b+c)	(-2a-1)
$\Delta P(gh)^a\rho^b d^c$	(b+1)	(2a-3b-c-1)	(-2a-2)
$\nu(gh)^a\rho^b d^c$	(b)	(2a-3b+c+2)	(-2a-1)
$h(gh)^a\rho^b d^c$	(b)	(2a-3b+c+1)	(-2a)
$t(gh)^a\rho^b d^c$	(b)	(2a-3b+c)	(-2a+1)
$D(gh)^a\rho^b d^c$	(b)	(2a-3b+c+1)	(-2a)
$L(gh)^2\rho^b d^c$	(b)	(2a-3b+c+1)	(-2a)

In order to obtain dimensionless groups in the left hand column, the M, L, and T exponents in each row must simultaneously be zero. For example, the first row gives rise to the following:

Simultaneous Equations	Solution
b+1 = 0	a = - 1/2
2a-3b+c = 0	b = 01
-2a-1 = 0	c = -2

The dimensionless parameter associated with the first row becomes $\frac{\dot{m}}{\rho d^2\sqrt{gh}}$. For convenience of physical interpretation

this quantity is arbitrarily modified to $\frac{\dot{m}}{\rho\left(\frac{\pi d^2}{4}\right)\sqrt{2gh}}$. In a similar manner the dimensionless quantities associated with the remaining rows of the table are obtained as $\frac{\Delta P/\rho g}{h}$, $\frac{d\sqrt{2gh}}{\nu}$, $\frac{h}{d}$, $\frac{t\sqrt{2gh}}{d}$, $\frac{D}{d}$, and $\frac{L}{d}$ respectively. Again it is convenient, for ease of physical interpretation, to replace $\frac{t\sqrt{2gh}}{d}$ by $\frac{1}{2}\left(\frac{d}{h}\right)\left(\frac{t\sqrt{2gh}}{d}\right)$, or $\frac{t}{\sqrt{2h/g}}$. The final result is written as

$$\frac{\dot{m}}{\rho\left(\frac{\pi d^2}{4}\right)\sqrt{2gh}} = F\left[\frac{t}{\sqrt{2h/g}}, \frac{\Delta P/\rho g}{h}, \frac{d\sqrt{2gh}}{\nu}, \frac{h}{d}, \frac{D}{d}, \frac{L}{d}\right] \quad \text{(A2)}$$

APPENDIX B

Analysis Based on Transient Flow in the Absence of Viscous Effects for Zero Pressure Drop

In the analysis considered here transient flow conditions are treated, and local acceleration effects are accounted for. The system analyzed is shown in FIG. 3. For simplicity the flow is assumed to be one dimensional.[1] It is convenient in this case to apply conservation of energy to a control volume surrounding the fluid remaining in the container at any given instant of time.

Conservation of energy gives

$$\left[\begin{array}{c}\text{Rate of increase of}\\ \text{fluid energy in the}\\ \text{container}\end{array}\right] + \left[\begin{array}{c}\text{Net rate}\\ \text{of energy}\\ \text{outflow}\end{array}\right] = \left[\begin{array}{l}\text{Rate of work done}\\ \text{on the fluid by}\\ \text{pressure forces at}\\ \text{boundaries where}\\ \text{fluid motion occurs.}\end{array}\right] \qquad \text{(B1)}$$

---

[1] A more exact treatment would involve the two dimensional streamline pattern of the flow, and the local acceleration effects would be more accurately evaluated by employing the virtual mass (Ref. 37) of the fluid in the container rather than the actual mass.

where both potential and kinetic energies must be accounted for. When expressed in terms of symbols this relation becomes

$$\frac{d}{dt}\left[(\rho Ay)g\,\frac{y}{2} + (\rho Ay)\,\frac{V_1^2}{2}\right] + \left[(\rho aV_2)\,\frac{V_2^2}{2}\right] = \left[P_1AV_1 - P_2aV_2\right] \quad \text{(B2)}$$

Since P_2 is chosen equal to P_1 for this analysis and since $AV_1 = aV_2$ from equation (4), the net rate of work done by the external pressure forces (given by the right hand side of the above equation) is zero. Inserting $V_1 = -\,dy/dt$ and $V_2 = -\,\frac{A}{a}\frac{dy}{dt}$ makes it possible, after some manipulation, to rewrite equation (B2) as

$$\frac{d^2y}{dt^2} = -g + \frac{\beta^2\left(\frac{dy}{dt}\right)^2}{2y} \quad \text{(B3)}$$

where $\beta^2 = \left[\left(\frac{A}{a}\right)^2 - 1\right]$. Notice that if $a = A$ (or $\beta = 0$) $a = A$, $\beta^2 = 0$. For this the situation reduces to the case of a fluid cylinder of constant area A, and the equation (B3) gives the acceleration as $d^2y/dt^2 = -g$.

In general $dy/dt = 0$ at $t = 0$ (zero initial discharge flow rate), and local acceleration effects dominate. Equation (B3) shows that $d^2y/dt^2 \approx -g$ for small values of time when dy/dt is negligibly small. However, once dy/dt becomes sufficiently large the convective acceleration effect, as indicated by the value of $\frac{\beta^2(dy/dt)^2}{2y}$ in equation (B3), increases and the local acceleration effect, as indicated by d^2y/dt^2, decreases in magnitude.

For large values of β ($a \ll A$) the local acceleration effect diminishes very rapidly when dy/dt is still quite small. Once the local acceleration effect becomes negligible, equation (B3) predicts $dy/dt = -\frac{1}{\beta}\sqrt{2gy}$ in agreement with the result given in equation (7) for quasi-steady flow.

Equation (B3) can be expressed in dimensionless form as

$$\frac{d^2[y/h]}{d\left[\frac{1}{\beta}\left(\frac{t}{\sqrt{2h/g}}\right)\right]^2} = -2\beta^2\left\{1 - \frac{1}{4\left(\frac{y}{h}\right)}\frac{d[y/h]}{d\,\frac{1}{\beta}\left(\frac{t}{\sqrt{2h/g}}\right)}\right\}^2 \qquad \text{(B4)}$$

The above differential equation was solved by means of digital computer calculations. The results, for various β values, are given in FIG. 6. The dimensionless mass flow rate values were obtained from the same program and are given in FIG. 7.

APPENDIX C

Analysis Based on Transient Flow for Discharge of a Container Through a Tube

The system analyzed here is shown in FIG. 2. In this analysis transient flow conditions are treated taking into account local acceleration effects, viscous forces and pressure drop. It is assumed that

(1) the flow is one dimensional
(2) friction effects in the container are negligible so that the pressure at the entrance to the tube is given by Bernoulli's equation
(3) the friction coefficient for the flow through the tube is constant.

FIGURE 20 shows the system configuration at any instant of time. In this case, it is convenient to apply conservation of momentum to the fluid within the control volume (dashed line) surrounding the fluid in the tube.

Conservation of momentum gives

$$\left[\begin{array}{c}\text{Rate of increase of}\\ \text{momentum of the fluid}\\ \text{in the control volume}\end{array}\right] =$$

$$\left[\begin{array}{c}\text{Net momentum}\\ \text{going into the}\\ \text{control volume}\end{array}\right] + \left[\begin{array}{c}\text{Net force acting}\\ \text{on the control}\\ \text{volume}\end{array}\right] \quad \text{(C1)}$$

Here the net force accounts for gravity, pressure and viscous forces. Since the cross-sectional area of the tube is a constant the velocity of the fluid within the control volume is constant along the length of the tube and its rate of change of momentum is given by $\frac{d}{dt}\left[\rho aL\left(-\frac{A}{a}\frac{dy}{dt}\right)\right]$. Because the amount of fluid entering the control volume at Q is the same as the amount leaving it at R (by continuity), the net amount of momentum entering the control volume is zero. By assumption (2), the pressure at Q is given by $P_1' = P_1 + \rho g(y - L) - \frac{1}{2}\rho\beta^2\left(\frac{dy}{dt}\right)^2$. Finally, according to the third assumption the frictional force on the control volume is

$$\tau \cdot \pi d \cdot L = c_f \cdot \frac{1}{2}\rho\left(-\frac{A}{a}\frac{dy}{dt}\right)^2 \cdot \pi dL$$

Notice that the friction coefficient c_f introduced here is analogous to the skin friction coefficient used for flat plates. It is equal to $\frac{f}{4}$, where f is the conventional friction factor for pipes given in equation (27). Hence, equation (C1) becomes

$$\frac{d}{dt}\left[\rho aL\left(-\frac{A}{a}\frac{dy}{dt}\right)\right] = \left[P_1 + \rho g(y - L) - \frac{1}{2}\rho\,\beta^2\left(\frac{dy}{dt}\right)^2\right]a - P_2 a$$
$$+ \rho gLa - \left[c_f \cdot \frac{1}{2}\rho\left(-\frac{A}{a}\frac{dy}{dt}\right)^2 \cdot \pi dL\right] \qquad (C2)$$

Dividing throughout by $(-\rho AL)$, equation (C2) can be rearranged to yeild

$$\frac{d^2y}{dt^2} - \left[\frac{\beta^2 a}{2LA} + \frac{2c_f}{d}\frac{A}{a}\right]\left(\frac{dy}{dt}\right)^2 + \left[\frac{g}{L}\frac{a}{A}\right]y =$$
$$- \frac{(P_1 - P_2)\,a}{\rho AL} \qquad (C3)$$

Equation (C3) has the same general character as equation (B3) of Appendix B and the conclusions about the relative importance of local and convective acceleration effects remain the same. The only difference between the two is that equation (C3) has terms which account for an external pressure drop and viscous forces whereas these have been excluded in equation (B3).

Equation (C3) can be expressed in dimensionless form as

$$\left(\frac{L}{h}\right)\frac{d^2y^*}{dt^{*2}} - \left[\frac{\beta^2}{2}\frac{a}{A} + 2c_f\frac{L}{d}\cdot\frac{A}{a}\right]\left(\frac{dy^*}{dt^*}\right)^2 + 2\beta^2\frac{a}{A}y^* =$$
$$- \left(\frac{P_1 - P_2}{\rho gh}\right)2\beta^2\frac{a}{A} \qquad (C4)$$

where $y^* = \frac{y}{h}$ and $t^* = \frac{1}{\beta}\frac{t}{\sqrt{2h/g}}$. This equation has to be solved with the initial conditions, $y^* = 0$ and $\frac{dy^*}{dt^*} = 0$ at $t^* = 0$.

Comparison of equation (C4) with the result of the dimensional analysis given by equation (3b) shows that indeed, the dimensionless liquid height (or alternately the dimensionless mass flow rate) is a function of the dimensionless parameters indicated in the dimensional analysis. Of course, it should be noted that the skin friction coefficient c_f $\left(= \frac{f}{4}\right)$ appearing in equation (C4) is essentially a function of the Reynolds number, $\frac{d\sqrt{2gh}}{\nu}$, appearing in equations (2b) and (3b). Also $\frac{L}{h}$, the coefficient of $\frac{d^2y^*}{dt^{*2}}$ in equation (C4), is given by $\left[\frac{L}{d} \Big/ \frac{h}{d}\right]$.

Equation (C4), with the indicated initial conditions has been solved for various values of the dimensionless parameters by the Fourth Order Runge-Kutta method with a 0.001 step. The solution is terminated when y^* reached a value near $\frac{L}{h}$, because physically when $y^* = \frac{L}{h}$, the tank is empty. The results are discussed in the text of the report.

APPENDIX D

Method of Least Squares Curve Fitting Applied to Instantaneous Fluid Height Measurements

The instantaneous fluid height, y, in a container during discharge, based on quasi-steady flow theiry, is given by

$$y = h - \frac{C_D}{\beta} \; 2g\left(h + \Delta P/\rho g\right)^{\frac{1}{2}} + \frac{C_D^{\,2}}{\beta^2} \; \frac{gt^2}{2} \qquad \text{(D1)}$$

This equation can be simplified by defining new terms as

$$B = \frac{C_D}{\beta} \sqrt{g/2} \qquad \text{(D2)}$$

and

$$S = \left(h + \Delta P/\rho g\right) \qquad \text{(D3)}$$

Equation (D1) can now be written as

$$y = h - 2SBt + B^2t^2 \qquad \text{(D4)}$$

For a fixed initial fluid height and external pressure drop, both h and S are known constants. The instantaneous fluid height, y, and time, t, are determined experimentally. With these data available, it is possible to determine the value of B which gives the best curve fit.

Equation (D4) is a curve of second order in the variable t, which has a smooth curve fit.. Let Q be defined as the sum of the squares of the deviations of the individual data points from the curve given by equation (D4).

$$Q = \sum_{i=1}^{n} \varepsilon_i = \sum_{i=1}^{n} (y_i - \hat{y}_i)^2 \qquad (D5)$$

where the variables are defined as

Q = sum of the squares of the deviations

ε_i = deviation of i^{th} data point

n = number of data points

$\hat{y}_i$ = value of y at time t_i given by equation (D4)

y_i = experimental value of y at time t_i

Substitution of equation (D4) in equation (D5) results in

$$Q = \sum_{i=1}^{n} y_i - (h - 2BSt_i + B^2 t_i^2)^2 \qquad (D6)$$

It is desired to minimize the value of Q by adjusting the value of B. This is done by taking the derivative of equation (D6) with respect to B, setting the result equal to zero, and solving for the value of B which results in a minimum value for Q,

$$\frac{\partial Q}{\partial B} = \sum_{i=1}^{n} \frac{2}{2B} y_i - (h - 2BSt_i + B^2 t_i^2)^2 = 0 \qquad (D7)$$

Differentiation as indicated by equation (D7) and rearrangement result in

$$\frac{\partial Q}{\partial B} = B^2 \sum_{i=1}^{n} t_i^4 - 3SB^2 \sum_{i=1}^{n} t_i^3 + (Bh + 2S^2B) \sum_{i=1}^{n} t_i^2$$

$$- B \sum_{i=1}^{n} t_i^2 y_i + S \sum_{i=1}^{n} t_i y_i - hS \sum_{i=1}^{n} t_i = 0 \qquad \text{(D8)}$$

This equation can be written as

$$G_3B^3 + G_2B^2 + G_1B + G_o = 0 \qquad \text{(D9)}$$

where

$$G_3 = \sum_{i=1}^{n} t_i^4 \qquad \text{(D10)}$$

$$G_2 = -3S \sum_{i=1}^{n} t_i^3 \qquad \text{(D11)}$$

$$G_1 = (h + 2S^2) \sum_{i=1}^{n} t_i^2 - \sum_{i=1}^{n} t_i^2 y_i \qquad \text{(D12)}$$

$$G_o = S \sum_{i=1}^{n} t_i y_i - hS \sum_{i=1}^{n} t_i \qquad \text{(D13)}$$

The constants G_o to G_3 are determined from the experimental data as indicated. This gives B as the variable in a non-homogeneous cubic equation. A useful method of determining the roots of equation (D9) is Newton's method (Ref. 19). The above system of equations has been programmed, enabling the rapid determination of discharge coefficient, non-dimensional height and non-dimensional mass flow rates shown by FIG. through .

APPENDIX E

Dimensional Analysis of Stratification in a Fluid Without Primary Flow

It was shown in the text of this report that the thickness of the stratification layer, Δ, represented as,

$$\Delta = f\ (k,\ \rho,\ c,\ t,\ g,\ \beta,\ (T_w - T_b),\ H\ \mu,\ P,\ A_s) \qquad (E1)$$

Listed below are the parameters with their corresponding dimensions in terms of mass, M, time, t, length, L, and temperature, .

Symbol	Parameter	Dimensions
Δ	depth of stratification	L
k	thermal conductivity	$MLT^{-3}\theta^{-1}$
ρ	density	ML^{-3}
c	specific heat	$L^2T^2\theta^{-1}$
t	time	T
g	gravitational field	LT^{-2}
β	coefficient of expansion	θ^{-1}
(T_w-T_b)	wall temperature gradient	
H	height of fluid contained in vessel	L
μ	dynamic viscosity	$ML^{-1}T^{-1}$
P	heated perimeter	L
A_s	cross-sectional area of fluid	L^2

Equation (E1) is rewritten in dimensional form

$$L = [MLT^{-3}\Theta^{-1}]^{a}\ [ML^{-3}]^{b}\ [L^{2}T^{-2}\Theta^{-1}]^{c}\ [T]^{d}\ [LT^{-2}]^{e}\ [\Theta^{-1}]^{f}\ [\Theta]^{g}\ [L]^{h}\ [ML^{-1}T^{-1}]^{i}\ [L]^{j}\ [L^{2}]^{h} \qquad (E2)$$

Since L alone exists on the left-hand side of equation (E2), the sum of the exponents of the three remaining dimensions on the right-hand side of the equation must sum to zero. Accordingly, the sum of the exponents of L on the right-hand side of the equation must sum to one. Listed below are the four dimensions and their corresponding exponents summed to the value as explained above.

Dimension

M	$a + b + i = 0$
L	$a - 3b + 2c + e + h - i + j + 2k = 1$
T	$-3a - 2c + d + 2e - i = 0$
Θ	$-a - c - f + g = 0$

These are four equations containing eleven unknowns; so four of these unknown exponents must be solved in terms of the other seven. The exponents chosen are a, c, g, and h, respectively. These exponents are found in terms of the remaining exponents using the equations as given in the table. Equation (E1) can now be written as

$$\Delta = (k)^{-b-i}\ (\rho)^{b}\ (c)^{3/2\ b + i - e + d/2}\ (t)^{d}\ (g)^{e}\ (\beta)^{f}\ (T_w - T_b)^{f + 1/2\ b - e + d/2}\ (H)^{1 + b - d + e - j - 2k}\ (\mu)^{i}\ (P)^{j}\ (A_s)^{k} \qquad (E3)$$

All the parameters are grouped to yield:

$$\frac{\Delta}{H} = (k^{-1}\ \rho c^{3/2}(T_w-T_b)^{1/2}H)^b\ (c^{1/2}t(T_w-T_b)^{1/2}H^{-1})^d$$
$$(c^{-1}g(T_w-T_b)^{-1}H)^e\ (\beta(T_w-T_b))^f\ (c\mu k^{-1})^i \qquad \text{(E4)}$$
$$(PH^{-1})^j\ (A_sH^{-2})^k$$

Equation (E4) shows that

$$\frac{\Delta}{H} = F\left[\frac{\rho c^{3/2}\ (T_w-T_b)^{1/2}H}{k},\ \frac{c^{1/2}t\ (T_w-T_b)^{1/2}}{H},\right.$$
$$\left.\frac{gH}{c\ (T_w-T_b)},\ \beta(T_w-T_b),\ \frac{\mu\ c}{k},\ \frac{P}{H},\ \frac{A_s}{H^2}\right] \qquad \text{(E5)}$$

Some of these seven π-factors on which $\frac{\Delta}{H}$ depends can be re-arranged to give other more familiar dimensionless groups. Carrying out the manipulations $\frac{\Delta}{H}$ can be written as

$$\frac{\Delta}{H} = G\left[\frac{t}{\sqrt{H/g}},\ \frac{\mu\ c}{k},\ \frac{\rho^2 g\beta(T_w-T_b)\ H^3}{\mu^2},\ \frac{gH}{c\ (T_w-T_b)},\right.$$
$$\left.\frac{\rho c^{3/2}\ (T_w-T_b)^{1/2}H}{k},\ \frac{P}{H},\ \frac{A_s}{H^2}\right] \qquad \text{(E6)}$$

APPENDIX F

Analysis of Stratification Growth

The objective of the present analysis is to obtain a general relation between the stratified layer thickness, Δ, and elapsed time, t, in the absence of primary flow.

The physical model to be analysed is illustrated in FIG. 66. A fluid of initially uniform temperature T_{bi} is confined in a rectangular container, two opposite walls of which are kept at constant temperature, T_w. The remaining four walls are assumed to be adiabatic.

In order to simplify the problem, the following assumptions and approximations are made.

1. The temperature distribution, T, in the stratified layer is uniform and is equal to the temperature of the heated walls, T_w.
2. The boundary layer does not exist between the heated walls of the container and the stratified layer, thus the heat transfer in this region can be neglected.
3. In the unstratified region, heat transfer only takes place within the boundary layer. The bulk temperature, T_{bi}, in this region remains unchanged.

4. The temperature in Z-direction is constant in the stratified layer and equals the heated wall temperature, T_w. It changes from T_w to the initial temperature T_{bi} across the "interface" between the stratified region and the unstratified liquid.

5. The film heat transfer coefficient, $\bar{h}$, is approximated as follows*:

for Turbulent Boundary Layer $(Gr\ Pr > 10^{10})$

$$\bar{h} = 0.021 \frac{k}{H} (Gr\ Pr)^{2/5}$$

for Laminar Boundary Layer $(Gr\ Pr < 10^{8})$

$$\bar{h} = 0.555 \frac{k}{H} (Gr\ Pr)^{1/4}$$

where $\bar{h}$ = film heat transfer coefficient, Btu/hr ft^2 F

k = thermal conductivity of the heated container walls, Btu/hr ft F

H = height of the container, ft

Gr = Grashof number

Pr = Prandtl number

---

* Strictly speaking this heat transfer coefficient $\bar{h}$ is valid for the case of free-convection heat transfer from a vertical plate at T_w surrounded in an infinite medium at T_∞. See Kreith, "Principles of Heat Transfer," Ref. (33).

Refer now to FIG. 66, and consider the energy balance of a stratified layer of thickness, Δ. The increase of internal energy must equal the heat transfer from the heated walls to the liquid during the time interval dt.

The increase of internal energy of the stratified layer of thickness Δ is

$$q = \rho c \left(T_w - T_{bi}\right) A \, d\Delta \qquad \text{(F1)}$$

where ρ - density of the fluid at T_w, Lb/ft^3

c - specific heat of the fluid at T_w, Btu/Lb °F

T_w - temperature of the heated walls, °F

T_{bi} - initial bulk temperature of the confined fluid, °F

A - cross sectional area of the container, ft^2

$d\Delta$ - the increase of the stratified layer thickness during the time interval dt, ft.

The heat transfer from the heated walls to the confined liquid during the time interval dt is given by

$$q = \bar{h} \left(H - \Delta\right) P \left(T_w - T_{bi}\right) \, dt \qquad \text{(F2)}$$

where $\bar{h}$ - film heat transfer coefficient Btu/hr ft^2 F

H - height of the container, ft

Δ - stratified layer thickness at time t, ft

P - heated perimeter, ft

Equating equations (F1) and (F2), results in

$$\rho c \left(T_w - T_{bi}\right) A \, d\Delta = \bar{h} \left(H - \Delta\right) P \left(T_w - T_{bi}\right) dt \qquad (F3)$$

Substitution of expressions for A and P into equation (F3), (A = ab, P = 2b), yields

$$\frac{1}{H-\Delta} \, d\Delta \, \frac{2 \bar{h}}{a \rho c} \, dt \qquad (F4)$$

When the left hand side of equation (F 4) is integrated from $\Delta = 0$ to $\Delta = \Delta$, and the right hand side from $t = 0$ to $t = t$, the equation

$$- \ln \left(\frac{H-\Delta}{H}\right) = \frac{2 \bar{h}}{a \rho c} \, t \qquad (F5)$$

is obtained.

After rearrangement, equation (F 5) becomes

$$\frac{\Delta}{H} = 1 - \exp. \left(- \frac{2 \bar{h}}{a \rho c} \, t\right), \qquad (F6)$$

which relates the dimensionless stratified layer thickness to time.

In the case of a turbulent boundary layer, equation (F 6) can be combined with assumption 5 to yield the following expression for the stratification growth,

$$\frac{\Delta}{H} = 1 - \exp. \left[-0.042 \left(Gr \, Pr\right)^{2/5} \theta\right] \qquad (F7)$$

where

$\theta = \frac{t\alpha}{aH}$, a dimensionless time characterized by the geometry of the container and the physical properties of the confined fluid.

$\alpha = \frac{k}{\rho c}$, thermal diffusivity of the fluid evaluated at mean temperature, ft^2/hr

For the case of laminar boundary layer, the expression is

$$\frac{\Delta}{H} = 1 - \exp. \left[- 1.11 \left(Gr\ Pr\right)^{1/4}\ \theta\right] \qquad (F8)$$

Numerical Example

For clarity and better understanding of the problem, a numerical example with specified geometry of the container, for a turbulent boundary layer, is presented below. The results are plotted in FIG. 68. Stratification growth in water, at $T_{bi} = 60°F$, confined in a container with heated walls, at temperature $T_w = 100°F$, is calculated. All the properties are evaluated at the mean temperature, $T_m = 1/2 \left(T_w + T_{bi}\right) = 80°F$.

$$a = 0.25 \text{ ft}$$

$$H = 1 \text{ ft}$$

$$Pr = \frac{\mu c_p}{k} = 5.89$$

$$Gr = \frac{g\rho^2\beta}{\mu^2} \Delta T H^3 = 2.24 \quad 10^9$$

$$\left(Gr \times Pr\right) = 1.32 \times 10^{10} > 10^{10} \text{ turbulent boundary layer}$$

$$\frac{\alpha}{a\ H} = \frac{5.68 \times 10^{-3}}{0.25 \times 1\ ft^2} \frac{ft^2}{hr}$$

$$= 2.27 \times 10^{-2}\ 1/hr$$

$$= 6.3 \times 10^{-6}\ 1/sec$$

Substituting these values into equation (F7) and simplifying results in the following expression for the dimensionless stratification thickness:

$$\frac{\Delta}{H} = 1 - \exp.\ (-\ 0.0031\ t)$$

where the time, t, is given in seconds. This result is plotted in FIG. 68.